FLOW BEHAVIOUR OF LIQUID CRYSTALLINE PHASES OF BRANCHED CHAIN GLYCOLIPIDS

AZWA AMANINA BINTI MISLAN

FACULTY OF SCIENCE
UNIVERSITY OF MALAYA
KUALA LUMPUR

2019

FLOW BEHAVIOUR OF CRYSTALLINE PHASES OF BRANCHED CHAIN GLYCOLIPIDS

AZWA AMANINA BINTI MISLAN

DISSERTATION SUBMITTED IN FULFILMENT OF THE REQUIREMENTS FOR THE DEGREE OF MASTER OF SCIENCE

DEPARTMENT OF CHEMISTRY
FACULTY OF SCIENCE
UNIVERSITY OF MALAYA
KUALA LUMPUR

2019

UNIVERSITY OF MALAYA

ORIGINAL LITERARY WORK DECLARATION

Name of Candidate: **AZWA AMANINA BINTI MISLAN**

Matric No: **SGR160050**

Name of Degree: **MASTER OF SCIENCE**

Title of Project Paper/Research Report/Dissertation/Thesis ("this Work"):

FLOW BEHAVIOUR OF LIQUID CRYSTALLINE PHASES OF BRANCHED CHAIN GLYCOLIPIDS

Field of Study: **PHYSICAL CHEMISTRY**

I do solemnly and sincerely declare that:

(1)I am the sole author/writer of this Work;
(2)This Work is original;
(3)Any use of any work in which copyright exists was done by way of fair dealing and for permitted purposes and any excerpt or extract from, or reference to or reproduction of any copyright work has been disclosed expressly and sufficiently and the title of the Work and its authorship have been acknowledged in this Work;
(4)I do not have any actual knowledge nor do I ought reasonably to know that the making of this work constitutes an infringement of any copyright work;
(5)I hereby assign all and every rights in the copyright to this Work to the University of Malaya ("UM"), who henceforth shall be owner of the copyright in this Work and that any reproduction or use in any form or by any means whatsoever is prohibited without the written consent of UM having been first had and obtained;
(6)I am fully aware that if in the course of making this Work I have infringed any copyright whether intentionally or otherwise, I may be subject to legal action or any other action as may be determined by UM.

Candidate's Signature Date:

Subscribed and solemnly declared before,

Witness's Signature Date:

Name:

Designation:

FLOW BEHAVIOUR OF LIQUID CRYSTALLINE PHASES OF BRANCHED CHAIN GLYCOLIPIDS

ABSTRACT

Increase in environmental awareness has led to the demand of alternatives for the commercially available chemical surfactant. Glycolipids, being low toxicity, biodegradable and showing surface activity have became one of the candidate for alternatives which known as biosurfactants. In this study, glucose and maltose are attached to the Guerbet alcohol; 2-hexyl-1-decanol through glycosidic linkage to form branched chain glycolipid namely 2-hexyl-decyl-*β*-D-glucoside (*β*-Glc-$C_{10}C_6$) and 2-hexyl-decyl-*β*-D-maltoside (*β*-Mal-$C_{10}C_6$) respectively. The effect of different head group size on the thermotropic and lyotropic mesophases was investigated. The mesophases were determined by optical polarizing microscopy and small angle X-ray scattering. *β*-Mal-$C_{10}C_6$ only shows lamellar (L_α) phase in both conditions. The shear viscosity test indicates all mesophases in thermotropic and lyotropic conditions exhibits shear thinning behaviour. All rheological measurements were obtained in the linear viscoelastic regime. In general, the viscoelastic studies on thermotropic A rheometer was used to investigate the flow behaviour of *β*-Glc-$C_{10}C_6$ that exhibits inverse hexagonal phase (H_2) and inverse bicontinuous cubic phases (*Ia*3*d* and *Pn*3*m*) in thermotropic and lyotropic conditions respectively. H_2 (*β*-Glc-$C_{10}C_6$) and L_α (*β*-Mal-$C_{10}C_6$) phases show that *G'* and *G"* increase with the frequency indicating the typical viscoelastic response for non-Newtonian fluid at the selected temperatures. The lyotropic inverse bicontinuous cubic of *β*-Glc-$C_{10}C_6$ containing different water concentrations shows the dominance of *G'* over *G"* at the range of frequency and temperature tested. A similar finding was observed for lyotropic L_α phase of *β*-Mal-$C_{10}C_6$ but with a lower magnitude of structural strength.

Keywords: Liquid crystals, Rheology, Guerbet glycolipids, Self-assembly

KELAKUAN ALIRAN FASA CECAIR HABLUR BAGI GLIKOLIPID BERCABANG

ABSTRAK

Peningkatan kesedaran alam sekitar telah menyebabkan permintaan alternatif terhadap surfaktan kimia komersial meningkat. Glikolipid yang rendah ketoksikan, terbiodegradasikan dengan aktiviti permukaan menjadikannya sebagai salah satu calon untuk surfaktan alternatif yang dikenali sebagai biosurfaktan. Dalam kajian ini, glukosa atau maltosa dicantumkan pada alkohol Guerbet; 2-heksil-1-dekanol melalui ikatan glikosida untuk membentuk glikolipid rantai bercabang iaitu 2-heksildesil-β-D-glukosida (β-Glc-$C_{10}C_6$) dan 2-heksildesil-β-D-maltosida (β-Mal-$C_{10}C_6$). Kesan kumpulan kepala yang berbeza saiz terhadap mesofasa termotropik dan liotropik dikaji. Sifat ricihan reologinya turut dicirikan. Mesofasa ini ditentukan melalui mikroskopi pengutuban optik dan serakan sinar-X bersudut-kecil. Reometer digunakan untuk mengkaji kelakuan aliran β-Glc-$C_{10}C_6$ yang mempamerkan fasa heksagonal songsang (H_2) dan fasa kubik dwisambungan songsang (*Ia3d* dan *Pn3m*) masing-masing pada keadaan termotropik dan liotropik. β-Mal-$C_{10}C_6$ hanya menunjukkan fasa lamella (L_α) dalam kedua-dua keadaan. Ujian ricihan kelikatan menunjukkan semua mesofasa mempunyai sifat penipisan ricihan. Semua pengukuran reologi diperolehi dalam rejim viskoelastik linear. Umumnya, kajian viskoelastik ke atas fasa termotropik H_2 (β-Glc-$C_{10}C_6$) dan L_α (β-Mal-$C_{10}C_6$) menunjukkan *G'* dan *G"* meningkat dengan frekuensi, dan ini merupakan tindak balas viskoelastik tipikal bagi cecair bukan Newtonian pada suhu dipilih. Fasa kubik dwisambungan songsang liotropik β-Glc-$C_{10}C_6$ yang mengandungi kepekatan air yang berbeza, menunjukkan dominasi *G'* terhadap *G"* pada kekerapan dan suhu yang dikaji. Penemuan serupa diperoleh untuk fasa L_α liotropik β-Mal-$C_{10}C_6$ tetapi dengan magnitud kekuatan struktur yang lebih rendah.

Kata kunci: Cecair hablur, Reologi, Glikolipid Guerbet, Swa-penyusunan

ACKNOWLEDGEMENTS

The postgraduate phase has been a journey of self-discovery and certainly a memorable one. Years ago, I would have never imagined myself pursuing higher education yet here I am, at this exact moment, as where I should be. It was not an easy task but as Nelson Mandela once said "it always seems impossible until it's done" and I could not agree more. I may not be able to name every person, but I would love to thank every single soul, who directly or indirectly involved in helping me completing my Master's degree.

First, I would like to express my highest gratitude to my supervisor, Dr. Noor Idayu Mat Zahid for her endless guidance and support during my study. She motivated me to be better and taught me the value of kindness and tolerance with one another. Whenever I was lost, she helped me to regain my motivation and because of her, I begin to pique my interest in fundamental sciences, a topic that was unfamiliar to me in the past. I would also like to thank Dr. Siti Munirah Saharin for her assistance in completing my project.

I want to extend my acknowledgement to my partner, Muhammad Jamil Afif for his patience, support and lame jokes whenever I was down and demotivated. I would like to thank my "thesis support team" for their companionship and helpful bits of advices; Fiqa, Zarif, and Jeevithra. Of course, all these are possible with the help of my laboratory mates; Nur Asmak Nabila, Melonney Patrick, Wan Farah Nasuha and Siti Syaidatul Atiqah.

Lastly, I would not be here without my parents' unconditional love and continuous assistance. They wanted the best for me and the least I can do is realizing their dreams to see their daughter be useful and serve the community. This achievement is impossible without them. Thank you.

TABLE OF CONTENTS

Abstract ..... **iii**

Abstrak ..... **iv**

Acknowledgements ..... **v**

Table of Contents ..... **vi**

List of Figures ..... **ix**

List of Tables ..... **xiii**

List of Equations ..... **xiv**

List of Schemes ..... **xv**

List of Symbols and Abbreviations ..... **xvi**

List of Appendices ..... **xviii**

CHAPTER 1: INTRODUCTION **1**

1.1 Research Background 1

1.2 Problem Statement 2

1.3 Objectives 4

1.4 Research Scope 4

1.5 Thesis Outline 6

CHAPTER 2: LITERATURE REVIEW **7**

2.1 Liquid Crystal 7

2.1.1 Thermotropic Liquid Crystal 9

2.1.2 Lyotropic Liquid Crystal 15

2.2 Glycolipid 19

2.2.1 Natural Glycolipid 19

2.2.2 Synthetic Glycolipid 21

2.3 Rheology 23

2.3.1 Fundamental Rheological Variables 24

2.3.2 Newtonian and Non-Newtonian Behaviour 25

2.3.3 Viscoelasticity 26

2.3.4 Rheological Tests on Glycolipids 28

CHAPTER 3: METHODOLOGY 32

3.1 Synthesis of Branched Chain Glycolipid 32

3.1.1 Materials 33

3.1.2 Glycosidation of β-D-glucopyranoside 34

3.1.3 Glycosidation of β-D-maltopyranoside 35

3.1.4 General Deacetylation Procedure 35

3.1.5 Characterization Using Nuclear Magnetic Resonance (NMR) 36

3.2 Physico-Chemical Characterization of Branched Chain Glycolipid 38

3.2.1 Thermogravimetric Analysis (TGA) 39

3.2.2 Optical Polarizing Microscopy (OPM) 40

3.2.3 Small Angle X-ray Scattering (SAXS) 43

3.2.4 Rheological Measurement 46

CHAPTER 4: RESULTS AND DISCUSSION 50

4.1 Synthesis and Chemical Characterization of Glycosides 50

4.2 Thermal Analysis 56

4.2.1 Thermogravimetric Analysis (TGA) 56

4.3 Liquid Crystal Characterization 58

4.3.1 Optical Polarizing Microscopy (OPM) 58

4.3.2 Small Angle X-ray Scattering (SAXS) 60

4.4 Rheological Behaviour 63

4.4.1 Viscosity Test……...64

4.4.2 Amplitude Sweep……70

4.4.3 Frequency Sweep……74

CHAPTER 5: CONCLUSION 80

REFERENCES 82

LIST OF PUBLICATIONS AND PAPERS PRESENTED 95

APPENDIX 98

LIST OF FIGURES

Figure 1.1	General molecular structure of a glycolipid.	2
Figure 2.1	Schematic drawing of the alignment of mesogen.	8
Figure 2.2	General molecular structure of a material possessing liquid crystalline property.	9
Figure 2.3	Phase transition from solid to liquid crystal to liquid on heating. Redrawn from (Vertogen & de Jeu, 2012).	9
Figure 2.4	The chemical structure of p-n-Hexyl-p´-cyanobiphenyl (left) and molecular arrangement of nematic phase (right) together with their liquid crystal phase behaviour. Cr, N and I stand for crystal, nematic and isotropic phase respectively. Redrawn from (Jákli & Saupe, 2006) and (Dierking, 2003).	10
Figure 2.5	Schematic drawing (left) and example of compounds showing smectic phases (right) together with their liquid crystal phase behaviour. Cr, SmA, SmC and I stand for crystal, smectic A, smectic C and isotropic phase respectively. Redrawn from (Demus et al., 2011) and (Jákli & Saupe, 2006).	11
Figure 2.6	The molecular arrangement of the chiral nematic phase (top). Redrawn from (Yu et al., 2018), and chemical structure of cholesteryl benzoate (bottom) Cr, N and I stand for crystal, nematic and isotropic phase respectively. Redrawn from (Jákli & Saupe, 2006).	12
Figure 2.7	Examples of discotic mesogens. (a) Phthalocyanine and (b) triphenylene. Redrawn from (Bushby & Lozman, 2002).	13
Figure 2.8	Schematic drawing of discotic liquid crystal phases. Redrawn from (Jákli & Saupe, 2006) and (Bushby & Lozman, 2002).	13
Figure 2.9	The different molecular shape design of glycolipids. Redrawn from (Vill & Hashim, 2002).	14
Figure 2.10	The schematic drawing of amphiphilic molecule. The hydrophilic and hydrophobic parts have different affinity towards the solvent. Redrawn from (Vill & Hashim, 2002).	15
Figure 2.11	The schematic drawing of lamellar phase. Redrawn from (Singh & Dunmur, 2002).	17
Figure 2.12	The schematic drawing of normal hexagonal (left) and inverse hexagonal (right) phase. Redrawn from (Collings & Hird, 1997).	17

Figure 2.13	The schematic diagram of the bicontinuous cubic phases. From left to right; *Pn*3*m*, *Im*3*m* and *Ia*3*d*. [Reprinted (adapted) with permission from ref. (Hashim et al., 2011). Copyright 2011 Elsevier].	18
Figure 2.14	The general structure of glycosphingolipids. R indicates the long fatty acid chain. Redrawn from (Vill & Hashim, 2002).	20
Figure 2.15	The structure of monogalactosyl diacylglycerol (MGDG).	20
Figure 2.16	Examples of single chain glycolipids, sorbitan ester (left) and alkyl polyglucoside (right). The number of glucose units, m usually consists of one to five glucoside parts (Sułek et al., 2013). Redrawn from (Iglauer et al., 2010) and (Sułek et al., 2013).	22
Figure 2.17	The chemical structures of a few Guerbet glycolipids having different types of sugar head group and length of chain branching. (a) 2-ethyl hexyl-α-D-mannoside, (b) 2-butyl-octyl-β-D-xyloside and (c) 2-octyl-dodecyl-β-D-maltoside. Redrawn from (Liew et al., 2015; Patrick et al., 2018; Saari et al., 2018).	23
Figure 2.18	Two parallel plates confining a sample. Redrawn from (Barnes et al., 1989).	24
Figure 2.19	The flow curve (left) and viscosity curve (right) of Newtonian behaviour. Redrawn from (Barnes et al., 1989).	25
Figure 2.20	The flow curve (left) and viscosity curve (right) of (a) ideally viscous (b) shear thinning and (c) shear thickening flow behaviours. Redrawn from (Mezger, 2014).	26
Figure 2.21	The viscoelastic spectrum as a function of frequency (ω). [Reprinted (adapted) with permission from ref. (Mezzenga et al., 2005). Copyright 2005 Langmuir].	27
Figure 3.1	The chemical structure of 2-hexyl-decyl-β-D-glucoside (left) and 2-hexyl-decyl-β-D-maltoside (right) respectively.	32
Figure 3.2	An illustration of a (a) spinning nucleus where B is the magnetic field and (b) the two spin states of nucleus. Redrawn from (Wade Jr, 2013).	36
Figure 3.3	Illustration of shielding effect due to the presence of lone pairs in oxygen atom connected directly to the proton.	37
Figure 3.4	The schematic diagram of a nuclear magnetic resonance spectrometer, redrawn from (Günther, 2013).	38
Figure 3.5	Basic setup of a thermogravimetric analyser. Redrawn from (Haines, 2012).	39

Figure 3.6	Typical optical polarizing microscope instrument, redrawn from (Dimitruk & Davidson, 2013).	41
Figure 3.7	Sample preparation for thermotropic study.	42
Figure 3.8	Sample preparation for lyotropic study.	43
Figure 3.9	The configuration of SAXS instrument. Redrawn from (Zhang, Chen, et al., 2018).	44
Figure 3.10	Illustration of Bragg's Law. Redrawn from (Tyler et al., 2015).	45
Figure 3.11	The schematic drawing of parallel plate and cone plate. Redrawn from (Mezger, 2014).	48
Figure 4.1	^{1}H-NMR spectrum of β-Glc-$C_{10}C_6$. The coloured boxes marked on the spectrum to denote hydrogen in different chemical environments i.e. blue, $-CH_3$ groups; yellow, $-CH_2$ groups; red, –CH group and black, sugar head. The asterisk (*) represents the hydrogen atom at C-1 carbon position.	53
Figure 4.2	^{1}H-NMR spectrum of β-Mal-$C_{10}C_6$. The coloured boxes marked on the spectrum to denote hydrogen in different chemical environments i.e. blue, $-CH_3$ groups; yellow, $-CH_2$ groups; red, –CH group and black, sugar head. The red and purple coloured asterisk (*) represent the hydrogen atom at C-1 and C-1'carbon position, respectively.	54
Figure 4.3	^{13}C-NMR spectrum of β-Glc-$C_{10}C_6$. The coloured boxes marked on the spectrum to denote carbon in different chemical environments i.e. blue, $-CH_3$ groups; yellow, $-CH_2$ groups; red, –CH group and black, sugar head. The asterisk (*) represents the carbon in $-OCH_2$ group of the aliphatic chain the enlarged peaks are available in the appendix B.	55
Figure 4.4	^{13}C-NMR spectrum of β-Mal-$C_{10}C_6$. The coloured boxes marked on the spectrum to denote carbon in different chemical environments i.e. blue, $-CH_3$ groups; yellow, $-CH_2$ groups; red, –CH group and black, carbon in the sugar head. The asterisk (*) represents the carbon in $-OCH_2$ group of the aliphatic chain. The insets show magnified peaks of certain areas.	56
Figure 4.5	TGA and DTG thermograms of β-Glc-$C_{10}C_6$ and β-Mal-$C_{10}C_6$ at a heating scan rate of 5°C min^{-1}.	57
Figure 4.6	OPM textures of (a) H_2 of dry β-Glc-$C_{10}C_6$ ($\times$ 10); (b) L_α of dry β-Mal-$C_{10}C_6$ ($\times$ 10). The inset shows the coexistence of maltese cross (highlight white). The OPM micrograph of (c) V_2 of hydrated β-Glc-$C_{10}C_6$ ($\times$ 10); and (d) L_α of hydrated β-Mal-$C_{10}C_6$ ($\times$ 10) were obtained in water contact penetration scan. W denotes water and all textures were captured at room temperature.	59

Figure 4.7 SAXS patterns under thermotropic and lyotropic conditions at 30°C indicating (a) H_2 phase of dry β-Glc-$C_{10}C_6$; (b) L_α phase of dry β-Mal-$C_{10}C_6$; (c) inverse bicontinuous cubic phases of hydrated β-Glc-$C_{10}C_6$ and (d) L_α phases of hydrated β-Mal-$C_{10}C_6$. In (c) and (d) the various water concentrations of 30% (w/w), 50% (w/w) and 80% (w/w) are represented by bottom line, middle line top line, respectively. The corresponding lattice parameters are also reported in the figure. 62

Figure 4.8 Viscosity,η versus shear rate,$\dot{\gamma}$ for (a) H_2 phase of β-Glc-$C_{10}C_6$ and (b) L_α phase of β-Mal-$C_{10}C_6$ at selected temperatures. 66

Figure 4.9 Viscosity,η versus shear rate,$\dot{\gamma}$ for β-Glc-$C_{10}C_6$ at different water concentrations of (a) 30% (w/w), (b) 50% (w/w) and (c) 80% (w/w) and at selected temperatures. The inset shows the larger scale of shear-thinning behaviour for 80% (w/w) cubic *Ia3d* phase at 37°C. 67

Figure 4.10 Viscosity,η versus shear rate,$\dot{\gamma}$ for β-Mal-$C_{10}C_6$ at different water concentrations of (a) 30% (w/w) (b) 50% (w/w) (c) 80% (w/w) and at selected temperatures. The insets show the larger scale of shear-thinning behaviour at designated temperatures. 69

Figure 4.11 Storage modulus, *G'* and loss modulus, *G"* versus strain for (a) H_2 phase of β-Glc-$C_{10}C_6$ and (b) L_α phase of β-Mal-$C_{10}C_6$ at selected temperatures. 71

Figure 4.12 Storage modulus, *G'* and loss modulus, *G"* versus strain for β-Glc-$C_{10}C_6$ at different water concentrations of (a) 30% (w/w) (b) 50% (w/w) and (c) 80% (w/w) and at selected temperatures. 73

Figure 4.13 Storage modulus, *G'* and loss modulus, *G"* versus strain for β-Mal-$C_{10}C_6$ at different water concentrations of (a) 30% (w/w) (b) 50% (w/w) and (c) 80% (w/w) and at selected temperatures. 74

Figure 4.14 Storage modulus, *G'* and loss modulus, *G"* versus angular frequency, ω for (a) H_2 phase of β-Glc-$C_{10}C_6$ and (b) L_α phase of β-Mal-$C_{10}C_6$ at selected temperatures. The strain for H_2 phase and L_α phase is 0.24% and 0.32% respectively. 76

Figure 4.15 Storage modulus, *G'* and loss modulus, *G"* versus angular frequency, ω for β-Glc-$C_{10}C_6$ at different water concentrations of (a) 30% (w/w), (b) 50% (w/w) and (c) 80% (w/w) and at selected temperatures. 78

Figure 4.16 Storage modulus, *G'* and loss modulus, *G"* versus angular frequency, ω for β-Mal-$C_{10}C_6$ at different water concentrations of (a) 30% (w/w), (b) 50% (w/w) and (c) 80% (w/w) and at selected temperatures. 79

LIST OF TABLES

Table 2.1	Previous rheological studies on materials exhibiting liquid crystalline phases.	29
Table 4.1	Percentage yield of β-Glc-$C_{10}C_6$.	51
Table 4.2	Percentage yield of β-Mal-$C_{10}C_6$.	51
Table 4.3	Data of thermal degradation of β-Glc-$C_{10}C_6$ and β-Mal-$C_{10}C_6$.	58
Table 4.4	The transition temperature of thermotropic study obtained from OPM for both samples. The temperature measurement error is $\pm 1°C$.	60
Table 4.5	Phase assignments and lattice parameters at 30°C for β-Glc-$C_{10}C_6$ and β-Mal-$C_{10}C_6$ in dry and at selected water concentrations. The error in lattice parameter is ± 0.1 Å.	63
Table 4.6	The LVE region limit of H_2 phase of β-Glc-$C_{10}C_6$ and L_α phase of β-Mal-$C_{10}C_6$ at selected temperatures.	72

LIST OF EQUATIONS

Equation 2.1	Order parameter, S	7
Equation 2.2	Critical packing parameter, CPP	15
Equation 2.3	Shear rate, $\dot{\gamma}$	24
Equation 2.4	Shear stress, τ	24
Equation 2.5	Shear viscosity, η	24
Equation 2.6	Longest relaxation time, τ_{max}	27
Equation 3.1	Bragg's Law	44

LIST OF SCHEMES

Scheme 3.1 The reaction scheme for (a) glucoside and (b) maltoside synthesis. 33

LIST OF SYMBOLS AND ABBREVIATIONS

% (w/w)	:	Mass fraction
α	:	Alpha
β	:	Beta
CPP	:	Critical Packing Parameter
D-NMR	:	Deuterated Nuclear Magnetic Resonance
ΔH	:	Enthalpy
DTG	:	Derivative Thermogravimetry
e.g.	:	Example gratia; for example
et al.	:	et alia; and others
etc.	:	et cetera; and the others
G'	:	Storage moduli
G"	:	Loss moduli
Glc	:	Glucose
H_1	:	Normal hexagonal phase
H_2	:	Inverse hexagonal phase
h	:	Height
Iso	:	Isotropic phase
i.e.	:	id est; that is
L_α	:	Lamellar phase
Mal	:	Maltose
$\hat{n}$	:	Director axis
η	:	Shear viscosity
η'	:	Dynamic viscosity
N	:	Nematic phase

N*	:	Nematic cholesteric phase
NMR	:	Nuclear Magnetic Resonance
OPM	:	Optical Polarizing Microscopy
p	:	Pitch
S	:	Order parameter
SmA	:	Smectic A phase
SmC	:	Smectic C phase
SAXS	:	Small Angle X-ray Scattering
τ	:	Shear stress
τ_f	:	Yield stress
τ_{max}	:	Longest relaxation time
T_c	:	Clearing temperature
TGA	:	Thermogravimetric Analysis
T_g	:	Glass transition temperature
TLC	:	Thin Layer Chromatography
T_m	:	Melting temperature
v	:	Velocity
V_2	:	Inverse bicontinuous cubic phase
ω	:	Angular frequency
XRD	:	X-ray Diffraction
$\dot{\gamma}$	:	Shear rate

LIST OF APPENDICES

Appendix A	^{1}H-NMR Spectra	98
Appendix B	^{13}C-NMR Spectra	102
Appendix C	TGA and DTG Thermograms	106

CHAPTER 1: INTRODUCTION

1.1 Research Background

Glycolipids are one of the major components of the cell membrane. They are found on the outer layer of the membrane cell and they are crucial in cellular processes such as cell recognition and apoptosis (Kren & Martínková, 2001). For the past few years, glycolipids have emerged as a model for studying the cell membrane since they are important in regulating the bio membrane function (Dembitsky, 2004). Despite being studied extensively, certain topics involving glycolipids like the existence of glycosphingolipids in rafts are still debated for over a decade (Hakomori, 2008). Furthermore, new postulations such as lateral phase separation, the formation of lipid domains, lateral pressure and curvature elasticity of membranes have been recently discussed and proved imperative in comprehending the membrane stability (Zahid et al., 2013).

Glycolipids may be categorized as a single chain or branched chain, both of which can be synthesized in the laboratories. The general molecular structure of glycolipids comprises of sugar, linked to an alkyl chain by a linker as shown in Figure 1.1. A variety of glycolipids can be produced depending on their chemical structure design. The sugar head can be either mono-, di-, oligo- and polysaccharides such as xylose (Liew et al., 2015), galactose (Hashim et al., 2011), cellulose (George & Sabapathi, 2015) and maltotriose (Vill et al., 1989). It was demonstrated that the modification of the sugar head (e.g. galactose, mannose) in single and branched chain glycosides greatly changed their phase behaviour (Sakya & Seddon, 1997; Seddon et al., 2003). Moreover, most single chain glycosides exhibited only one phase which was smectic A (Vill & Hashim, 2002) as opposed to the numerous lamellar and non-lamellar phases exhibited by branched chain glycosides (Brooks et al., 2011; Hashim et al., 2006; Mannock & McElhaney, 2004). Ether (Vill et al., 2000) or ester (Liu et al., 1999) groups are usually chosen as linkers as

much as sulphur (Sakya et al., 1994) and amide (Attard et al., 1994) linkages. The phase behaviour is also governed by the length of the alkyl chain. For example, lengthening the alkyl chain has been shown to improve the thermal stability of single chained glycolipids (Karukstis et al., 2012) while increasing the alkyl chain length of branched chain glycosides will result in the formation of columnar phases (Hashim et al., 2006). In addition, unsaturation can also affect the physical properties of glycolipids. Curved phases are anticipated when the double bond is introduced in the molecule structure since the hydrophilic head group is smaller compared to the volume occupied by the hydrophobic tail group (Mannock & McElhaney, 2004; Yamashita et al., 2008).

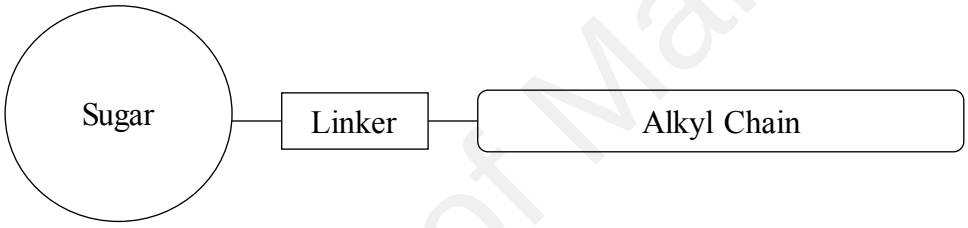

Figure 1.1: General molecular structure of a glycolipid.

1.2 Problem Statement

Glycolipids are amphiphiles which display liquid crystalline properties due to the de-mixing tendency of the polar and non-polar parts of the molecule (Hashim et al., 2006). The hydrophilic part comprises a sugar head group while the aliphatic hydrocarbon chain builds up the hydrophobic part of the molecule. The intermolecular interactions and self-assembly were thoroughly investigated to understand their phase behaviour. The structure-property relationship was immensely rationalized (Mannock & McElhaney, 2004; Vill et al., 1989; Vill & Hashim, 2002; von Minden et al., 2002) for instance, increasing the length of hydrocarbon tail leads to higher thermal stability in thermotropic and lyotropic phases (Boyd et al., 2000; Sakya & Seddon, 1997) since they have stronger Van der Waals interactions, thus greater energy is required to melt them.

In contrast to morphology studies, the report on rheological studies for all of the known liquid crystalline structures in the glycolipid system is limited. The viscoelastic and plastic (Pouzot et al., 2007) behaviour that controls their responses to stress are still in discussion. For instance, the shear study of cubic phase is predominantly challenging due to the mesophase possessing several relaxation mechanisms upon stress (Mezzenga et al., 2005). In addition, no specific rheological signature has been accepted for all known self-assembled nanostructures of surfactant–water binary system (Mezzenga et al., 2005). Furthermore, the availability of shear rheology for thermotropic glycolipid is sparse compared to the lyotropic. This is because glycolipid is hygroscopic thus fundamental studies on "dry" glycolipid is challenging (Hashim et al., 2018) but possible if precautionary steps were taken prior to measurement which was included in Chapter 3. To the our best knowledge, no viscoelastic study has been reported yet for the Guerbet glycolipids.

Additionally, the increase of environmental awareness has led to the demand for alternatives for the commercially available chemical surfactant. The attractive features of glycolipids such as low toxicity, biodegradability and surface activity made them a prime candidate as biosurfactant in the cosmetics and pharmaceutical industry (Misran et al., 2008). Furthermore, they have enormous potential in drug delivery systems (Chen et al., 2014). They also act as non-ionic surfactants that are used in the manufacturing of detergents, personal care products (von Rybinski & Hill, 1998), agrochemicals (Mnif & Ghribi, 2016), adhesives (van Thillo et al., 2002) and templating for nano-materials (Ji et al., 2005). Hence, it is important to evaluate their flow behaviour for commercial application to satisfy consumer demands. For instance, the viscosity test provide insights related to the internal structure of the material, thus offering understanding of their processability in large scale manufacturing. A general example to clarify the premise is that most personal care products (e.g. toothpaste, lotion, shampoo) require shear thinning

behaviour whereby increasing the shear rate (e.g. rubbing) will decrease its viscosity. If a toothpaste exhibits shear thickening behaviour that thicken instead of thinning upon rubbing, this would result in difficulty to spread it inside the mouth and cause unpleasant experience to the consumer. Hence, rheological study will allow the manufacturer to formulate the best texture by assessing the viscoelastic property and in turn, satisfy the consumer's request.

1.3 Objectives

The overall goal is to study the flow behaviour of liquid crystalline phases formed by synthetic glycolipids. The specific aims of this project are listed as follows:

a) To synthesize nature-like branched-chain glycolipids possessing different sugar head groups with identical tail group ($-C_{10}C_6$).
b) To identify and determine their thermotropic and lyotropic liquid crystalline phases.
c) To assess the rheological behaviour for the different liquid crystalline phases.

1.4 Research Scope

The scope of research was divided into two parts; the synthesis of branched chain glycolipids namely 2-hexyl-decyl-β-D-glucoside (β-Glc-$C_{10}C_6$) and 2-hexyl-decyl-β-D-maltoside (β-Mal-$C_{10}C_6$) followed by physico-chemical characterization of both compounds. Their physico-chemical analysis mainly focus on liquid crystalline phases characterization and rheological measurement in thermotropic and lyotropic conditions. In thermotropic study, the phase/flow behaviour changed with temperature while in the lyotropic study, the phase/flow behaviour changed with both temperature and solvent.

Synthetic glycolipids have been chosen in this study due to the difficulty to extract and purify natural glycolipids even though the latter is abundant in nature. The two types of glycolipids were synthesized using Lewis acid glycosidation method which is cost

effective and a well-established method (Hashim et al., 2006). β-anomer of both glucoside and maltoside are selected instead of α-anomer since the latter required doubled the amount of catalyst to produce satisfactory yield (Hashim et al., 2006). The purification process of α-anomer of glycosides is alsp considerably laborious (Wing & BeMiller, 1969).

Most natural glycolipids found in the cell membrane are double chained such as monogalactosyl diacylglycerol and digalactosyl diacylglycerol (both found in chloroplasts) (Metzler, 2003). Since natural glycolipids are difficult to be extracted and purified in large quantity, the naturally mimicking glycolipids are highly sought after especially in biophysical studies. In this project, the branched hydrophobic tail was made from Guerbet alcohol namely 2-hexyl-1-decanol. Generally, Guerbet alcohol contains two asymmetric chains which differ by two methylene units, and the two chains branch at the 2- or β-carbon position, which is also chiral. The chain branching makes the alcohol less volatile while the material remains as a liquid to a very low temperature and shows low irritation tendency (Hashim et al., 2018).

Over the past few years, numerous studies on the self-assembly of branched-chain glycolipids have been published especially in hydrated condition (Liew et al., 2015; Mannock & McElhaney, 2004; Patrick et al., 2018; Saari et al., 2018; Yamashita et al., 2008; Zahid et al., 2013). Understanding the phase behaviour of these compounds serve as a basis for the fundamental study of the cell membrane. In contrast to morphology studies, there has been a limited number of rheological studies for all of the known liquid crystalline structures in the glycolipid system. Thus, the quantification of their viscoelastic property enables the understanding of relaxation mechanism in their self-assemblies.

1.5 Thesis Outline

The thesis outline is divided into five chapters.

Chapter 1 represents a brief overview of the research background, problem statement and objectives of this project. The research scope is also narrowed down and through this chapter, the significance of the rheological study for glycolipids is also highlighted due to their potential to be utilized as surfactant in various industrial fields such as cosmeceutical and biotechnology.

Chapter 2, the literature review section briefly describes the glycolipids and liquid crystal theories. In this chapter, the fundamental of rheology is discussed in Section 2.3 onward. The literature review on rheological studies of relevant materials is also included in this chapter.

Chapter 3 focuses on the methodology to synthesize Guerbet glycolipids from glucose and maltose sugar. Then, followed by theory and principle of the techniques including nuclear magnetic resonance (NMR), thermogravimetric analysis (TGA), optical polarizing microscopy (OPM) and small-angle X-ray scattering (SAXS). Finally, the general principle of rheometry is also described.

Chapter 4 provides the results and discussion of this project. First, the thermal analysis was discussed followed by the physico-chemical characterization of the glycolipids. Next, their flow behaviour in thermotropic and lyotropic condition were elaborated which includes viscosity test, strain test, and frequency sweep.

Chapter 5 provides the conclusion and summary of the project which is outlined based on the research outcomes. Additionally, possible future study is also shortly discussed as a continuation of this project.

CHAPTER 2: LITERATURE REVIEW

2.1 Liquid Crystal

An Austrian scientist, Friedrich Reinitzer was the first one to report on the "double melting" phenomenon in the 19th century. He noticed that cholesterol acetate and cholesterol benzoate turned cloudy when heated. Upon further heating, they become clear. He also described that these cholesterol derivatives became coloured upon cooling. He later consulted a German physicist, Otto Lehmann who proceeded to characterize the phase under the polarizing microscope (Goodby & Gray, 1998). Together, they were both credited as the founder of liquid crystal with Lehmann suggested the term "liquid crystal" (Friedel, 1922).

Liquid crystal is an intermediate state of matter between the ordered solid state crystal and isotropic liquid (Dierking, 2003). Although they appeared to be liquid, they exhibit long-range order either position or orientation, or both (Ermakov et al., 2016). Thus, their appearance is liquid-like and yet, they behave like solid crystals. The compounds that exhibit liquid crystal phase are called mesogen and they tend to align in one common axis known as director ($\hat{n}$) as shown in Figure 2.1. To calculate the degree of orientational order present in a liquid crystal phase, order parameter, (S) is introduced in Equation 2.1.

$$\boldsymbol{S = \frac{1}{2} \langle 3\ cos^2 \theta - 1 \rangle} \quad \textbf{(Equation 2.1)}$$

where θ is the angle between the long axis of mesogen and the director ($\hat{n}$) while the angular bracket represents a statistical average of $cos^2 \theta$. When the order parameter value is equal to one ($S = 1$), the material is in solid crystal state. However, when the material is in the isotropic liquid state, the average value of $cos^2 \theta$, ($\langle cos^2 \theta \rangle$) becomes $\frac{1}{3}$. This makes the order parameter to become zero ($S = 0$). Hence, liquid crystals will have orientational order parameter varies between zero and one i.e. $0 < S < 1$. Several

instrumentation methods can be used to determine the order parameter such as X-ray Diffraction (XRD) or deuterium nuclear magnetic resonance (D-NMR) (Meier et al., 2012).

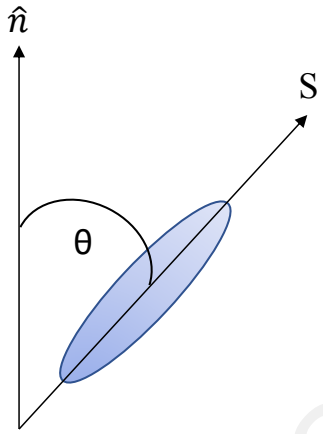

Figure 2.1 : Schematic drawing of the alignment of mesogen.

Typically, for a compound to qualify as liquid crystal, they must have a rigid π-electrons system with a flexible long alkyl chain, also known as the spacer. The rigid core cannot possess liquid crystalline property by itself. Hence the addition of a flexible spacer will further assist in the formation of liquid crystal. Various substitutions can be applied to the molecular structure to acquire the different types of liquid crystal phase, also known as mesophase. For example, Thaker et al. (Thaker et al., 2010) reported the difference in melting point, mesophase stability and wider liquid crystalline phase range when naphthalene was used as the rigid core compared to phenyl. The presence of a lateral group ($–CH_3$) in phenyl structure caused a change in the molecular structure and broadening of the molecule. Hence, the transition temperature was lowered for all phases. The general molecular structure of a typical mesogen is depicted in Figure 2.2.

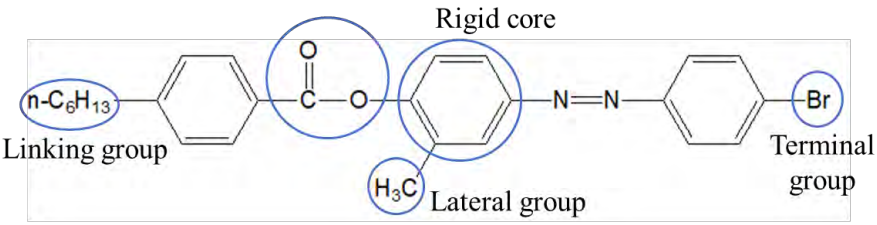

Figure 2.2 : The general molecular structure of a mesogen.

Certain mesogens may or may not exhibit melting temperature, T_m which is the transition temperature from crystal solid to liquid crystal. When heated, the liquid crystal phase turns to isotropic liquid and this transition temperature is termed as clearing temperature, T_c (see Figure 2.3). There are two main classes of liquid crystals namely thermotropic and lyotropic liquid crystals. Additionally, some mesogens are called amphitropic liquid crystal in which they can self-assemble in both dry or solvated conditions (Hashim et al., 2012).

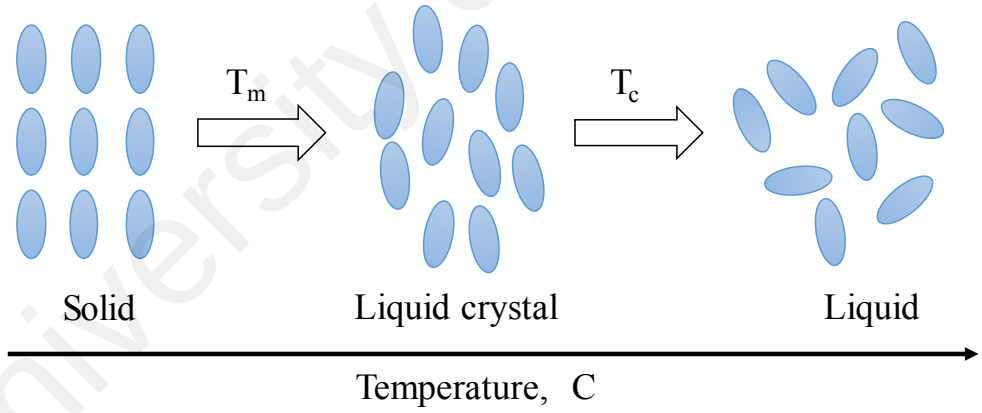

Figure 2.3 : Phase transition from solid to liquid crystal to liquid on heating. Redrawn from (Vertogen & de Jeu, 2012).

2.1.1 Thermotropic Liquid Crystal

According to IUPAC (Barón, 2001), thermotropic mesophase is formed by heating a solid or cooling an isotropic liquid, or by heating or cooling a thermodynamically stable mesophase. In short, the mesophase is influenced by temperature change. The type of

mesophase formed is strongly affected by the molecular structure of the mesogen. There are two types of molecular structures found in liquid crystals that will be discussed in the next section.

Monophilic Liquid Crystals

Monophilic liquid crystals can be characterized by the simple shape of the mesogenic compound. The simplest and most common liquid crystal phase is the nematic phase (N) which arises from the rod-shaped (calamitic) molecule. This phase possess long-range orientational yet no positional order. An example of mesogen with nematic phase is *p-n*-Hexyl-*p'*-cyanobiphenyl as shown in Figure 2.4. The widely known application of nematic liquid crystals (often in a twisted form) is the liquid crystal display (LCD) in which the weakly aligned director ($\hat{n}$) is manipulated using electric effect and their optical property (Hoogboom et al., 2006).

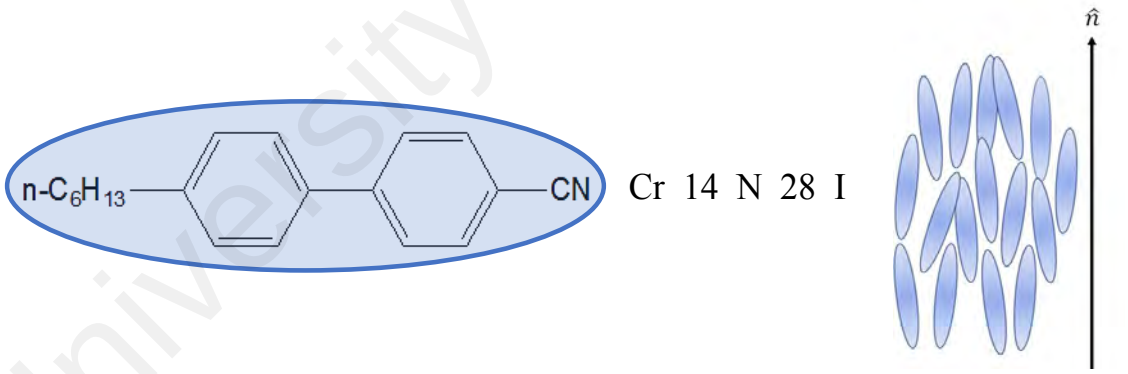

Figure 2.4 : The chemical structure of *p-n*-Hexyl-*p'*-cyanobiphenyl (left) and molecular arrangement of nematic phase (right) together with their liquid crystal phase behaviour. Cr, N and I stand for crystal, nematic and isotropic phase respectively. Redrawn from (Jákli & Saupe, 2006) and (Dierking, 2003).

When calamitic molecules possesses both orientational and positional order, they form the smectic phase. This phase is still fluid-like yet they tend to position themselves in layers. There are many types of smectic phase depending on the extent and the nature of ordering (Sengupta, 2013), however the most common phases are smectic A (SmA) and

smectic C (SmC). In SmA mesophase, the director ($\hat{n}$) is parallel to the layer normal. In SmC mesophase, the molecular arrangement is identical to SmA but the director ($\hat{n}$) is tilted away from the layer normal (Jákli & Saupe, 2006). The schematic drawing of SmA and SmC is shown in Figure 2.5.

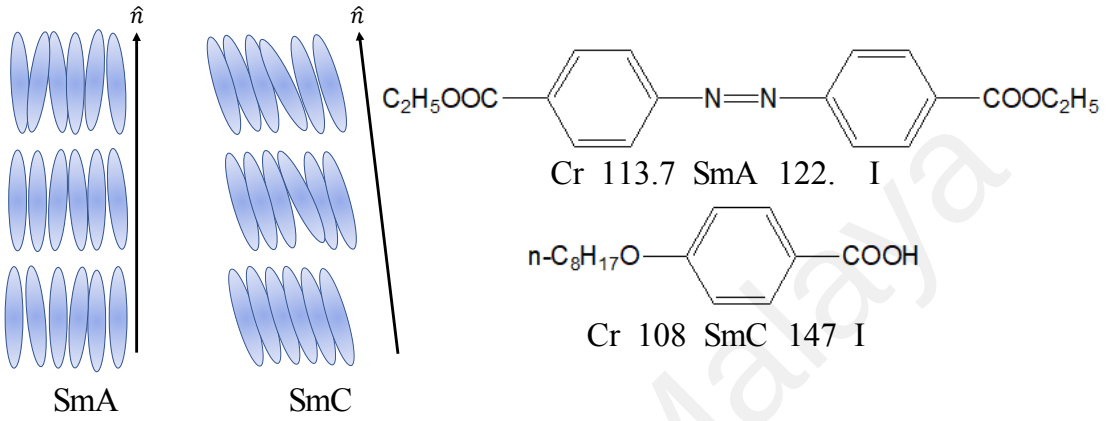

Figure 2.5 : Schematic drawing (left) and example of compounds showing smectic phases (right) together with their liquid crystal phase behaviour. Cr, SmA, SmC and I stand for crystal, smectic A, smectic C and isotropic phase respectively. Redrawn from (Demus et al., 2011) and (Jákli & Saupe, 2006).

Cholesteric phase (N*), also known as chiral nematic phase is a different form of the nematic phase. They may be found right before the isotropic phase temperature (Vertogen & de Jeu, 2012). The formation of chiral nematic is possible when the mesogen contains a chiral centre whereby the director ($\hat{n}$) twist around an axis that is perpendicular to the long molecular axis like cholesteryl benzoate (Dierking, 2014) as shown in Figure 2.6. Pitch (p) is the distance at which the director makes a 360° turn.

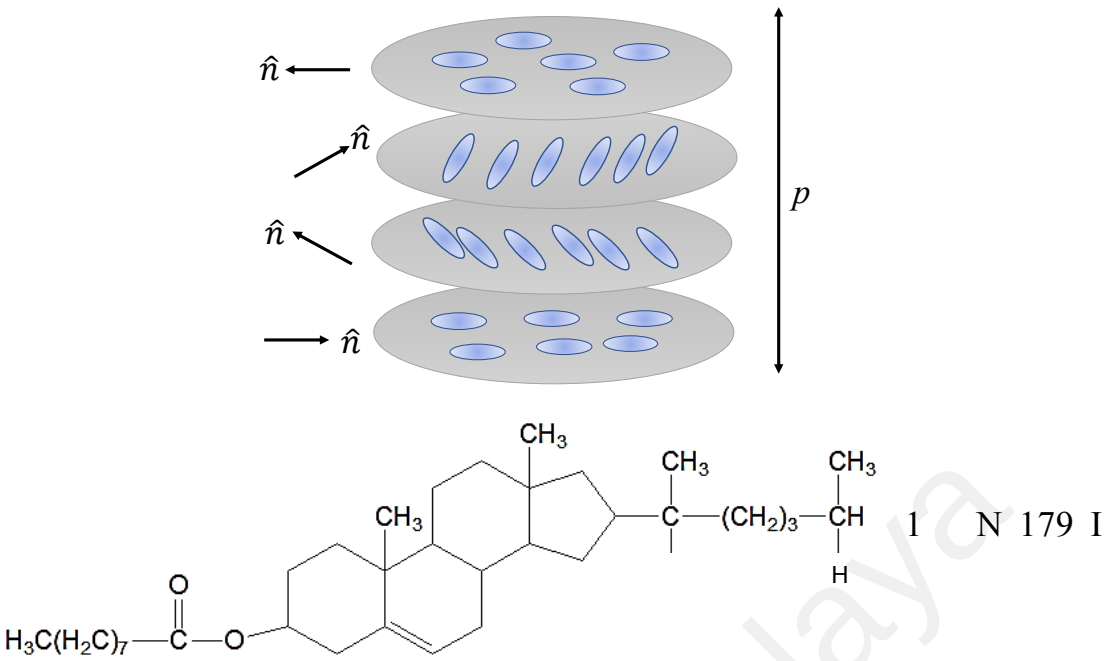

Figure 2.6 : The molecular arrangement of the chiral nematic phase (top). Redrawn from (Yu et al., 2018), and chemical structure of cholesteryl benzoate (bottom) together with their liquid crystal phase behaviour. Cr, N and I stand for crystal, nematic and isotropic phase respectively. Redrawn from (Jákli & Saupe, 2006).

Discotic liquid crystals are formed by disc-shaped mesogen, often stacking over one another to form columns. The term "discotic" actually refers to the shape of the mesogen instead of the mesophases and it can either be columnar or nematic (Demus et al., 2011) though the former is more favourable than the latter (Sengupta, 2013). The mesogen commonly has long aliphatic substituents (alkyl or alkoxy) surrounding the flat cores, which frequently comprise of the aromatic ring (see Figure 2.7).

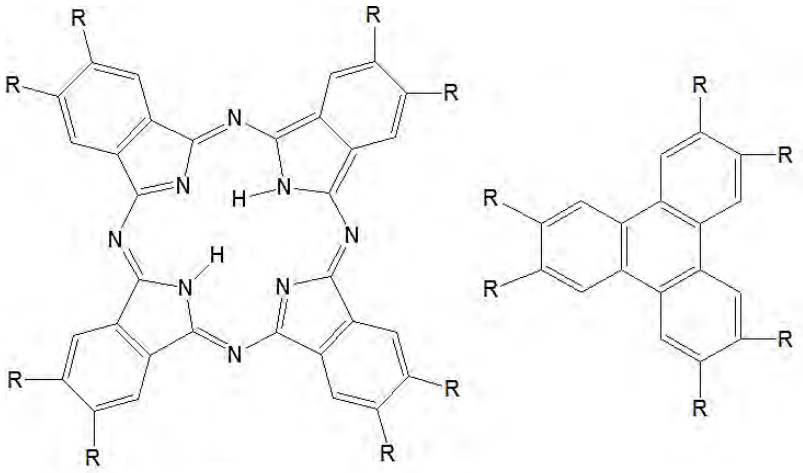

Figure 2.7 : Examples of discotic mesogens. (a) Phthalocyanine and (b) triphenylene. Redrawn from (Bushby & Lozman, 2002).

The simplest mesophase formed by the disc-shaped mesogen is the nematic (N_D) phase. This phase is the least ordered and in a way similar to the nematic phase of rod-shaped (calamitic) mesogen except that it is optically negative (Chandrasekhar & Ranganath, 1990). In columnar phase (Col), the mesogen may organize in several modes of stacking such as hexagonal, rectangular and oblique (see Figure 2.8). Interestingly, certain columnar liquid crystals are considered as 1D fluid since they are fluid-like along the columns yet solid-like in a two-dimensional array of columns (Jákli & Saupe, 2006).

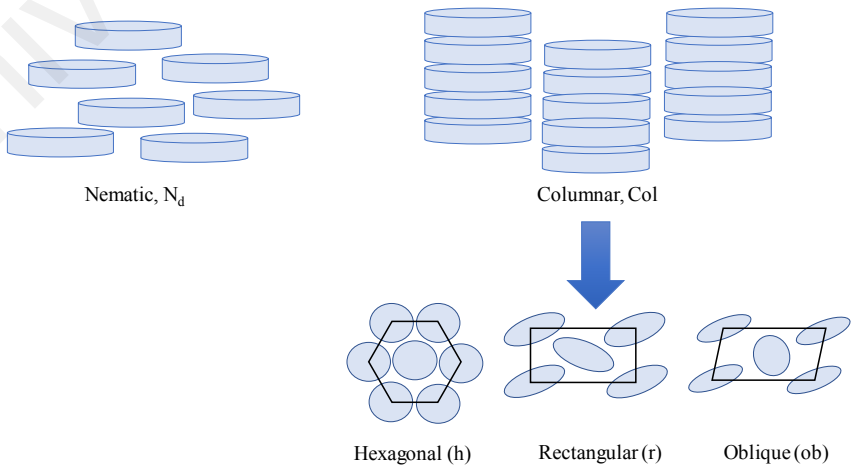

Figure 2.8 : Schematic drawing of discotic liquid crystal phases. Redrawn from (Jákli & Saupe, 2006) and (Bushby & Lozman, 2002).

In addition, they form chiral discotic liquid crystals when a chiral centre is incorporated within the discotic mesogen or in a mixture of discotic nematic and chiral dopants (Langner et al., 1995). For this mesophase, the director moves in a helical fashion similar to the chiral nematic phase.

Amphiphilic Liquid Crystals

Amphiphilic mesogens consist of two incompatible molecular parts, i.e. hydrophilic and hydrophobic parts which are present within a molecule. Hence, they exhibit microphase separation and creates amphiphilic liquid crystals (Vill & Hashim, 2002). Glycolipids are one of many examples of amphiphilic liquid crystals in which the hydrophilic sugar molecule (polar) is attached to the hydrophobic aliphatic alkyl chain (non-polar). The mesophase formed is influenced by the molecular shape of the amphiphiles as shown in Figure 2.9.

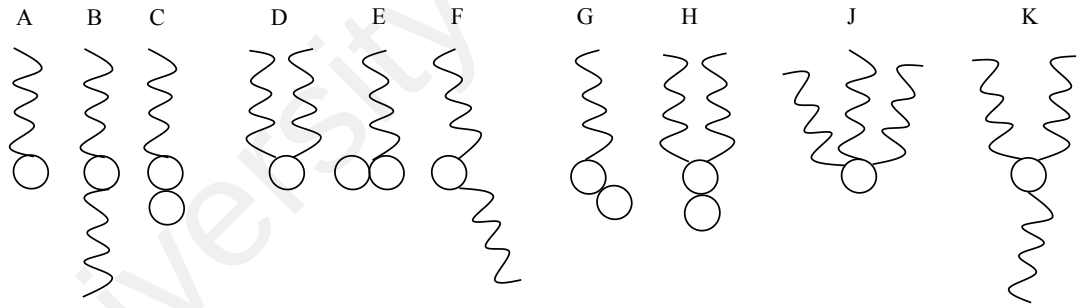

Figure 2.9 : The different molecular shape design of glycolipids. Redrawn from (Vill & Hashim, 2002).

A, B, and C are expected to form the smectic phase resulting from the elongated shape of the mesogens. D and E have pie-shaped and forked mesogen respectively, while F is non-linear dialkylated sugar, all of which prefer to form the hexagonal columnar phase. Next, the mesophase of banana-shaped amphiphiles, G and elongated fork, H is situated at a borderline between lamellar and columnar phase with the possibility of forming

bicontinuous cubic phase. J has a cone-shaped mesogen and is able to form the discontinuous cubic phase. Lastly, K has dissymmetric star-like amphiphiles that makes the formation of rectangular and tetragonal columnar phase possible. Besides that, star-like mesogen tends to form columnar phase (Vill & Hashim, 2002).

2.1.2 Lyotropic Liquid Crystal

A mesomorphic compound that could form a liquid crystal phase by both temperature and solvent effects is known as lyotropic liquid crystals. Mesogen that exhibits lyotropic liquid crystals are mostly amphiphiles and sometimes oils (Jákli & Saupe, 2006). The schematic drawing of an amphiphilic molecule is depicted in Figure 2.10 in which the water loving part (hydrophilic head) will readily solvate when the solvent (usually water) is introduced into the system. Consequently, this induces fluidity in the binary system due to water filling in the void space around the liquid crystal molecules (Liang et al., 2005).

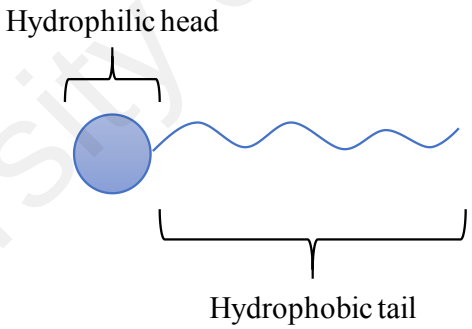

Figure 2.10 : The schematic drawing of amphiphilic molecule. The hydrophilic and hydrophobic parts have different affinity towards the solvent. Redrawn from (Vill & Hashim, 2002).

Generally, the type of mesophase formed by an amphiphile can be predicted from the critical packing parameter as proposed by Jacob Israelachvili (Israelachvili, 1994). The equation is given in Equation 2.2.

$$CPP = \frac{v}{a_o l_c} \qquad \textbf{(Equation 2.2)}$$

where v is the volume of the hydrophobic chain, a_o is the interfacial area occupied by the hydrophilic group and l_o is the length of the hydrocarbon chain. The normal structure is anticipated when the CPP is less than one (CPP<1). Conversely, CPP greater than one (CPP >1) will give the inverse structure. For non-lamellar phases, the lyotropic nomenclature distinguishes the normal and the inverse structures with the subscripts 1, and 2 respectively. It has been reported that the incorporation of bulky chain will instigate the formation of inverse structures such as inverse bicontinuous cubic and inverse hexagonal phases (Hashim et al., 2012).

Lyotropic liquid crystals have prevalent application due to their self-assembly compatibility with the living systems such as the possibility of gene therapy that utilizes the lyotropic lamellar phase of DNA complexes and cationic liquids (Rädler et al., 1997). Since ~40% of commercial drugs are poorly water soluble (Williams et al., 2013), several attempts have been made to use the lyotropic liquid crystals in the drug-delivery system (Kazemi et al., 2018; Müller-Goymann, 2004). In addtion, they are also used in consumer products such as surfactants in the cosmeceutical industry (Misran et al., 2008).

Three common types of lyotropic mesophases are lamellar, hexagonal and cubic phases. In the lamellar mesophase, the mesogens are usually separated by the water solvent (Singh & Dunmur, 2002). Similar to the biological cell membrane, the amphiphilic molecules position themselves in such a way that the polar head is in contact with the water while the non-polar tail avoids the water. The double layer is usually smaller than twice the amphiphilic molecule length while the bilayer and water layer thickness values are influenced by the temperature and amount of water content in the system. The layers can slide over each other easily, making it the most liquid-like mesophase over the other lyotropic phases. Figure 2.11 shows the schematic drawing of the lamellar phase.

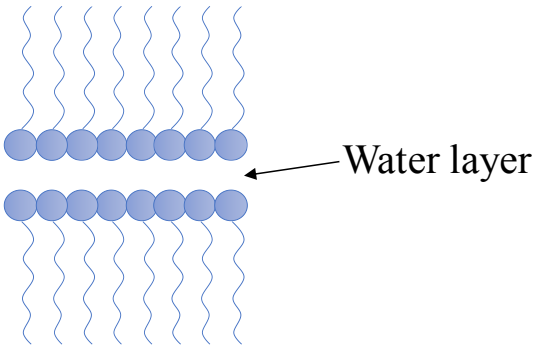

Figure 2.11 : The schematic drawing of lamellar phase. Redrawn from (Singh & Dunmur, 2002).

The hexagonal phase corresponds to the hexagonal arrangement of the molecular aggregate (see Figure 2.12). The water-continuous, normal hexagonal phase (H_1) is more common compared to the inverse hexagonal phase (H_2) which is alkyl chain-continuous. The normal hexagonal phase usually has a larger diameter compared to the inverse hexagonal phase because of the overlapping of the non-polar chain in the latter which results in a closer-packed cylinder (Fairhurst et al., 1998).

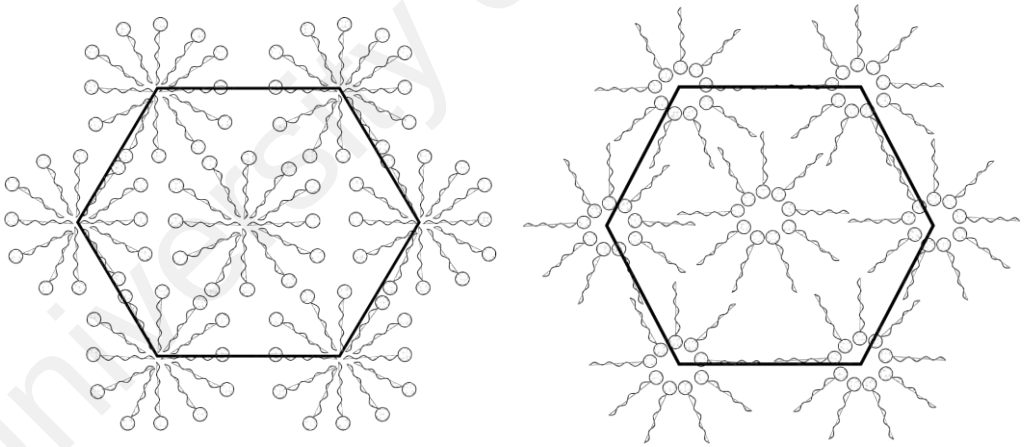

Figure 2.12 : The schematic drawing of normal hexagonal (left) and inverse hexagonal (right) phase. Redrawn from (Collings & Hird, 1997).

The cubic phase is also known as the viscous isotropic phase because they are optically isotropic. Furthermore, they are often observed at low curvatures and are extremely viscous when compared with lamellar and hexagonal phases. The cubic phase structure consists of the bicontinuous lipid bilayer that is curved and extends in three dimensions,

separating two identical networks of water channel (Shah et al., 2001). The cubic liquid crystalline texture appeared black under the optical polarizing microscope since they exhibit cubic symmetries (Hyde, 2001) and sometimes overlooked under the polarizing microscope because they appeared similar to the isotropic phase (Collings & Hird, 1997). Three fundamentals triply periodic minimal (TPMS) namely primitive (P), Schwarz diamond (D) and Schoen gyroid (G) minimal surfaces are the basis of cubic phase. Based on these three surfaces, three bicontinuous mesophases are established; the most common is gyroid (*Ia*3*d*), followed by diamond (*Im*3*m*) and primitive bicontinuous mesophase (*Pn*3*m*) as shown in Figure 2.13.

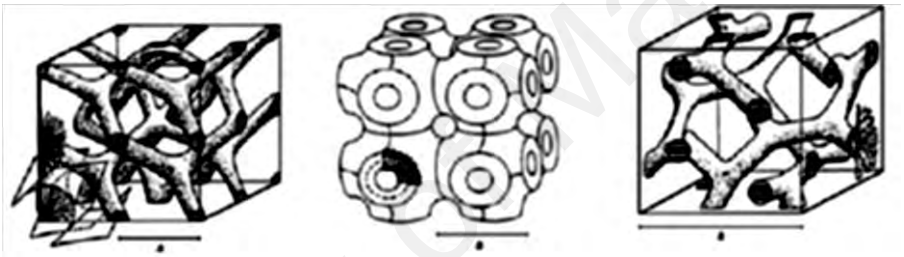

Figure 2.13 : The schematic diagram of the bicontinuous cubic phases. From left to right; *Pn*3*m*, *Im*3*m* and *Ia*3*d*. [Reprinted (adapted) with permission from ref. (Hashim et al., 2011). Copyright 2011 Elsevier].

Recently, the cubic phase is gaining headlines for being potentially used in sustained drug release matrix due to their highly ordered nanostructures (Chen et al., 2014). For example, It has been reported that a wide range of drugs have shown controlled release in cubic phases such as insulin (Sadhale & Shah, 1999), vitamin E and aspirin (Wyatt & Dorschel, 1992). Lipids are often used to form the cubic phase (Chen et al., 2014) due to their environmentally friendly features. One of the possible lipid candidates is glycolipids.

2.2 Glycolipid

The IUPAC definition of glycolipids are compounds containing at least one monosaccharide moieties bound by a glycosidic linkage to a hydrophobic moiety (Lafiandra et al., 2012). Glycolipid is abundant in nature and crucial in most living organisms performing function such as cell recognition and membrane fusion (Goodby, 1998). This membrane component is also related to various diseases for example, the defects in the catabolism of glycosaminoglycans cause a rare lysosomal disease generally known as mucopolysaccharidoses (Heywood et al., 2015). Another example is Gaucher disease which is an autosomal recessive disorder that occurs when glucocerebroside accumulates in the kidney and spleen. The disease was caused by the deficiency of glucocerebrosidase, an enzyme that catalyses the hydrolysis of glucocerebroside to ceramide and glucose (Hruska et al., 2008). This demonstrates the importance and effect of glycolipids in the human body. Thus, this section will discuss glycolipids in nature followed by the demand for synthetic glycolipids.

2.2.1 Natural Glycolipid

Several types of glycolipids can be found in nature namely glycosphingolipids, glycoglycerolipids, and glycosyl phosphopolyprenols. Glycosphingolipids have a carbohydrate moiety that is covalently bonded to the sphingoid bases such as dihydrosphingosine. It is commonly found in mammalians and also microorganisms, particularly in the nerve tissues and brain. They can be further divided into three main classes which are cerebrosides, globosides, and gangliosides (Goodby, 1998). Research has shown that the natural killer T (NKT) cells, a type of lymphocyte involved in the immune system were able to recognize *Sphingomonas*, a glycosphingolipids from gram-negative bacteria that is abundant in our environment (Kinjo et al., 2005).

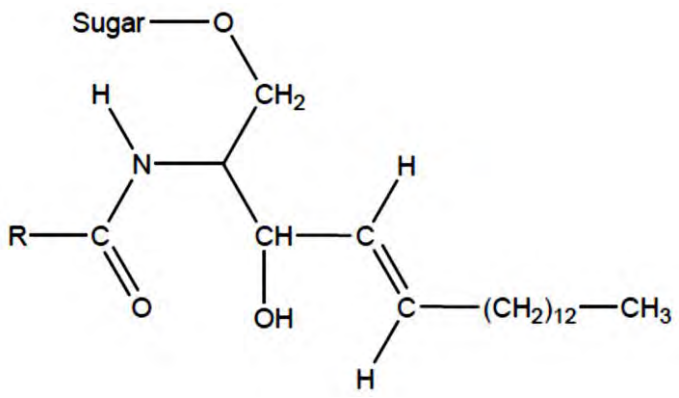

Figure 2.14 : The general structure of glycosphingolipids. R indicates the long fatty acid chain. Redrawn from (Vill & Hashim, 2002).

Glycoglycerolipids have 1,2-di-*O*-acyl-*sn*-glycerols joined by a glycosidic linkage at the position *sn*-3 to a sugar head (Vill et al., 1989). It is highly abundant in cyanobacterias, chloroplast in plants and eukaryotic algae. For example, monogalactosyl diacylglycerol (MGDG) is a galactolipid that can be found on photosynthetic thylakoid membranes which is critical for the plants growth in a phosphate limiting environment.

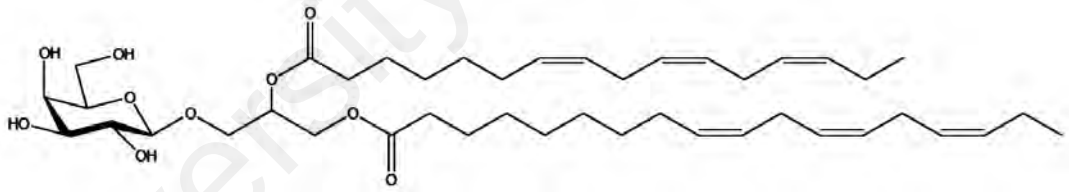

Figure 2.15 : The structure of monogalactosyl diacylglycerol (MGDG).

Glycosyl phosphopolyprenols are biochemically unique compared to the other glycolipids due to the sugar linkage by a phosphate bridge with the lipid. Moreover, this lipid originated from a completely separate biosynthetic route than the others. Their biosynthesis are partially shared with the pathway that leads to sterols and polyisoprenoidquinones. Hence, they are known as lipid-linked intermediate because they supply glycosyl residues to the suitable acceptors whereas glycolipids are seen as

intermediates and acceptors of further sugar residues or metabolism end products (Hemming, 1985).

Although glycolipids are abundant in nature, the extraction, purification, and total synthesis are proven difficult (van Boeckel & van Boom, 1980; van Boeckel et al., 1981). Despite that, the extraction of natural glycolipids is possible and has been reported before. For example, a research group had isolated the naturally branched chain glycolipids known as simplexide from Caribbean marine sponges *'Plokartis Simplex'* (Costantino et al., 1999). However, synthetic glycolipids are still preferred as a medium to study the natural glycolipids since they can be produced on a large scale using a relatively economic procedure (Vill et al., 1989).

2.2.2 Synthetic Glycolipid

Synthetic glycolipids can be categorized into two types i.e. single chain and branched chain. The single chain glycolipids form a class of surfactants known as sugar-based surfactants. Common examples include sucrose ester, sorbitan ester and alkyl polyglucosides (APGs). Some of their chemical structures are shown in Figure 2.16. The most widely-used and known sugar-based surfactant is alkyl polyglucosides which have been commercially utilized in the industries such as lubricants for water (Sułek et al., 2013). It is also used as a nonionic surfactant in household products such as detergent and soaps because they are less toxic, environmentally friendly and biodegradable (Ferrer et al., 2002; Sadtler et al., 2004). They are slightly different from the usual chemical surfactant since their self-assembly is governed by the hydrogen-bonding network between the sugar moieties (Imura et al., 2007). However, since they have single chains, they exclusively form the lamellar phase in dry condition (Vill & Hashim, 2002) which limits their range of liquid crystalline phases, resulting in limited ability to form curved interfaces such as hexagonal phase (Nguan et al., 2010).

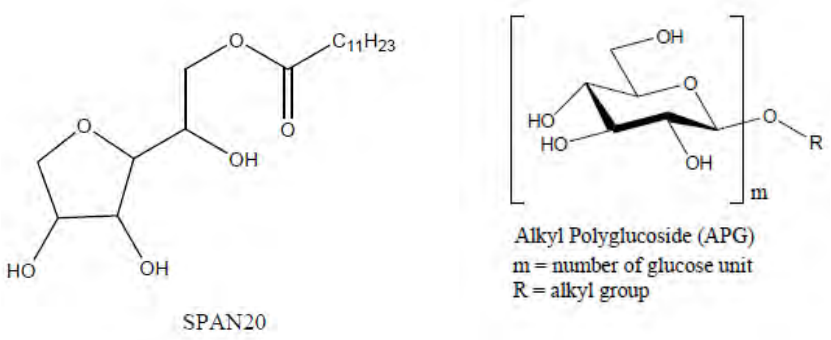

Figure 2.16 : Examples of single chain glycolipids, sorbitan ester (left) and alkyl polyglucoside (right). The number of glucose units, m usually consists of one to five glucoside parts (Sułek et al., 2013). Redrawn from (Iglauer et al., 2010) and (Sułek et al., 2013).

To overcome this limitation, synthetically produced branched chained glycolipids have been gaining interest due to their similarities to natural glycolipids. A relatively new synthesis design (Hashim et al., 2006) has been described recently using Guerbet alcohol as the starting material. The term Guerbet comes from Marcel Guerbet who pioneered the Guerbet chemistry in the 1890s (O'Lenick Jr, 2001). With this method, various glycolipids with different sugar headgroups and branched chain lengths can be synthesized (see Figure 2.17). For example, the phase behaviour of a series of Guerbet *β*-D-xylosides, glucosides and maltosides have been reported recently (Brooks et al., 2011; Liew et al., 2015; Saari et al., 2018). Besides, the nano-structured self-assembly of *β*-dominant (~90%) anomeric mixtures of Guerbet glucoside and maltoside have also been studied for its potential application in drug delivery and release (Ahmad et al., 2012).

Compared to the lyotropic glycolipids, there is no known application for thermotropic glycolipids (Hashim et al., 2018) due to the hygroscopic nature of sugar and thus, the usage of dry glycolipids for consumers are limited and challenging to be implemented. However, studies on thermotropic glycolipids have showed the presence of ferroelectric property (Vill et al., 1988) and the existence of a tilted bilayer organization

(Abeygunaratne et al., 2006). Hence, no knowledge left unused because the research on dry glycolipids self-assemblies will subsequently lead to the lyotropic study that is related to the biological system, which in return may lead to a possible nature-like innovations (Patrick et al., 2018).

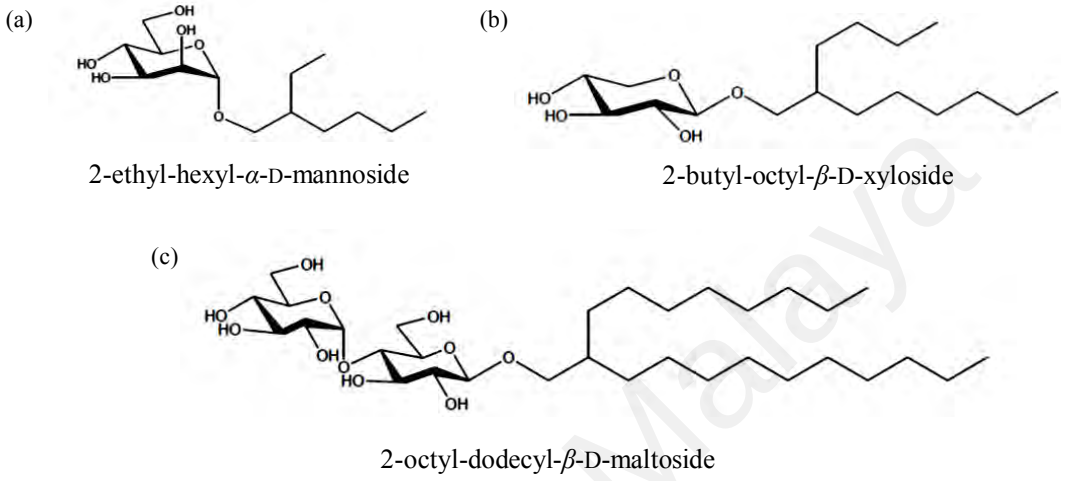

Figure 2.17 : The chemical structures of a few Guerbet glycolipids having different types of sugar head group and length of chain branching. (a) 2-ethyl hexyl-*α*-D-mannoside, (b) 2-butyl-octyl-*β*-D-xyloside and (c) 2-octyl-dodecyl-*β*-D-maltoside. Redrawn from (Liew et al., 2015; Patrick et al., 2018; Saari et al., 2018).

2.3 Rheology

To extend the application of glycolipids, the rheological study is essential in gaining insight into the flow behaviour of the different liquid crystalline phases formed. The term rheology was introduced by E. C. Bingham of Lafayette College with the advice of his colleague and defined as a study of flow and deformation of materials (Barnes et al., 1989). Later in 1929, the definition was widely used when the American Society of Rheology was established. The emergence of the rheology study is recent but rapid due to the discovery of the viscoelastic property of flamethrowers during the World War (Barnes et al., 1989). Since then, rheology has been applied to many fields such as pharmaceuticals, food industries, biotechnology and even daily items such as the toothpaste.

2.3.1 Fundamental Rheological Variables

The description of the fundamentals rheological variables can be explained by a sample confined between two parallel plates as shown in Figure 2.18.

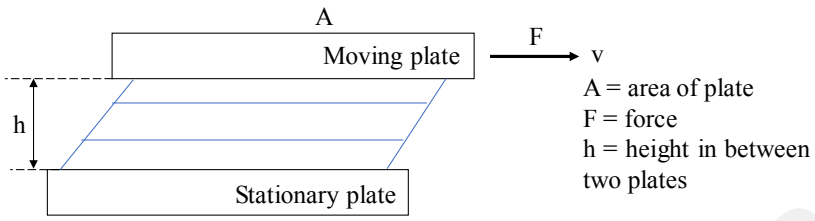

Figure 2.18 : Two parallel plates confining a sample. Redrawn from (Barnes et al., 1989).

When a sample is sandwiched between the two plates where one is moving at velocity, v while one is stationary, it creates a velocity gradient also known as shear rate, $\dot{\gamma}$. It describes how fast the sample is made to flow in s^{-1} and is represented by Equation 2.3.

$$\dot{\gamma} = \frac{v_{top} - v_{bottom}}{h} = \frac{v}{h} \qquad \textbf{(Equation 2.3)}$$

On the other hand, shear stress, τ is the force that causes the sample to flow. It is the force needed to move the plate divided by the area of the moving plate (Equation 2.4).

$$\tau = \frac{Force}{Area} = \frac{Newton}{m^2} = Pa \qquad \textbf{(Equation 2.4)}$$

Shear viscosity, η is defined as the fluid's internal resistance to flow and is equal to shear stress divided by shear rate in Equation 2.5.

$$\eta = \frac{Shear\ stress, \tau}{shear\ rate, \dot{\gamma}} = \frac{Pa}{s^{-1}} = Pa.s \qquad \textbf{(Equation 2.5)}$$

For most samples, a certain minimum force needs to be exerted for the sample to flow. The minimum force is called yield stress, τ_f. It is usually obtained by extrapolating the flow curve in a graph of shear stress versus shear rate.

2.3.2 Newtonian and Non-Newtonian Behaviour

Under rheology, there is a sub-field known as viscometry. This field gives information on the ability of the material to flow. Scientifically, viscosity is defined as the measure of internal resistance of the fluid to flow (Mezger, 2006). The viscosity can be calculated by using Equation 2.5 and although it is dependent on shear rate, it is also affected by physical properties such as temperature, pressure, and time. Upon testing, the fluids can be categorized as having Newtonian or non-Newtonian behaviour.

Newtonian Behaviour

A material is considered as an ideally viscous fluid or Newtonian behaviour when the shear stress produced is proportional to the increase in shear rate while the viscosity is independent of the shear rate as shown in Figure 2.19. Some examples of fluids with Newtonian behaviour is water and silicone oil. Any fluids that deviate from this behaviour is considered as non-Newtonian fluid.

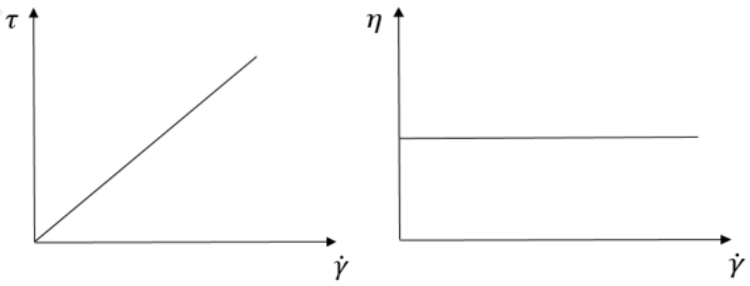

Figure 2.19 : The flow curve (left) and viscosity curve (right) of Newtonian behaviour. Redrawn from (Barnes et al., 1989).

Non-Newtonian Behaviour

When a material has shear thinning behaviour, the viscosity decreases with increasing shear rates. This is also called as pseudoplastic behaviour in which the particle size and its flow orientation can be changed when a force is act upon it. For instance, pseudoplasticity was observed in depectinized fruits juices when they were heated (Saravacos, 1970). The opposite of pseudoplasticity is dilatancy in which a material exhibits shear thickening behaviour and hence, they are called dilatant material. This type of behaviour is generally undesirable since it can cause blockage in pipe systems in which the viscosity of the material increases as the shear rate increases. Despite that, dilatant material has the potential to be employed in body armour (Ding et al., 2013; Li et al., 2008).

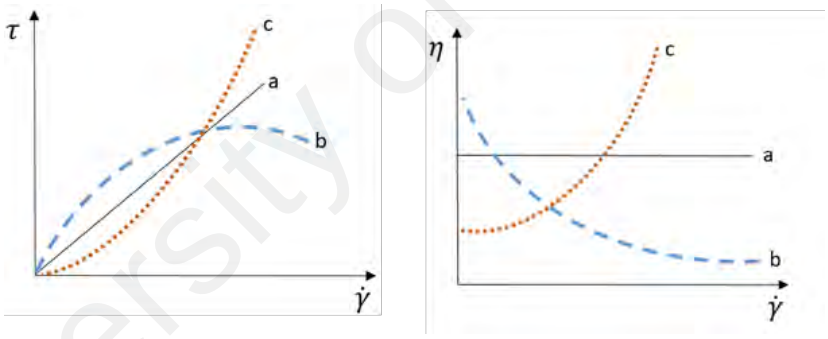

Figure 2.20 : The flow curve (left) and viscosity curve (right) of (a) ideally viscous (b) shear thinning and (c) shear thickening flow behaviours. Redrawn from (Mezger, 2014).

2.3.3 Viscoelasticity

It is common for a material to exhibit a mixture of viscous and elastic behaviour when a small deformation is applied, also known as viscoelasticity. Typically, this property is represented in the viscoelastic spectrum as shown in Figure 2.21 and the frequency scan is preferred than the temperature scan since it gives detailed information and illustrates the viscoelasticity of the liquid crystalline phases (Mezzenga et al., 2005).

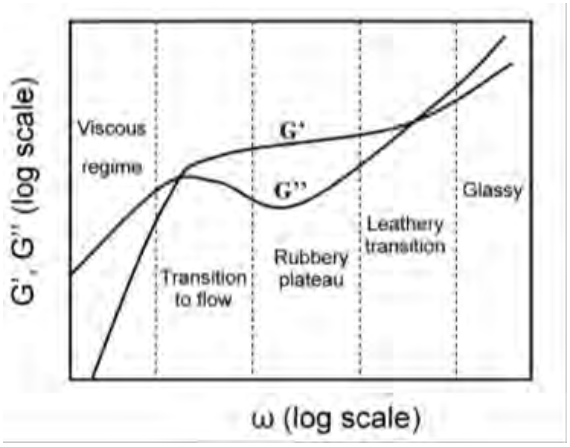

Figure 2.21 : The viscoelastic spectrum as a function of frequency (ω). [Reprinted (adapted) with permission from ref. (Mezzenga et al., 2005). Copyright 2005 Langmuir].

To describe the material behaviour, storage modulus or *G'* is used to indicate the solid-like portion at any frequency while loss modulus or *G"* is used to indicate the liquid-like portion. The *G'* and *G"* data can be represented in several different ways by rheometer such as the loss tangent (tan δ) and dynamic viscosity (η') but *G' G"* is preferred since they contain extra information that is unavailable in the former. The spectrum above is divided into five regions where the behavioural changes are affected by the values of *G' G"* as the frequency increases.

At low frequency, *G"* has a higher value than *G'* which indicates that the superior behaviour is viscous. Both *G'* and *G"* steadily increase as the frequency increases where at one point *G'* will surpass *G"*. The longest relaxation time, τ_{max} can be calculated using Equation 2.6 by taking the crossover value between *G'* and *G"*.

$$\boldsymbol{\tau_{max} = \frac{1}{\omega}} \qquad \textbf{(Equation 2.6)}$$

The longest relaxation time is defined as the time at which the structured fluid relaxes back to its equilibrium configuration when perturbed (Mezzenga et al., 2005). When the

frequency approaches $1/\tau_{max}$, the material behaves like a viscoelastic material rather than fluid-like. Above that, the material exhibits rubbery behaviour as *G'* becomes dominant and *G"* may consistently decrease to a minimum before it starts increasing again. Then at the leather transition region, *G"* will once again dominate after a second crossover. Lastly, at extremely high frequency the material behaves like a glassy material.

2.3.4 Rheological Tests on Glycolipids

The rheology of lyotropic system of glycolipids was mostly involving APGs due to their commercial values. However, certain mesophases such as inverse hexagonal and inverse micellar (discontinuous) cubic phase (Rodriguez-Abreu et al., 2005) are still considered underexplored. It was shown that droplet sizes affected the flow behaviour of glycolipids as demonstrated by Boris Niraula and co-workers (Niraula et al., 2004). In his study, the emulsion of homologous glucopyranosides of different chain lengths ($C_7 - C_{10}$) were prepared and they found the samples exhibited smaller droplet size as the length of alkyl chain at tail group increases. Additionally, the shear viscosity of the longer tail group was remarkably higher than that of the shorter tail and thus, they displayed a wider linear viscoelastic (LVE) region. After six months, the *G'* value of LVE region did not differ significantly from the original which implies the emulsion system had good storage stability. Indeed, rheological testing can be implemented as a standard procedure to evaluate the suitability of glycolipids to be used as biosurfactants for the consumers. Table 2.1 listed a few rheological studies of liquid crystalline phases exhibited by various materials including glycolipid.

Table 2.1 : Previous rheological studies on materials exhibiting liquid crystalline phases.

Reference	Surfactant/Lipids	Liquid Crystalline Phase	Flow Behaviour
(Mezzenga et al., 2005)	▪ Dimodan U/J ▪ Monolinolein (C18:0)	▪ Lamellar ▪ Hexagonal ▪ Bicontinuous cubic (double diamond)	▪ Plastic ▪ Viscoelastic ▪ Complex rheological behavior
(Zhao et al., 2011)	▪ Dodecyl polyoxypropylene ether	▪ Lamellar	▪ Elastic gel-like
(Pouzot et al., 2007)	▪ Dimodan U/J ▪ Limonene oil	▪ Discontinuos cubic (*Fd3m*)	▪ Hard gel-like
(Elbadawi et al., 2015)	▪ Glucopone ▪ Heptane	▪ Bicontinuous cubic (*Ia3d*)	▪ Solid-like

Supramolecular gels are made up of three-dimensional networks as a result of the molecular self-assembly (Zhang, Hu, et al., 2018). Within it, another class of self-assembly emerged, simply known as supramolecular soft materials. Supramolecular soft materials are synthesized from low molecular weight compounds that possess a unique tendency to form various architectures via non-covalent interaction such as hydrogen bonding, π-π stacking, van der Waals forces, and dipole-dipole interaction. Their potential applications in the medical field (Ye et al., 2014), solar cells (Zhang et al., 2014) and optical devices (Vidyasagar et al., 2011) have been discussed elsewhere. Recently, the synthesis and rheology of glycolipid-based supramolecular soft material by using cashew nut shell liquid have been reported (Lalitha et al., 2018). In general, the material displayed viscoelastic solid behaviour since *G' > G"* which demonstrates the mechanical strength of the material toward external stress which was suitable for possible application in the future. Another research group (Wang et al., 2017) has successfully synthesized a series of glycolipids containing 4,6-*O*-benzylidene acetal protected D-glucosamide and triazole. Similarly, the viscoelastic behaviour of the sample was investigated to give an insight into their mechanical strength. One of the compounds had a propyl chain as the

terminal group showed the best hydrogelator performance with concentration as low as 0.15% wt. At the same time, they also form hydrogels in solvent mixtures of dimethyl sulfoxide or ethanol with water. The flow test on this particular compound in a mixture of ethanol: water (*v*/*v*) of the ratio of 1:2 at 2.0 mg mL^{-1} had edisplayd greater storage modulus, *G'* compared to loss modulus, *G"*, which meant they were elastic semi-solid.

Cellulose is a polysaccharide that consists of polymerized D-glucose and it is the most abundant organic polymer ever discovered (Sun et al., 2016). There have been reports on using cellulose nanocrystals in drug delivery (Roman et al., 2009), topical cream application (Taheri & Mohammadi, 2015) and many more. Thus, the flow test was crucial to ensure optimum performances. Sulfonated cellulose nanocrystals were produced by extraction from cotton showed a shear thinning behaviour in the aqueous system. Moreover, at the measuring temperature of 10°C, it was found that the lower concentration cellulose nanocrystals exhibited viscous behaviour but gradually transformed into elastic behaviour with the transition-to-gel observed in between the elastic and viscous behaviour. Furthermore, hydrochloric acid treated cellulose nanocrystals from softwood kraft pulp showed significantly greater shear thinning behaviour compared to the sulfuric acid treated cellulose nanocrystals (Araki et al., 1999).

The rheological characterization of cubic phase is somewhat difficult since they are thought to have several relaxation mechanisms when stress is applied (Jones & McLeish, 1995, 1999; Montalvo et al., 1996). Despite that, several publications have been reported to explain their relaxation patterns. For example, the discontinuous cubic phase of *Fd*3*m* made up of inverted micellar in the ternary mixture of monolinolein/limonene oil/water displayed a hard-gel like behaviour with well-defined yield stress (Pouzot et al., 2007). Their relaxation mechanism was found to be similar to bicontinuous cubic *Ia*3*d* and *Pn*3*m* mesophases yet *Fd*3*m* had slower relaxation time which arised from a few plausible

reasons. First, the water diffusion from different sizes of micelles as the result of different Laplace pressure gradient. Second, the repositioning of the disfigured interfaces into dodecahedral and hexakaidecahedral structures and lastly the packing perturbation in micellar structure back to the *Fd*3*m* lattice.

In 2005, a research team had studied the shear rheology of mesophases in monoglyceride/water system. It was found that the bicontinuous cubic phase displayed complex rheological behaviour yet could be modelled following a multiple Maxwell model (Mezzenga et al., 2005). Besides, the rheological study on ultra-swollen lipid phases of limonopalmitolein and 1,2 distearoyl phosphatidylglycerol have been reported recently (Speziale et al., 2018). It was revealed that the longest relaxation time, τ_{max} of *Ia*3*d* and *Pn*3*m* decreased as the lattice parameter and water content increased. When the two mesophases were compared at the same water content, the *Ia*3*d* cubic phase experienced longer relaxation time due to their close-packed arrangement of 3D minimal surfaces of the lipid bilayer resulting in a smaller water channel. Currently, most opinions agreed that the lamellar phase is the most fluid-like mesophase, described as plastic fluid undergoing yielding followed by hexagonal phase that exhibits reasonably viscoelastic fluid and lastly the most rigid is the cubic phase (Sagalowicz et al., 2006).

CHAPTER 3: METHODOLOGY

3.1 Synthesis of Branched Chain Glycolipid

In this work, the studied compounds were synthesized following a previously reported procedure (Hashim et al., 2006). This procedure was used to synthesize two types of Guerbet glycolipids with similar lipid tail length but different head group size namely 2-hexyl-decyl-*β*-D-glucoside and 2-hexyl-decyl-*β*-D-maltoside. Figure 3.1 shows the chemical structure of the two compounds.

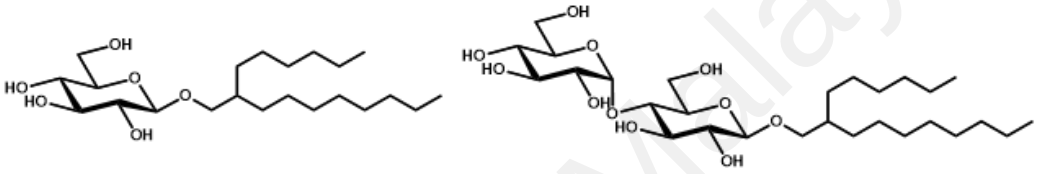

Figure 3.1 : The chemical structure of 2-hexyl-decyl-*β*-D-glucoside (left) and 2-hexyl-decyl-*β*-D-maltoside (right) respectively.

The general synthesis route involves three consecutive steps which are peracetylation, glycosidation and deacetylation. The aim of peracetylation is to protect the hydroxyl (-OH) group in the sugar structure from interfering with the chemical reaction. However, in this project, this step is not carried out since the peracetate sugars of glucose and maltose are commercially inexpensive and available in large quantity.

Hence, the first synthesis step conducted was the glycosidation instead of peracetylation. Glycosidation involves the attachment between a carbohydrate to a functional group of a different molecule such as an alcohol. In this study, boron trifluoride diethyl etherate was used as a catalyst since it has incomplete octet and an empty 2p orbital, making it a Lewis acid. This is where the term “Lewis acid glycosidation” came from. During the reaction, an acetoxy group at the C-1 position was replaced with the branched chain hydrocarbon tail of the Guerbet alcohol. Lastly, deacetylation is a reaction

to remove the acetyl group from the sugar head to obtain the final product. The reaction scheme involving glycosidation and deacetylation is shown in Scheme 3.1.

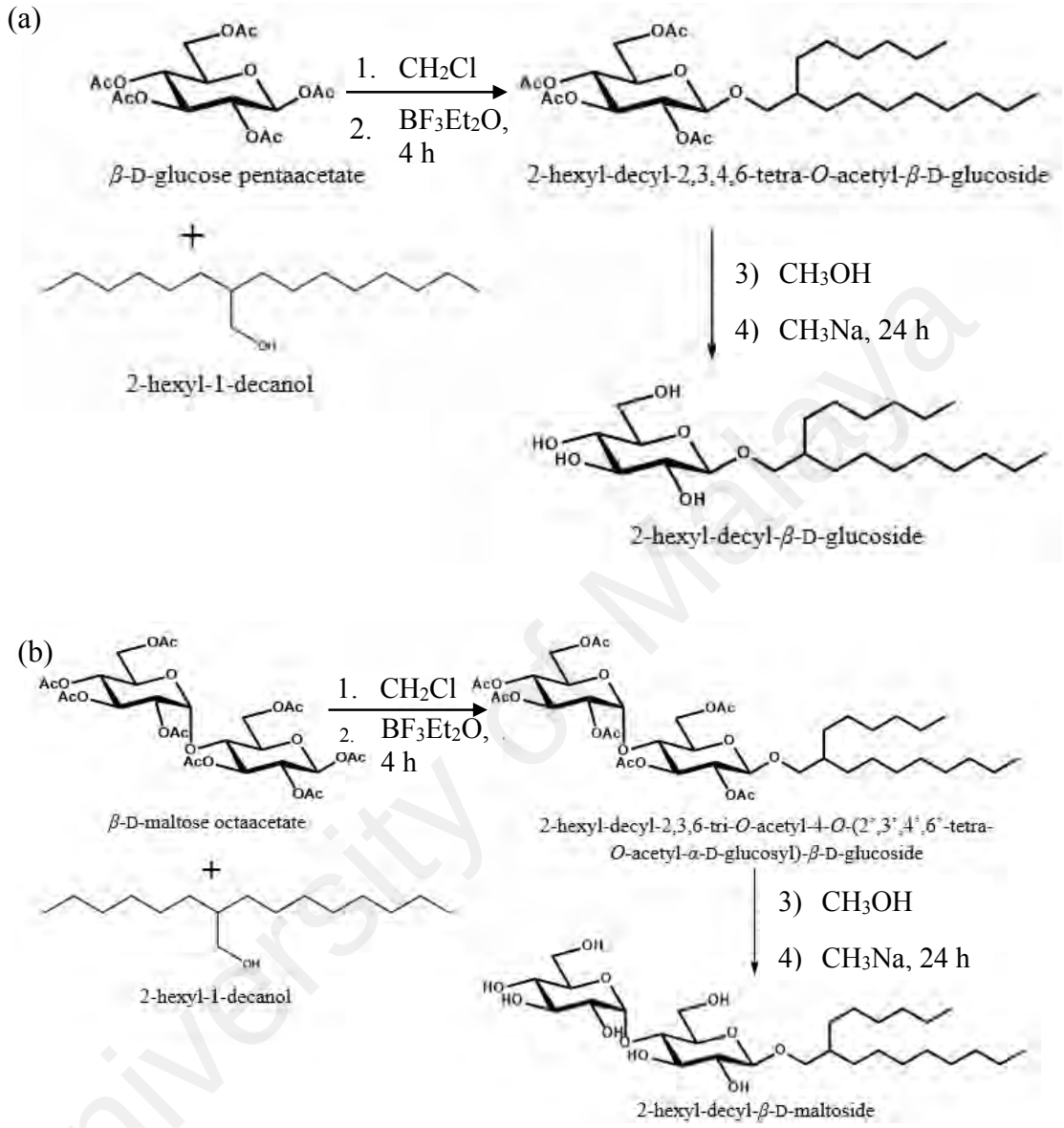

Scheme 3.1 : The reaction scheme for (a) glucoside and (b) maltoside synthesis.

3.1.1 Materials

The starting material *β*-D-glucose pentaacetate (98%) was acquired from Merck while *β*-D-maltose octaacetate (98%) was purchased from Carbonsynth Limited. Boron trifluoride diethyl etherate, sodium methoxide (97%), sodium hydrogen carbonate, diphosphorus pentoxide, dichloromethane, *n*-hexane, ethyl acetate and methanol were

purchased from Merck. The Guerbet alcohol, 2-hexyl-1-decanol (97%) was purchased from Sigma-Aldrich. Magnesium sulphate and acetonitrile were purchased from Riendemann Schmidt. All chemicals and solvents were used without further purification.

Thin Layer Chromatography (TLC) was used to monitor the synthesis progress. This method was also used to separate non-volatile mixtures and determining their purity (Santiago & Strobel, 2013). This technique is cheap, quick, has high sensitivity and reproducibility. In addition, TLC is usually performed on TLC plates that is made of aluminium, glass or plastic coated with adsorbent (Meyers & Meyers, 2008). For TLC, Silica Gel 60 F254 coated on aluminium sheets from Merck were used. Since glycolipid is not ultraviolet (UV) active, staining solution mixture of ethanol, water and sulphuric acid (90:8:2) was used to develop the TLC. It was then immersed in the staining solution and subsequently heated with the heat gun.

The separation of α- and β-anomers were applied after glycosidation by flash column chromatography. The stationary phase consisted of silica gel with pore size of 0.035–0.070 mm, (Silica Gel 60 Å) while a solution mixture of hexane–ethyl acetate was used as the mobile phase. Bellow pump was applied to provide external pressure into the column and hence provide a faster and consistent eluent flow.

3.1.2 Glycosidation of β-D-glucopyranoside

A mixture of β-D-glucose pentaacetate (6 g, 15.4 mmol, 1.0 equiv.) and 2-hexyl-1-decanol (5.8 ml, 20.0 mmol, 1.3 equiv.) was dissolved in 100 ml dichloromethane in a 250 ml round bottom flask. The reaction mixture was stirred at room temperature. Then boron trifluoride diethyl etherate (2.9 ml, 23.1 mmol, 1.5 equiv.) was added dropwise into the solution mixture via syringe. The solution mixture was stirred for four hours and the progress of reaction was monitored by TLC (hexane:ethyl acetate, 2:1). After four hours, the solution mixture was later quenched by saturated sodium hydrogen carbonate solution

thrice. The organic layer was separated from aqueous part and washed with water. Then the organic layer was dried over anhydrous magnesium sulphate, filtered and concentrated. The product was further separated using hexane–acetonitrile system to remove excess alcohol. The acetonitrile layer was collected and evaporated. The crude product was purified by column chromatography (hexane–ethyl acetate, 5:1). The chemical structure of collected product was confirmed by ^{1}H- and ^{13}C-NMR spectroscopy. Both spectra are available in the Appendix A and B respectively.

3.1.3 Glycosidation of *β*-D-maltopyranoside

β-D-maltose octaacetate of 6 g (8.8 mmol, 1.0 equiv.) and 2-hexyl-1-decanol (3.3 ml, 11.4 mmol, 1.3 equiv.) were mixed in 120 ml of dichloromethane. Boron trifluoride diethyl etherate (1.63 ml, 13.2 mmol, 1.5 equiv.) was added dropwise. The subsequent steps followed the glycosidation of *β*-D-glucopyranoside. Next, the crude product obtained was purified by column chromatography using hexane–ethyl acetate of the ratio 2.5:1. The chemical structure of the collected product was confirmed by using ^{1}H- and ^{13}C-NMR spectroscopy (see Appendix A and B respectively for the spectra).

3.1.4 General Deacetylation Procedure

The purified product obtained from the column chromatography was dissolved in methanol (1 g in 30 ml). Then, sodium methoxide was added to the solution until the solution turned basic. The reaction was stirred for 24 hours at room temperature. The solution was neutralized with Amberlite IR-20. Then, the Amberlite IR-20 was filtered and the solvent was evaporated. The product was further dried in vacuum oven for 48 hours at 50°C. The complete replacement of acetate groups by hydroxyl groups on the sugar head was confirmed by ^{1}H-NMR spectra. Their ^{1}H- and ^{13}C-NMR are given in Appendix A and B respectively.

3.1.5 Characterization Using Nuclear Magnetic Resonance (NMR)

This technique is a non-destructive method to analyse the chemical characters of matter by exploiting their magnetic properties. The basic principle is that nucleus (e.g. proton, ^{1}H) has nuclear spin when they have odd mass or atomic number. In turn, they become electrically charged and emit magnetic fields as illustrated in Figure 3.2(a). Initially, the proton spins in random direction. When an external magnetic field, B_o is applied, the direction of magnetic field of proton can align along with the external field and this is called as α-spin state. If the direction of proton's magnetic field is the opposite of the external field, it is known as β-spin state. Between these two states, the former has lower energy state than the latter hence, it is more stable. The change in spin state can only occur when the proton has equal energy with the energy difference between the two states as shown in Figure 3.2(b). This phenomenon is recognized as resonance (Wade Jr, 2013).

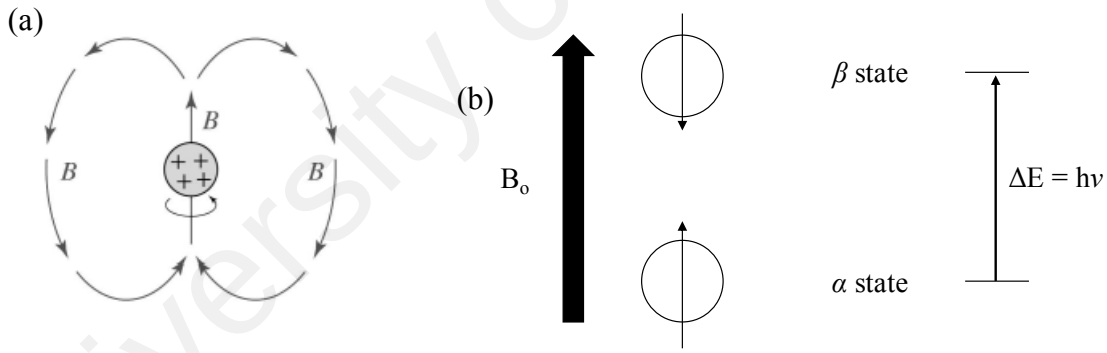

Figure 3.2 : An illustration of a (a) spinning nucleus where B is the magnetic field and (b) the two spin states of nucleus. Redrawn from (Wade Jr, 2013).

The proton is surrounded by an electron that emits its own magnetic field which will hinder the proton from the external field since the secondary field produced by the electron is the opposite direction of the applied external field (Duer, 2008). The shielding effect depends on the chemical environment of the proton. For example, the proton connected directly to the oxygen atom will be absorbed at higher field compared to the proton adjacent to the carbon atom due to the presence of lone pairs in oxygen as shown below in Figure 3.3. This will give rise to different chemical shifts that can be interpreted from the spectrum.

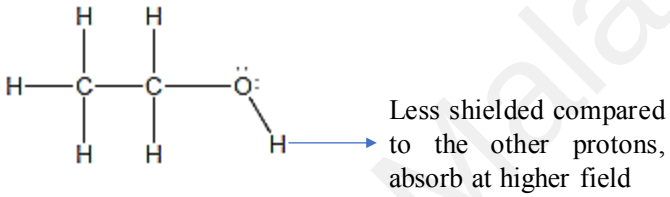

Figure 3.3 : Illustration of shielding effect due to the presence of lone pairs in oxygen atom connected directly to the proton.

Carbon-13 NMR (^{13}C-NMR) is often run simultaneously with proton NMR (^{1}H-NMR) to enforce the chemical structure determination. However, the natural abundance of isotope ^{13}C is only around 1% compared to the natural isotope ^{12}C. Thus, the signal produced is weaker and took longer measurement time than that of ^{1}H-NMR. To overcome this issue, Fourier Transform NMR (FT-NMR) spectroscopy has been developed whereby the magnetic nuclei are irradiated with a pulse of radio frequency close to their resonant frequency. Some of the energy will be absorbed by the nuclei and precess at their resonant frequency. The precession of various nuclei at slightly different frequencies gives out free induction decay (FID), a complex signal that decays as the nuclei lose the energy they gained from the pulse. The average of many FIDs will be recorded and the computer converts it into a spectrum (Wade Jr, 2013). The typical setup of nuclear magnetic spectrometer is shown in Figure 3.4.

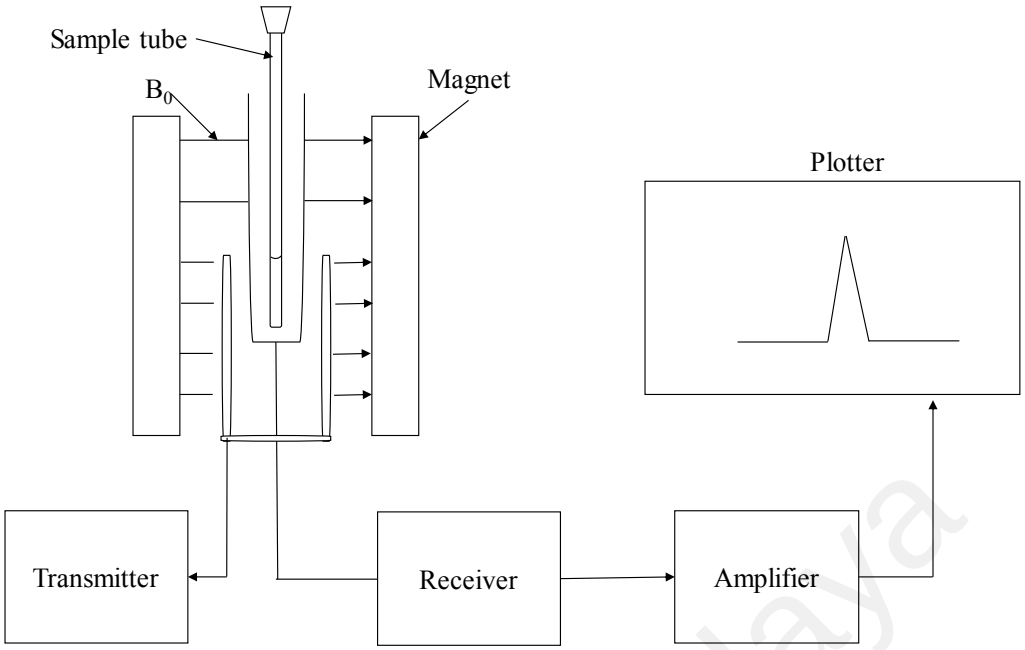

Figure 3.4 : The schematic diagram of a nuclear magnetic resonance spectrometer, redrawn from (Günther, 2013).

Measurement

Nuclear Magnetic Resonance (NMR) technique particularly ^{1}H- and ^{13}C-NMR was used to assess the chemical structure and anomeric purity of the synthesized compounds. The NMR measurement was taken using Bruker Avance 400 NMR spectrometer at 25°C. Chloroform-d was used as solvent for protected glycolipids while methanol-d_4 for deprotected glycolipids. The residual solvent peak for chloroform-d is 7.26 ppm in ^{1}H-NMR and 77.23 ppm in ^{13}C-NMR. As for methanol-d_4, residual solvent peak appeared at 4.87 ppm and 49.15 ppm in ^{1}H-NMR and ^{13}C-NMR respectively.

3.2 Physico-Chemical Characterization of Branched Chain Glycolipid

The two branched-chain glycosides were first subjected to thermal analysis measurement using thermogravimetric analysis (TGA). Their liquid crystalline phases were identified and determined by a combination of various techniques namely optical polarizing microscopy (OPM) and small-angle X-ray scattering (SAXS). Finally, the

rheological measurement was performed to characterize the flow behaviour of the mesophases.

3.2.1 Thermogravimetric Analysis (TGA)

TGA is a type of thermal analysis that monitor the mass loss as a function of temperature in a controlled environment by using thermogravimetric analyzer or more commonly known as thermobalance (Haines, 2012). The mass loss could be caused by changes such as oxidation, decomposition or dehydration. The main aim of TGA is to predict the thermal stability and decomposition temperature of the material. The temperature of the sample is detected by the thermocouple placed as close as possible to the sample (Gaisford et al., 2016) and the mass changes is recorded by the analytical balance that is placed outside of the furnace. The basic setup of a thermogravimetric analyzer is shown in Figure 3.5. The samples are heated at a rate of 10 or 20°C min^{-1} in most cases. Nevertheless, lowering heating rates is known to improve the resolution of overlapping weight losses.

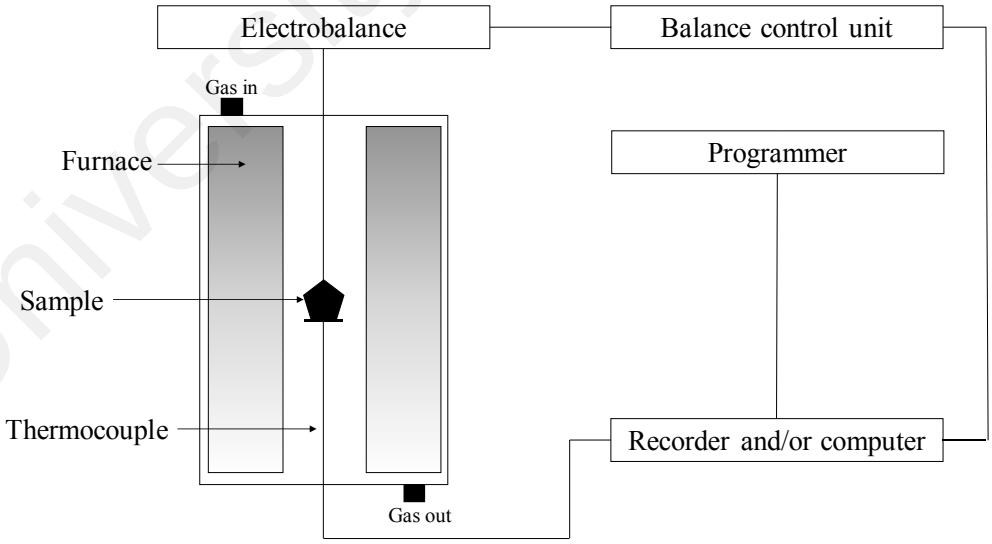

Figure 3.5 : Basic setup of a thermogravimetric analyser. Redrawn from (Haines, 2012).

Measurement

The glycolipids were dried for at least 24 hours over diphosphorus pentoxide before measurement to remove traces of moisture. Next, approximately 11 mg of sample was transferred into the aluminium pan before loaded into the sample holder of Netzsch STA449 F5 Jupiter. The sample was subjected to heating between 30–500°C at the scanning rate of 5°C min^{-1} in nitrogen atmosphere. The data analysis was performed with Proteus software.

3.2.2 Optical Polarizing Microscopy (OPM)

The function of optical polarizing microscope is to determine the texture and hence the identity of the mesomorphic compounds. It is also a convenient way to identify the transition temperature of the liquid crystalline compound. Polarized light differs from normal light because its light waves travel in one direction compared to the latter. Hence, this technique detects the defects within the liquid crystalline phase (Collings & Hird, 1997) in which different liquid crystalline phases will show different textures under the polarizing microscope. Hot-stage is often connected to the instrument to observe the different textures adapted by liquid crystalline phases at different temperatures.

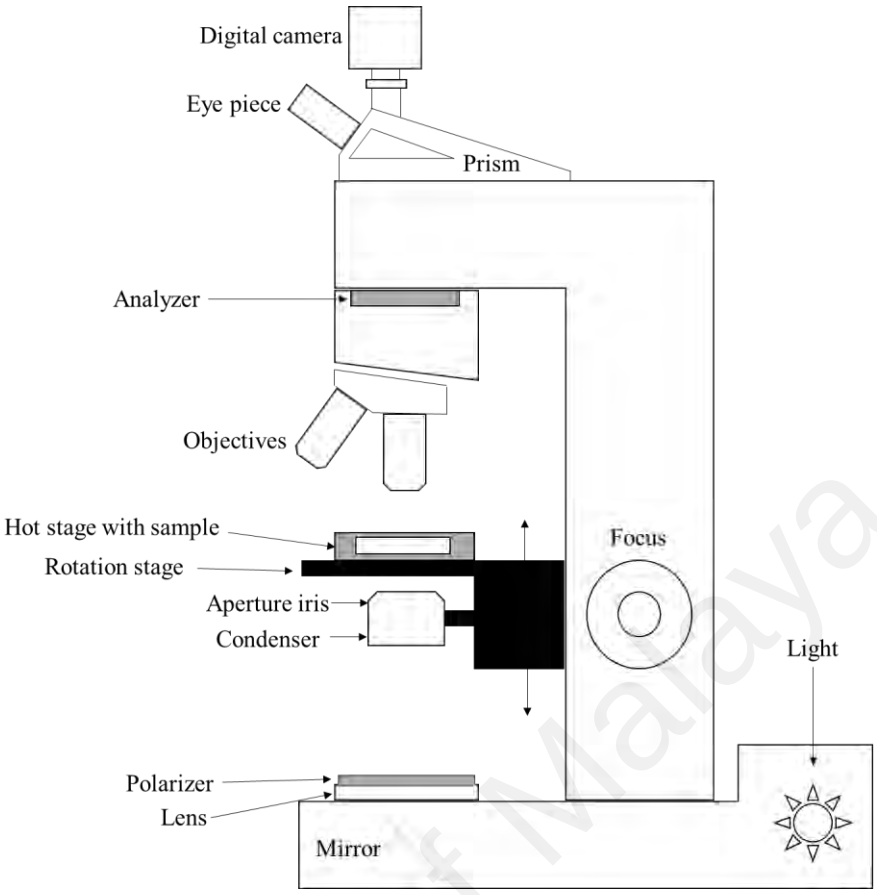

Figure 3.6 : Typical optical polarizing microscope instrument, redrawn from (Dimitruk & Davidson, 2013).

The optical polarizing microscope is equipped with two linear polarizers as shown in Figure 3.6. One is situated below the stage (polarizer) while another one is situated above the objective (analyzer). When the light goes through the first polarizer, it selects a single orientation among all waves which compose the light. The second polarizer is placed perpendicularly to the first one, obstructing the wave from passing through. When a birefringent sample is placed along the light beam, it will polarized the light into two separate wave, which will then recombine after they pass through the analyser through the constructive and destructive interferences (Carlton, 2011).

Thermotropic Phase Behaviour

In thermotropic study, the sample was lyophilized over diphosphorus pentoxide for at least 24 hours to remove all the trace water as the sugar glycolipids are hygroscopic. Then the dried sample was placed on a clean glass slide and covered with cover slip as shown in Figure 3.7. The cover slip was gently pressed and then positioned on the temperature-controlled hot stage for temperature variation study. The sample was heated to its isotropic phase at the rate of 5°C min^{-1} and then cooled down to room temperature at the rate of −2 C min^{-1}. The first thermal cycle purpose was to produce a flat and even sample thickness and also to remove the thermal history of the sample. Once cooled, the phase transition temperature was recorded during the second heating and the sample texture image was captured upon second cooling.

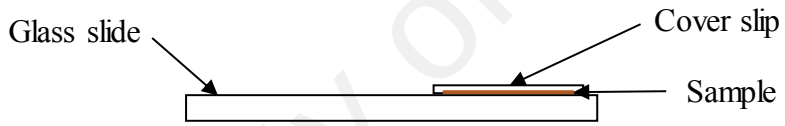

Figure 3.7 : Sample preparation for thermotropic study.

Lyotropic Phase Behaviour

Water contact penetration method was used to study the lyotropic phase behaviour. Figure 3.8 demonstrates the schematic diagram of water penetration technique. It has similar preparation method to the thermotropic study where the samples to be studied was placed on a clean glass slide and covered with the cover slip. It was heated until isotropic phase and cooled down to the room temperature to get a uniform sample thickness and to remove the sample thermal history. Then, a drop of water was added on the edge of the cover slip and the water will enter the sample via capillary action. A concentration gradient of excess water at the cover slip edge to neat surfactant was formed. The OPM

image of the solvated sample was captured at least after 30 minutes of equilibration during which precaution was taken to reduce water loss.

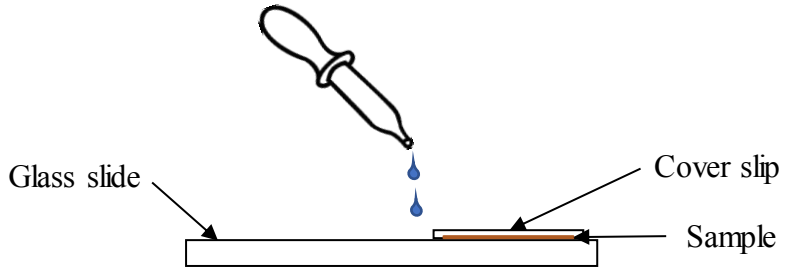

Figure 3.8 : Sample preparation for lyotropic study.

Measurement

The thermotropic and lyotropic studies were identified with Mettler Toledo FP82HT and observed with Olympus BX51 microscope fitted with cross-polarizing filters. The pictures of textures were captured with Olympus DP26 camera. Magnification factor used were ×10 and ×20. CellSans software was used to process the images of the mesophases.

3.2.3 Small Angle X-ray Scattering (SAXS)

This is a non-destructive technique which is used to determine the scattering intensity of a compound as a function of the scattering angle, with a resolution ranging typically from 10 to 1000 Å (i.e. with scattering angles < 5°). When the sample is bombarded with an intense X-ray beam, this will result in the scattering of X-rays which subsequently give the information of size, shape and components information of the sample (Heberle et al., 2012).

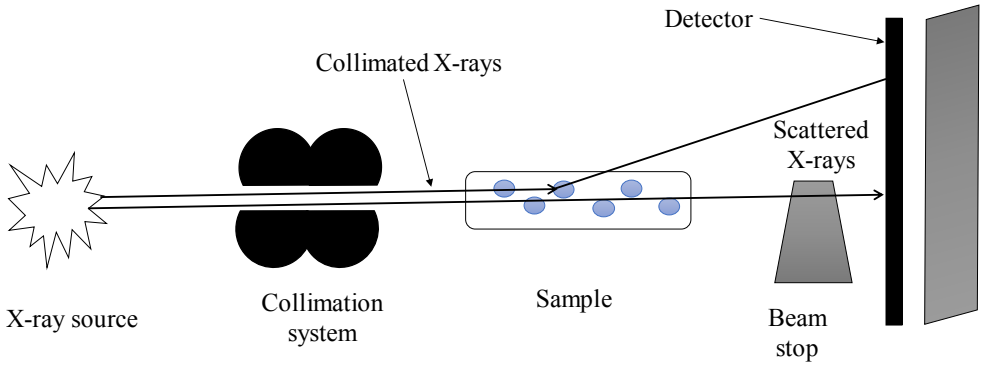

Figure 3.9 : The configuration of SAXS instrument. Redrawn from (Zhang, Chen, et al., 2018).

The SAXS instrument consists of X-ray source, a collimation system, sample holder, a beam stops and detector as shown in Figure 3.9. Once the X-ray source irradiate X-ray beam, it will pass through the collimation system where the beam will be narrowed down before it hits the sample. The scattering pattern resulting from the collision between sample and collimated X-ray beam is then picked up by the detector. The beam stop will prevent the strong X-ray beam from hitting the detector since it can mask some of the weak scattering pattern of the sample and also prevent detector breakage (Blanchet et al., 2015; Schnablegger & Singh, 2013).

$$\boldsymbol{n\lambda = 2d_{hkl} \sin \theta} \quad \textbf{(Equation 3.1)}$$

This technique is governed by Bragg's Law as given by Equation 3.1 where n is an integer, λ is the wavelength of the X-ray, d_{hkl} (with common unit of Å) is the repeated distance between two neighbouring planes of lattices (d-spacing), and θ is the scattering angle between the reflected X-ray and the plane formed by the sample surface. The Miller indices h, k and l are the family of equidistant reflection planes also known as the reciprocal lattice plane. The illustration of Bragg's Law is given in Figure 3.10.

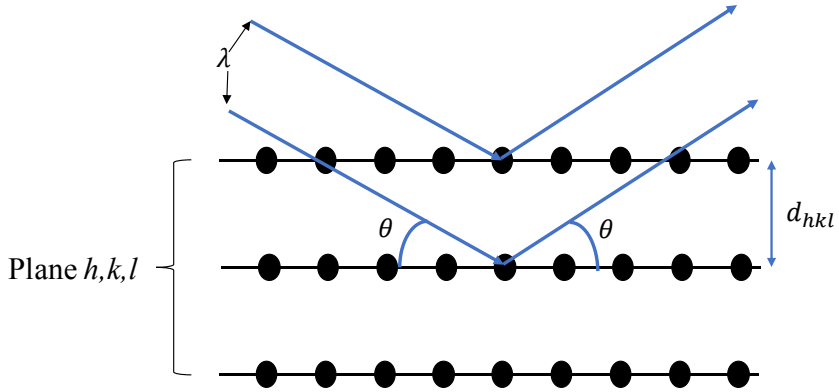

Figure 3.10 : Illustration of Bragg's Law. Redrawn from (Tyler et al., 2015).

In this thesis, SAXS study was emphasised to investigate the self-assembly of the chosen compound in dry and excess water by determining the reciprocal distances (with common unit of Å^{-1}), s_{hkl}, which is related to d_{hkl} by $s_{hkl} = 1/d_{hkl}$ (Tyler et al., 2015). Once the reciprocal distance is calculated, the space group and the structure of mesophase can be characterized. Commonly, SAXS patterns are represented by magnitude of the scattering vector, q (with common unit of Å^{-1}) rather than s_{hkl}. The q and s_{hkl} is related by $q = 2\pi s_{hkl}$.

Sample Preparation

First, the sample was dried overnight in vacuum until the day before measurement. The thermotropic phase study was conducted by loading the sample directly into the paste cell holder and immediately placed in the X-ray machine. The sample was heated up to isotropic temperature and then cooled to the room temperature. The sample was left overnight in the vacuum before the measurement was taken. For lyotropic study, a selection of hydrated samples at a water concentration of 30% (w/w), 50% (w/w) and 80% (w/w) samples were prepared by adding appropriate amounts of water and dry glycolipid (~100 mg) into a 1.5 ml micro centrifuge tube. The samples were then homogenized by repeated up and down centrifuging and then left to equilibrate at the

room temperature for at least three days to ensure the mesophases have fully stabilized prior to the SAXS measurement.

Measurement

In this experiment, SAXSess Anton Paar, Austria was used to obtain the scattering pattern of the mesophases. The instrument has X-ray tube model DX-Cu 12×0.45, SERFERT that function to generate the radiation of Cu-K_α at wavelength $\lambda = 1.\ 2$ Å at 40 kV and 50 mA. The measurements were carried out in line collimation mode under vacuum with the detector distance of 317 mm. Silver behenate ($\lambda = .8$ Å) was used as calibrant for all measurements. Peltier System (TCStage 300) was used to control the sample temperature (±0.1°C). Approximately 50 mg of dried or hydrated sample was transferred to a paste cell holder and loaded into the X-ray machine. During measurement, both dry and hydrated samples underwent 10 minutes equilibration at the chosen temperature and the acquisition time was 30 minutes. The primary beam was corrected using SAXStreat software. The corrected data was later processed by Space Group Indexing software (SGI program) to determine the space group of the liquid crystalline phases and its corresponding lattice parameter.

3.2.4 Rheological Measurement

The flow properties of the compound are determined by rheometry. The rheometer was used to measure how a liquid or slurry flows under applied force (Ollikainen, 2015). It measures the resulting deflection angle caused by the sample's resistance to flow and the test can be either conducted at a controlled shear rate (CSR mode) or controlled shear stress (CSS mode).

In CSR mode, the rotational speed is set beforehand at the rheometer and the shear rate is determined based on the gap and the rotational speed. Then, the flow resistance

moment, M (or shear force) of the material under investigation is measured. The torque is subsequently converted into rheological parameter of shear stress using the shear area of the measuring system. In CSS mode, the torque is set beforehand and the shear stress is determined from the torque and the shear area of the measuring system. The rotational speed is achieved by the plunger due to the applied torque is measured. It is then converted into rheological parameter of shear rate with a suitable measuring system factor (Barnes et al., 1989).

Measurement

The sample was dried in vacuum desiccator overnight before measurement. In thermotropic study, a small amount of sample was loaded directly on the measuring plate of Anton Paar's rheometer Physica MCR 301 precisely under the parallel plate with a diameter of 25 mm. Then the distance between parallel plate and the lower measuring plater (where the sample is applied) was set to 1 mm. The steady shear viscosity measurements were conducted at shear rates varied in the range of 0.001–1000 s^{-1}. For β-Glc-$C_{10}C_6$, the measurement was taken at 25°C and 37°C. Meanwhile for β-Mal-$C_{10}C_6$, the sample was characterized at 25°C, 37°C, 60°C and 90°C. It is worth mentioning that even though β-Mal-$C_{10}C_6$ has solid powder appearance, it is just as sticky as β-Glc-$C_{10}C_6$, thus we were able to carry out the testing using conventional method described above. All samples were equilibrated for 5 minutes at the desired temperature to ensure that the required mesophase was obtained before the measurement. The linear viscoelastic (LVE) region of all mesophases was determined in strain-controlled mode with frequency of 1 rad s^{-1} at shear strain amplitude from 0.01–100%. Then, the frequency sweep experiment was also conducted to determine the relaxation time of the liquid crystalline phases with pre-determined strain from LVE region. The hexagonal phase of β-Glc-$C_{10}C_6$ was determined at shear strain amplitude of 0.24% while the lamellar phase of β-Mal-$C_{10}C_6$

was measured at shear strain amplitude of 0.32% at an angular frequency from 0.1–100 rad s^{-1}.

The lyotropic samples were prepared according to the following manner. A selection of hydrated samples at water concentrations of 30% (w/w), 50% (w/w) and 80% (w/w) was prepared by adding the appropriate amount of water and dry glycolipid into a 5.0 mL centrifuge tube. Homogenization was carried out by centrifuging the sample at 5000 rotation per minute (rpm) for 5 minutes. The homogenized samples were left to equilibrate at the room temperature for at least three days before measurement. The measurement cell for β-Mal-$C_{10}C_6$ was a double gap concentric cylinder with a diameter of 26.7 mm. This particular system was chosen since the sample had low viscosity in combination with large surface area provided by the double gap set up. Temperature control was regulated with Peltier system from the outer concentric cylinder. Since β-Glc-$C_{10}C_6$ has viscous and gummy consistency, it was unable to homogenously mix with water. Hence, the measurement cell was modified to a cone plate with a diameter of 25 mm and 1° cone angle in which the measuring position is fixed at 0.051 mm. The difference between parallel plate and cone plate is shown in Figure 3.11 below.

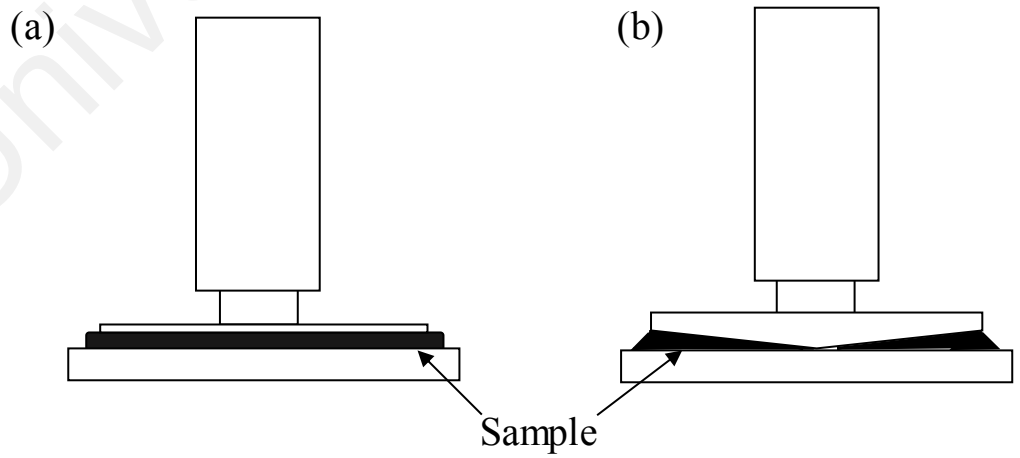

Figure 3.11 : The schematic drawing of parallel plate and cone plate. Redrawn from (Mezger, 2014).

Similar to thermotropic test, the shear rate for viscosity test of the hydrated samples were set in the range of 0.001 to 1000 s^{-1}. For β-Glc-$C_{10}C_6$, the measurement was conducted at 25°C and 37°C. As for β-Mal-$C_{10}C_6$, a selection of temperatures at 25°C, 37°C, 60°C and 90°C were selected for measurement. All samples were equilibrated for 5 minutes at the desired temperature before measurement. The LVE region of lyotropic samples was determined at 10 rad s^{-1} instead of 1 rad s^{-1} due to cluttered lines produced at 1 rad s^{-1} which made data interpretation difficult. The strain range was set to $4 \times 10^{-6} -$ 10%. The frequency sweep of both compounds was conducted from 0.628–628 rad s^{-1} with strain of 0.01% at all concentrations.

CHAPTER 4: RESULTS AND DISCUSSION

This section describes the synthesis and physico-chemical characterization of β-Glc-$C_{10}C_6$ and β-Mal-$C_{10}C_6$. First, the structure elucidation was conducted through ^{1}H-NMR and ^{13}C-NMR. The peak assignments for both compounds were briefly described followed by thermal analysis using TGA. Subsequently, the characterization of thermotropic and lyotropic liquid crystalline phases formed by both Guerbet glycosides was conducted using OPM and SAXS. The last section discusses the rheological behaviour of these thermotropic and lyotropic mesophases.

4.1 Synthesis and Chemical Characterization of Glycosides

Two types of glycosides have been synthesized using the synthesis method described in Chapter 3. The percentage yield of the reactions for each batch of β-Glc-$C_{10}C_6$ and β-Mal-$C_{10}C_6$ is tabulated in Table 4.1 and Table 4.2 respectively. The glucoside compounds gave yellowish gel while the maltoside appeared as white solid powder and very hygroscopic than the former. The lower yield of β-Glc-$C_{10}C_6$ compared to β-Mal-$C_{10}C_6$ mostly due to the similar affinity between the anomeric mixture of α-Glc-$C_{10}C_6$ and β-Glc-$C_{10}C_6$ to the silica gel during elution in flash column chromatography. During this step, TLC was actively conducted to check the elution of β-Glc-$C_{10}C_6$ and the collection of the desired β-Glc-$C_{10}C_6$ was stopped once mixture of both anomers present on the TLC plate. The properties of the sample did not change from batch to batch as supported by their NMR spectra. The NMR spectra for these two compounds are available in the Appendix section. Nonetheless, we include brief discussion of ^{1}H- and ^{13}C-NMR spectra and NMR data for both compounds in this section.

Table 4.1 : Percentage yield of *β*-Glc-$C_{10}C_6$.

Batch No.	*β*-D-Glucose Pentaacetate (Limiting Reactant)			*β*-Glc-$C_{10}C_6$ (Final Compound)			Percentage Yield (%)
	Molecular Formula	Molecular Weight (g mol^{-1})	Reactant Weight (g)	Molecular Formula	Molecular Weight (g mol^{-1})	Product Weight (g)	
1	$C_{16}H_{22}O_{11}$	390.34	6.00	$C_{22}H_{44}O_6$	404.58	1.10	17.7
2	$C_{16}H_{22}O_{11}$	390.34	6.00	$C_{22}H_{44}O_6$	404.58	0.37	5.88
3	$C_{16}H_{22}O_{11}$	390.34	6.02	$C_{22}H_{44}O_6$	404.58	0.10	1.6
4	$C_{16}H_{22}O_{11}$	390.34	6.00	$C_{22}H_{44}O_6$	404.58	0.48	7.7
5	$C_{16}H_{22}O_{11}$	390.34	6.00	$C_{22}H_{44}O_6$	404.58	0.11	1.80
6	$C_{16}H_{22}O_{11}$	390.34	6.03	$C_{22}H_{44}O_6$	404.58	0.73	11.8
7	$C_{16}H_{22}O_{11}$	390.34	6.01	$C_{22}H_{44}O_6$	404.58	0.86	13.8
8	$C_{16}H_{22}O_{11}$	390.34	6.00	$C_{22}H_{44}O_6$	404.58	0.85	13.6
9	$C_{16}H_{22}O_{11}$	390.34	6.02	$C_{22}H_{44}O_6$	404.58	1.14	18.4
10	$C_{16}H_{22}O_{11}$	390.34	6.03	$C_{22}H_{44}O_6$	404.58	0.83	13.3
11	$C_{16}H_{22}O_{11}$	390.34	6.12	$C_{22}H_{44}O_6$	404.58	0.67	10.6
12	$C_{16}H_{22}O_{11}$	390.34	6.01	$C_{22}H_{44}O_6$	404.58	0.56	9.0

Table 4.2 : Percentage yield of *β*-Mal-$C_{10}C_6$.

Batch No.	*β*-D-Maltose Octaacetate (Limiting Reactant)			*β*-Mal-$C_{10}C_6$ (Final Compound)			Percentage Yield (%)
	Molecular Formula	Molecular Weight (g mol^{-1})	Reactant Weight (g)	Molecular Formula	Molecular Weight (g mol^{-1})	Product Weight (g)	
1	$C_{28}H_{38}O_{19}$	678.59	6.00	$C_{28}H_{54}O_{11}$	566.73	1.45	29.6
2	$C_{28}H_{38}O_{19}$	678.59	6.01	$C_{28}H_{54}O_{11}$	566.73	1.19	23.8
3	$C_{28}H_{38}O_{19}$	678.59	6.00	$C_{28}H_{54}O_{11}$	566.73	0.94	18.8
4	$C_{28}H_{38}O_{19}$	678.59	6.00	$C_{28}H_{54}O_{11}$	566.73	1.23	24.5
5	$C_{28}H_{38}O_{19}$	678.59	6.00	$C_{28}H_{54}O_{11}$	566.73	1.05	21.0
6	$C_{28}H_{38}O_{19}$	678.59	6.00	$C_{28}H_{54}O_{11}$	566.73	0.89	17.8
7	$C_{28}H_{38}O_{19}$	678.59	6.01	$C_{28}H_{54}O_{11}$	566.73	1.44	28.7
8	$C_{28}H_{38}O_{19}$	678.59	6.01	$C_{28}H_{54}O_{11}$	566.73	1.65	33.0
9	$C_{28}H_{38}O_{19}$	678.59	6.08	$C_{28}H_{54}O_{11}$	566.73	1.43	28.5
10	$C_{28}H_{38}O_{19}$	678.59	6.07	$C_{28}H_{54}O_{11}$	566.73	0.80	15.9
11	$C_{28}H_{38}O_{19}$	678.59	6.03	$C_{28}H_{54}O_{11}$	566.73	1.12	22.3
12	$C_{28}H_{38}O_{19}$	678.59	6.00	$C_{28}H_{54}O_{11}$	566.73	1.06	21.2

The ^{1}H-NMR spectrum of β-Glc-$C_{10}C_6$ with important peaks to signify the characteristic of the compound is shown in Figure 4.1. The two terminal methyl groups ($–CH_3$) are represented by a triplet peak at ~0.92 ppm. Methylene bridge or methanediyl ($–CH_2$) of the alkyl chain are represented by a sharp peak at 1.32–1.43 ppm since they are in similar chemical environment.

The broad small peak at 1.63 ppm representing a hydrogen atom attached to the chiral carbon of the alkyl chain which is can be referred as methanetriyl group (–CH). The peaks from 3.20–3.88 ppm signify the hydrogen atoms in the sugar head. Finally, the hydrogen atom at C-1 carbon position is denoted by the peak at 4.24 ppm. This peak is shifted at the lowest field due to the deshielding effect of the two neighbouring oxygen atoms. ^{1}H-NMR data of β-Glc-$C_{10}C_6$ is as follows:

^{1}H-NMR (400 MHz, CD_3OD): δ (ppm) = 4.24 (d, 1H, $J_{1,2}$ = 8.0 Hz, H-1), 3.88 (dd, 1H, OCH_2a), 3.83 (dd, 1H, $J_{6a,6b}$ = 12.0 Hz, H-6a), 3.69 (dd, 1H, $J_{6a,6b}$ = 12.0 Hz, H-6b), 3.25–3.43 (m, 4H, OCH_2b, H-3, H-4, H-5), 3.20 (dd~t, 1H, H-2), 1.63 (m, 1H, CH), 1.32–1.43 (m, 24H, CH_2), 0.92 (t, 6H, J = 6.8 Hz, 2 x CH_3).

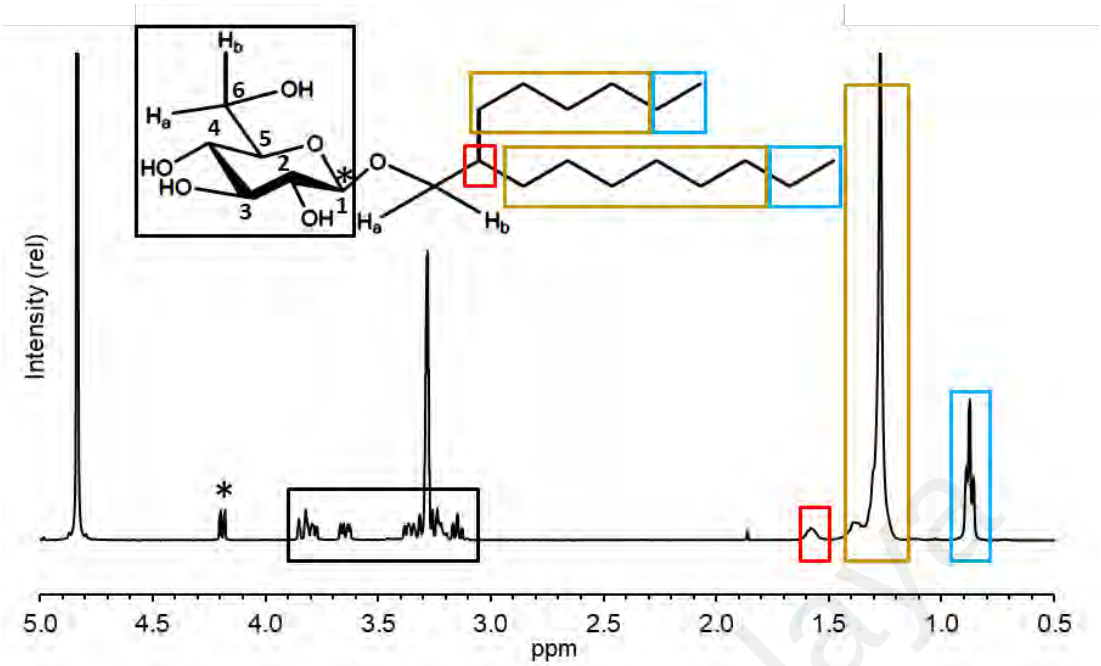

Figure 4.1 : ^{1}H-NMR spectrum of β-Glc-$C_{10}C_6$. The coloured boxes marked on the spectrum to denote hydrogen in different chemical environments i.e. blue, –CH_3 groups; yellow, –CH_2 groups; red, –CH group and black, sugar head. The asterisk (*) represents the hydrogen atom at C-1 carbon position.

The ^{1}H-NMR spectrum of β-Mal-$C_{10}C_6$ is shown in Figure 4.2. The peaks at higher field are mainly the aliphatic chain of the tail group which consists of –CH_3, –CH_2 and –CH groups at 0.92–1.63 ppm. The sugar head and ether linkage are shifted at lower field around 3.32–3.91 ppm due to their close proximity to oxygen atoms, causing deshielding effect since oxygen atom is electronegative. Hydrogen H-1 which is connected to carbon C-1 is seen at 4.26 ppm. While hydrogen H-1' is the hydrogen atom attached to the carbon C-1' of the second glucose unit. H-1' is more deshielded than that of H-1 (5.06 ppm vs. 4.26 ppm). ^{1}H-NMR data of β-Mal-$C_{10}C_6$ is as follows:

^{1}H-NMR (400 MHz, CD_3OD): δ (ppm) = 5.06 (d, 1H, $J_{1',2'}$ = 3.6 Hz, H-1'), .26 (d, 1H, $J_{1,2}$ = 8.0 Hz, H-1), 3.91 (dd, 1H, $J_{6a,6b}$ = 12.0 Hz, H-6a), 3.81 – 3.86 (m, 3H, H- ', H-6b, H-6a'), 3.67– 3.73 (m, 2H, H- ', H-6b'), 3. 8 – 3.65 (m, 2H, H-3, H-3'), 3. (dd, 1H, $J_{3,4}$ = 9.2 Hz, H-4), 3.36 – 3.48 (m, 3H, H-2', H-5, H-2), 3.23–3.36 (m, 2H, OCH_2), 1.63 (m, 1H, CH), 1.32–1.43 (m, 24H, CH_2), 0.92 (t, 6H, J = 6.8 Hz, 2 x CH_3).

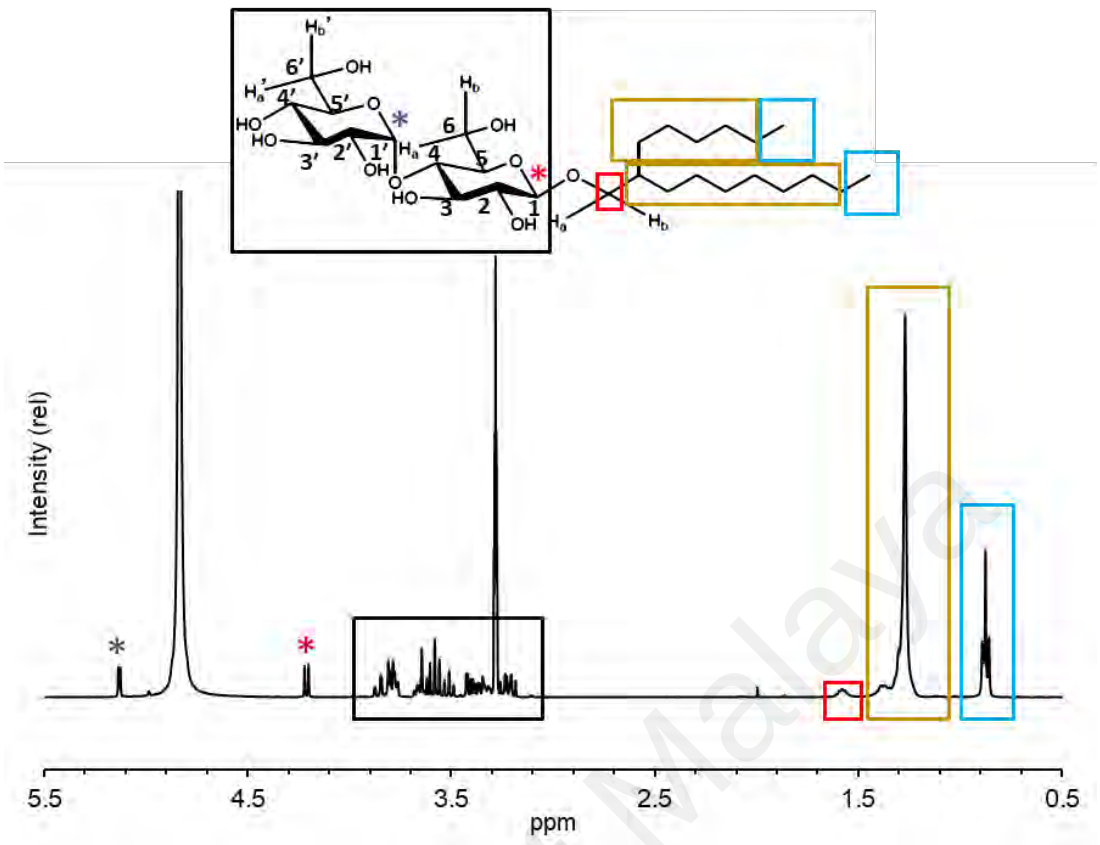

Figure 4.2 : ^{1}H-NMR spectrum of *β*-Mal-$C_{10}C_6$. The coloured boxes marked on the spectrum to denote hydrogen in different chemical environments i.e. blue, –CH_3 groups; yellow, –CH_2 groups; red, –CH group and black, sugar head. The red and purple coloured asterisk (*) represent the hydrogen atom at C-1 and C-1' carbon position, respectively.

Figure 4.3 shows the ^{13}C-NMR spectrum of *β*-Glc-$C_{10}C_6$.The peaks of aliphatic chain peaks are mainly observed at highest field of 13.0–38.1 ppm. The secondary carbons (–CH_2) are deshielded to lower field of 22.0–31.7 ppm compared to the primary carbons (–CH_3) at 13.0 ppm. The chiral carbon (–CH) denoted by red box is a tertiary carbon, thus it is shifted to an even lower field of 38.1 ppm. Similar to ^{1}H-NMR, the presence of electronegative atom will influence the ppm shift. For instance, the presence of oxygen atom in –OCH_2 group of the aliphatic chain cause deshielding effect to 72.6 ppm. Moreover, most of the carbon atoms in the sugar head is shifted to the lower field since they are connected to the hydroxyl (–OH) group. Finally, carbon C-1 which is connected to two oxygen atoms is shifted to the lowest field around 103.4 ppm since both oxygen

atoms withdraw electrons from the carbon atom. ^{13}C-NMR peak assignment of β-Glc-$C_{10}C_6$ is as follows:

^{13}C-NMR (100 MHz, CD_3OD): δ (ppm) = 103.4 (C-1), 76.8 (C-3), 76.5 (C-4), 73.8 (C-2), 72.6 (OCH_2), 70.3 (C-5), 61.4 (C-6), 38.1 (CH), 22.3–31.7 (CH_2), 13.0 (CH_3).

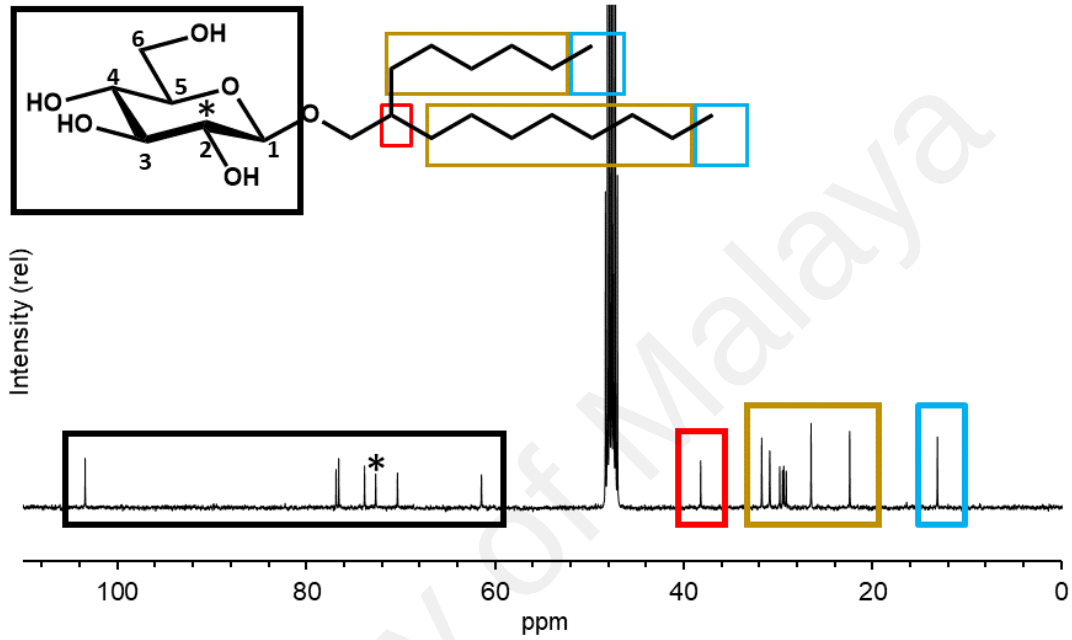

Figure 4.3 : ^{13}C-NMR spectrum of β-Glc-$C_{10}C_6$. The coloured boxes marked on the spectrum to denote carbon in different chemical environments i.e. blue, –CH_3 groups; yellow, –CH_2 groups; red, –CH group and black, sugar head. The asterisk (*) represents the carbon in –OCH_2 group of the aliphatic chain and the enlarged peaks are available in the appendix B.

Similar to β-Glc-$C_{10}C_6$, the peaks at higher field region of β-Mal-$C_{10}C_6$ represent the aliphatic chains at around 13.1–38.1 ppm (see Figure 4.4). The blue box denotes the primary carbon at 13.1 ppm while the yellow box denotes the secondary carbon at 22.3–31.7 ppm. The red box designates the tertiary carbon which is shifted to lower field of 38.1 ppm. The –OCH_2 group of the aliphatic chain is shifted to a lower field of 72.7 ppm since it is attached to an oxygen atom. The peaks for carbon in the sugar head appeared in the region of 60.8–103.3 ppm. The two peaks at the lowest field represent carbon C-1 (101.5 ppm) and C-1' (103.3 ppm). ^{13}C-NMR data of β-Mal-$C_{10}C_6$ is as follows:

^{13}C NMR (100 MHz, CD_3OD): δ (ppm) = 103.3 (C-1'), 101. (C-1), 79.9 (C-2), 76.5 (C-3'), 7 .2 (C -3), 73.7 (C-2'), 73. (C - '), 7 2.8 (C-5), 72.7 (OCH_2), 70.1 (C- ', C-4), 61.4 (C-6'), 60.8 (C-6), 38.1 (CH), 22.3–31.7 (CH_2), 13.1 (CH_3).

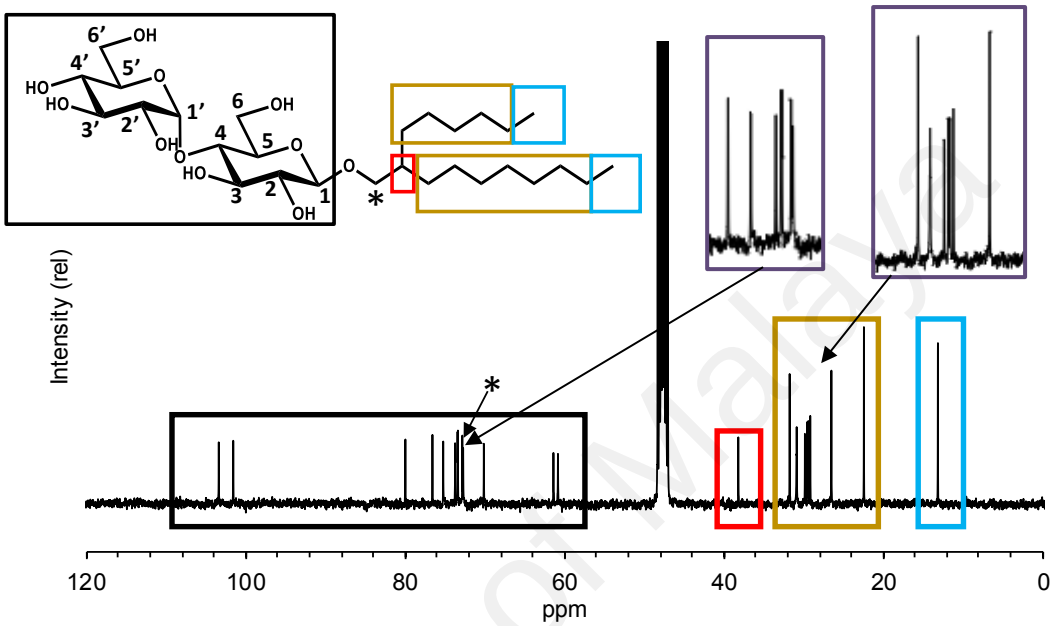

Figure 4.4 : ^{13}C-NMR spectrum of β-Mal-$C_{10}C_6$. The coloured boxes marked on the spectrum to denote carbon in different chemical environments i.e. blue, –CH_3 groups; yellow, –CH_2 groups; red, –CH group and black, carbon in the sugar head. The asterisk (*) represents the carbon in –OCH_2 group of the aliphatic chain. The insets show magnified peaks of certain areas.

4.2 Thermal Analysis

The thermal analysis is comprised of TGA to assess the decomposition temperature of the glycosides was presented in the following sub section.

4.2.1 Thermogravimetric Analysis (TGA)

Figure 4.5 shows the TGA thermograms for β-Glc-$C_{10}C_6$ and β-Mal-$C_{10}C_6$ heated at a constant rate of 5°C min^{-1}. The initial decomposition temperature of β-Glc-$C_{10}C_6$ was 200°C, while the major weight loss began rapidly at 280°C, leaving a residue of 3.2% at 500°C. The corresponding DTG curve indicated two peaks: a small peak at 234°C and a

large peak centred at 340°C, the latter likely due to the remaining weight loss. In the case of its maltoside counterpart, the weight loss started at 300°C and the corresponding DTG thermogram showed a peak centred at 337°C. The residual percentage of 10.2% was obtained at 500°C for β-Mal-$C_{10}C_6$.

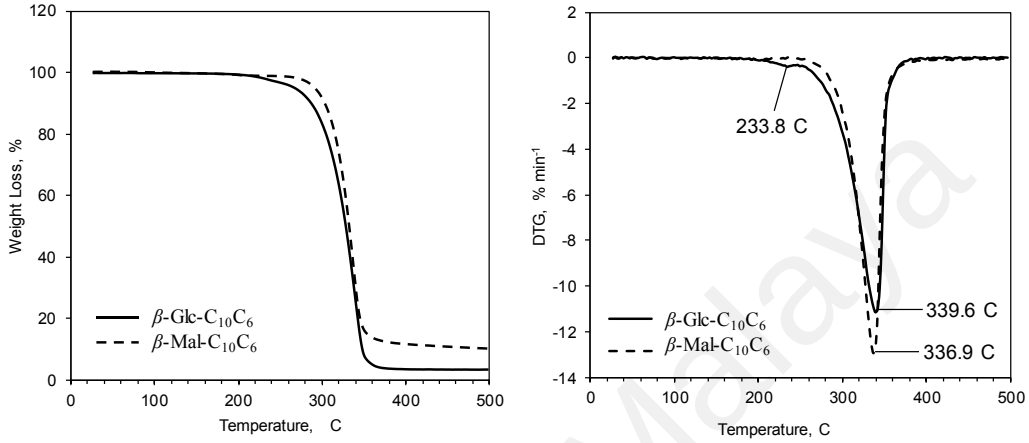

Figure 4.5 : (a) TGA and (b) DTG thermograms of β-Glc-$C_{10}C_6$ and β-Mal-$C_{10}C_6$ at a heating scan rate of 5°C min^{-1}.

The minor DTG peak at 234°C of β-Glc-$C_{10}C_6$ was likely due to the cleavage of the glycosidic bond, also known as transglycosylation. This led to the formation of oligosaccharides and loss of alcohol, a process commonly observed around 200–300°C (Hengemihle et al., 1984; Kawamoto et al., 2014) . The subsequent DTG peak which centred at 340°C could be associated with the fragmentation of the carbohydrates into a complex mixture of low-molecular-weight organic compounds and volatile products (Hengemihle et al., 1984; Kawamoto et al., 2014; Shafizadeh, 1982). As for β-Mal-$C_{10}C_6$, only a single DTG peak was observed at 337 °C which was due to the dissociation of the carbohydrate compounds. The minor DTG peak resulting from transglycosylation within the expected temperature range was not observed in maltoside. The presence of an extra $\alpha(1\rightarrow)$ glycosidic linkage that connected the two glucose units together in maltoside possibly required more heat for the process. That being the case, it

may have occurred at a slightly higher temperature and overlapped with the major thermal decomposition.

The remaining residue at 500°C represented by 3.2% and 10.2% for *β*-Glc-$C_{10}C_6$ and *β*-Mal-$C_{10}C_6$ respectively showed that the latter produced a higher percentage of char which could be correlated by an increase in saccharide units from monosaccharide (glucose) to the disaccharide (maltose). The summarized TGA data are tabulated in Table 4.3.

Table 4.3 : Data of thermal degradation of *β*-Glc-$C_{10}C_6$ and *β*-Mal-$C_{10}C_6$.

Sample	Temperature of Initial Decomposition (°C)	Temperature of Final Decomposition (°C)	Temperature of Maximum Decomposition Rate (°C)	Percent of Weight Loss (%)
***β*-Glc -$C_{10}C_6$**	200	260	234	3.0
	280	380	340	93.8
***β*-Mal-$C_{10}C_6$**	300	390	337	89.8

4.3 Liquid Crystal Characterization

The characterization of liquid crystal phase was conducted with the techniques described in Chapter 3 namely OPM and SAXS. OPM is a helpful technique in determining the liquid crystalline phase identity exhibited by the glycosides and SAXS acts as a quantitative analysis to evaluate the structural parameter of mesophase observed from OPM.

4.3.1 Optical Polarizing Microscopy (OPM)

Figure 4.6 shows the textures exhibited by the glycosides in thermotropic and lyotropic conditions. Upon heating, the anhydrous *β*-Glc-$C_{10}C_6$ and *β*-Mal-$C_{10}C_6$ turned to isotropic phase at 57°C and 189°C respectively (see Table 4.4), a finding comparable with

previously-reported data to within error. The latter had a higher clearing temperature, T_c than the former due to a large number of headgroup which increased the chance of hydrogen bonding in the molecules, resulting on a higher T_c.

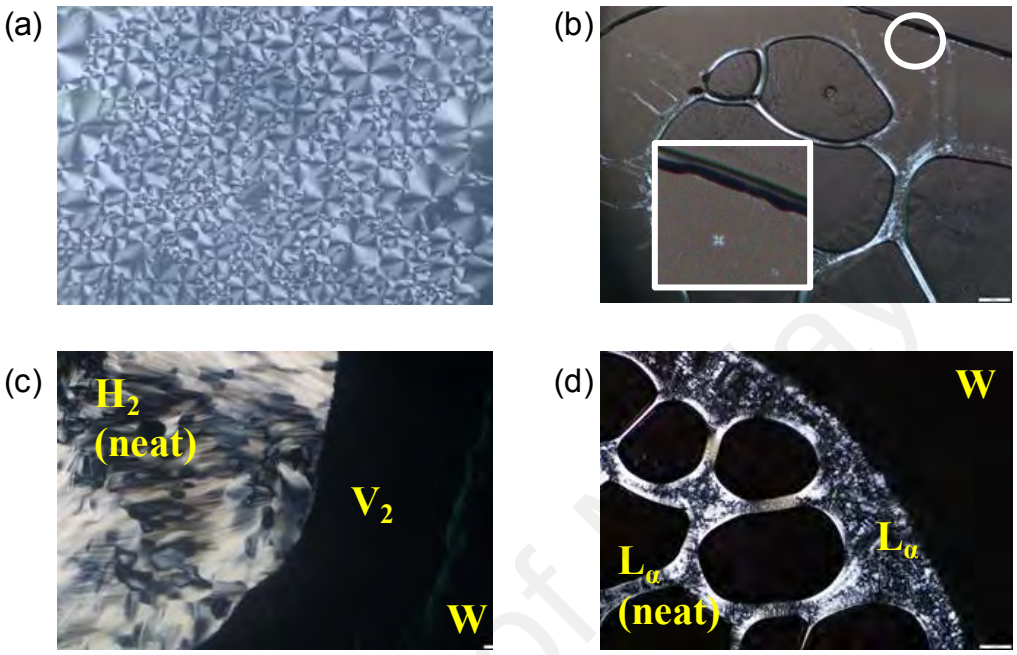

Figure 4.6: OPM textures of (a) H_2 of dry *β*-Glc-$C_{10}C_6$ (× 10); (b) L_α of dry *β*-Mal-$C_{10}C_6$ (× 10). The inset shows the coexistence of maltese cross (highlight white). The OPM micrograph of (c) V_2 of hydrated *β*-Glc-$C_{10}C_6$ (× 10); and (d) L_α of hydrated *β*-Mal-$C_{10}C_6$ (× 10) were obtained in water contact penetration scan. W denotes water and all textures were captured at room temperature.

On cooling at a scan rate of –2°C min^{-1}, *β*-Glc-$C_{10}C_6$ displayed a fan-shaped birefringent texture as shown in Figure 4.6(a). The strong birefringence appearance with larger domains are usually associated with inverse hexagonal phase. Evidently, the chain branching in Guerbet glycoside increased the hydrophobic volume, thus the shape factor would be greater than 1. This, according to Israelachvili (Israelachvili, 1994), favoured the formation of inverse structures.

Upon cooling the *β*-Mal-$C_{10}C_6$, an oily streak texture with birefringent bands across a pseudo-isotropic region were observed (see Figure 4.6 (b)). In the same figure, a maltese

cross structure was also seen which denotes the formation of L_α phase in β-Mal-$C_{10}C_6$. The formation of lamellar phase was preferred by β-Mal-$C_{10}C_6$ since the larger sugar head group resulted in a linear shape and hence favoured the formation of lamellar structures. In addition, branched-chain maltosides favoured a lamellar phase due to strong electrostatic interaction via hydrogen bonding in the hydrophilic region.

When water was added to the neat surface of the dry β-Glc-$C_{10}C_6$ at the room temperature, a viscous isotropic phase had replaced the birefringent texture at the higher water content (Figure 4.6(c)) which indicates the formation of the cubic phase. This mesophase was expected to belong to the inverse type due to molecular structure of β-Glc-$C_{10}C_6$ as discussed earlier. However, the L_α texture of β-Mal-$C_{10}C_6$ remained in the presence of water as shown in Figure 4.6(d).

Table 4.4 : The transition temperature of thermotropic study obtained from OPM for both samples. The temperature measurement error is $\pm$ 1°C.

Sample	Phase Type	Clearing Temperature (°C)
β-Glc-$C_{10}C_6$	H_2	57
β-Mal-$C_{10}C_6$	L_α	189

4.3.2 Small Angle X-ray Scattering (SAXS)

The scattering pattern of SAXS provides a proper identification of the liquid crystal phases observed by OPM. For example, SAXS provides information on the coexistence of liquid crystalline phases where one or both phases are isotropic, which cannot be established by OPM. Furthermore, SAXS enables determination of structural information of these mesophases. The SAXS pattern of the anhydrous β-Glc-$C_{10}C_6$ at 30°C revealed three peaks with the spacing ratios of √1, √3 and √ which was characteristic of H_2 phase (Figure 4.7(a)) with lattice parameter of 28.3 Å. Meanwhile, β-Mal-$C_{10}C_6$ (Figure 4.7 (b))

showed a the typical scattering pattern of L_α phase which was characterized by the reflections of 1, 2 and 3 having a lattice parameter value of 31.1 Å.

Previously, the partial binary phase diagram of β-Glc-$C_{10}C_6$ (Zahid et al., 2013) and β-Mal-$C_{10}C_6$ (Saari et al., 2018) have been reported. Based on the reported works, the excess water points for β-Glc-$C_{10}C_6$ and β-Mal-$C_{10}C_6$ were estimated at around 32% (w/w) and 40% (w/w) respectively. The higher water saturation point in Guerbet maltoside than its glucoside counterpart is anticipated due to a stronger intermolecular hydrogen bond between water molecules and the –OH groups in the maltose sugar. For a quantitative lyotropic investigation, three water concentrations have been chosen for SAXS measurements as well as for rheological study in the following section. The water concentrations of 30% (w/w) was selected to represent the lower hydration level (before excess water condition), while 50% (w/w) and 80% (w/w) were designated to describe the system of excess water condition. The published partial phase diagrams for both β-Glc-$C_{10}C_6$ and β-Mal-$C_{10}C_6$ showed that all phases observed were invariant with the temperatures investigated i.e. 25°C –60°C, which suggests that there was no significant removal of water molecules from the sugar head group as a result of the strong hydrogen bonding between the OH groups of the glycolipids and water.

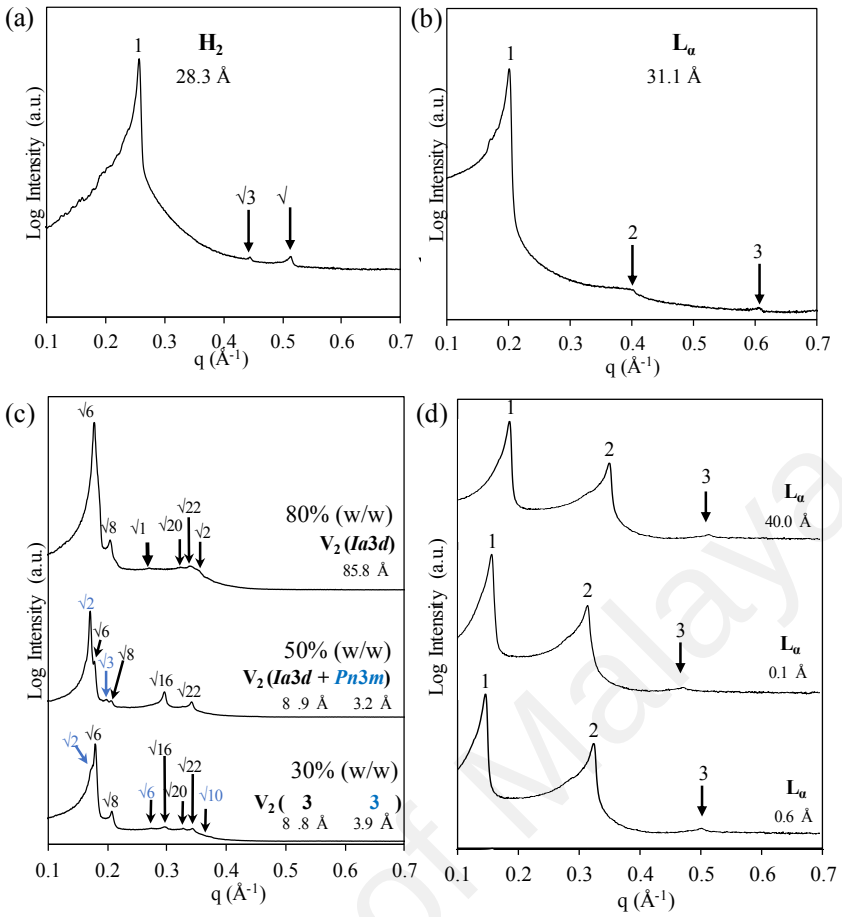

Figure 4.7: SAXS patterns under thermotropic and lyotropic conditions at 30°C indicating (a) H_2 phase of dry *β*-Glc-$C_{10}C_6$; (b) L_α phase of dry *β*-Mal-$C_{10}C_6$; (c) inverse bicontinuous cubic phases of hydrated *β*-Glc-$C_{10}C_6$ and (d) L_α phases of hydrated *β*-Mal-$C_{10}C_6$. In (c) and (d) the various water concentrations of 30% (w/w), 50% (w/w) and 80% (w/w) are represented by bottom line, middle line top line, respectively. The corresponding lattice parameters are also reported in the figure.

Figure 4.7(c) shows the scattering patterns of hydrated *β*-Glc-$C_{10}C_6$. At 30% (w/w), the SAXS patterns formed an *Ia*3*d* cubic phase that coexisted with *Pn*3*m*. This phase coexistence remained at excess water condition of 50% (w/w). The observation of unusual *Ia*3*d*/*Pn*3*m* coexistence of *β*-Glc-$C_{10}C_6$ at 30% (w/w) and in excess water of 50% (w/w) was backed up by the calculated ratio $a_{Ia3d/Pn3m}$ (1.614 and 1.592, respectively). This agreed within a few percent with the expected Bonnet relation $a_{Ia3d/Pn3m} = 1.576$. At 80% (w/w), a stable *Ia*3*d* cubic phase was detected. The formation of an *Ia*3*d* phase is rare since this phase has the most compact space filler and normally occurs at reduced

hydration (Seddon et al., 2006) The chain branching may play a role in stabilizing the *Ia3d* structure in excess water due to the presence of chiral and asymmetric *β*-carbon at C-2 position (Zahid et al., 2013).

In the case of *β*-Mal-$C_{10}C_6$ (Figure 4.7(d)), the L_α phase dominated the lyotropic phase behaviour at these water concentrations. This phase formation is usually governed by the hydrated head group whereby all the seven hydroxyls in maltose are surrounded by extensive water shell, hence, increasing the head group area triggering the formation of the lamellar structure in their fully hydrated system (Hashim et al., 2012). The formation of hydrogen bonding between water molecules and all hydroxyl groups in the head group results in larger effective headgroup area diminishing the hydrophobic chain effect and hence lead to zero mean curvature. The phase assignments and lattice parameters of the glycosides in dry and at selected water concentrations are shown in Table 4.5.

Table 4.5 : Phase assignments and lattice parameters at 30°C for *β*-Glc-$C_{10}C_6$ and *β*-Mal-$C_{10}C_6$ in dry and at selected water concentrations. The error in lattice parameter is ± 0.1 Å.

Water concentration	Phase (Lattice Parameter)	
	β-Glc-$C_{10}C_6$	*β*-Mal-$C_{10}C_6$
0 % (w/w)	H_2 (28.3 Å)	L_α (31.1 Å)
30 % (w/w)	*Ia3d* & *Pn3m* (85.8 Å & 53.9 Å)	L_α (40.0 Å)
50 % (w/w)	*Ia3d* & *Pn3m* (85.9Å & 53.2 Å)	L_α (40.1 Å)
80 % (w/w)	*Ia3d* (85.8 Å)	L_α (40.6 Å)

4.4 Rheological Behaviour

The flow behaviour of all liquid crystalline phases in thermotropic and lyotropic conditions formed by *β*-Glc-$C_{10}C_6$ and *β*-Mal-$C_{10}C_6$ was investigated in terms of viscosity test, amplitude sweep and frequency sweep. The viscosity test was to evaluate the viscosity of mesophase under shear stress. The amplitude sweep was carried out to

determine the linear viscoelastic (LVE) limit of the mesophase to ensure its structure was not destroyed in frequency sweep. Finally, the frequency sweep investigation determined the macroscopic properties, such as the ability of these liquid crystalline structures to store (*G'*) and dissipate (*G"*) energy which would be useful to understand their stability, processing, transportation, and storage (Matsumoto et al., 2009). Three different water concentrations i.e. 30% (w/w), 50% (w/w), and 80% (w/w) were selected to comprehend the lyotropic rheological behaviour. The effect of temperature in these experiments was also studied and deserves some discussion.

4.4.1 Viscosity Test

The viscosity test of the thermotropic liquid crystal phase was first discussed followed by the discussion of the viscosity of lyotropic mesophase at selected water concentrations. The experimental procedure was carried out as described in Chapter 3.

Thermotropic Study

The typical variation of the viscosity, η versus shear rate, $\dot{\gamma}$ is observed for H_2 phase and L_α phase of the extensively dried β-Glc-$C_{10}C_6$ and β-Mal-$C_{10}C_6$ (respectively) as shown in Figure 4.8. The results indicated that the viscosity decreased when the shear rate increased which implied shear thinning behaviour, also known as pseudoplastic behaviour. In general, lipid layers in the lamellar phase could move over each other easily. However, movement along the uni-axis (perpendicular to lipid layers) would be expected to be much more difficult since it involved distortion or re-alignment of bilayers (Tiddy, 1980). In the case of the hexagonal phase, the rods were expected to move in direction of the long axis as easily as lamellar phase lipid layers can slide over another, but to a lesser extent. Nevertheless, movement perpendicular to this direction involved modification of the hexagonal packing, disruption of the rods and was anticipated to be more difficult

than the parallel movement (Tiddy, 1980). Thus, the viscosity of the hexagonal phase would be expected to be relatively higher than the lamellar phase.

However, when comparing the plots of the H_2 phase of β-Glc-$C_{10}C_6$ at 25°C and 37°C with that of the L_α phase of β-Mal-$C_{10}C_6$ (see Figure 4.8 (a) and (b)), the results showed that the latter has higher viscosity. This unexpected behaviour was most probably due to the latter has seven hydroxyl groups in its sugar head which increases the hydrogen bond network and cause more resistance for the L_α phase to flow. On the other hand, the glucoside counterpart had monosaccharide head group with only four hydroxyl groups available with less hydrogen bond network and hence the H_2 phase of β-Glc-$C_{10}C_6$ is more fluid. The hydrogen bonds in self-assembly of glycolipids formed intralayer (formed between two sugars within the layer) and interlayer hydrogen bonds (formed between two neighbouring layers). This observation was supported by a molecular dynamics simulation of an anhydrous lamellar structure, which showed that maltoside had intermolecular hydrogen bonds formed between the headgroups (i.e. both intra- and interlayer) ranging from 6.7 to 7.2 (Manickam Achari et al., 2012). This value is almost double than that observed from a thermotropic lamellar simulation for glucoside (~4.8) (Ahmadi et al., 2014). In glucose and maltose headgroups the interlayer hydrogen bonds per lipid had the same value of 3.1. On the other hand, their intralayer hydrogen bonds per lipid differed considerably, where the former was 1.1 while the latter was 3.9 (Ahmadi et al., 2014; Manickam Achari et al., 2012). These reported findings showed that the intralayer hydrogen bonds played a significant role in making the L_α phase of β-Mal-$C_{10}C_6$ more viscous than the H_2 phase of β-Glc-$C_{10}C_6$.

It was also observed that when the temperature increases, the viscosity decreased by a factor of 10 in both H_2 and L_α phases. This could be explained by the fact that heat made the mesophases flow easily. As more heat was added into the system, the thermal motion

will destroy the delicate ordering of liquid crystalline phases (Chandrasekhar, 1992) , thus the viscosity decreased as a function of temperatures. Such a trend has been observed in several systems (Barra & Mitchell, 2013; Németh et al., 1998). It is important to note that the selected measurement temperatures for each compound was lower than their T_c value determined from OPM. Although the T_c of β-Mal-$C_{10}C_6$ is higher, at ~189°C, the temperature of measurements for β-Mal-$C_{10}C_6$ was limited to 90°C as the sugar compound experienced browning or caramelization due to the long duration of test which was consistent with anomalous behaviour observed in strain test at the specific temperature.

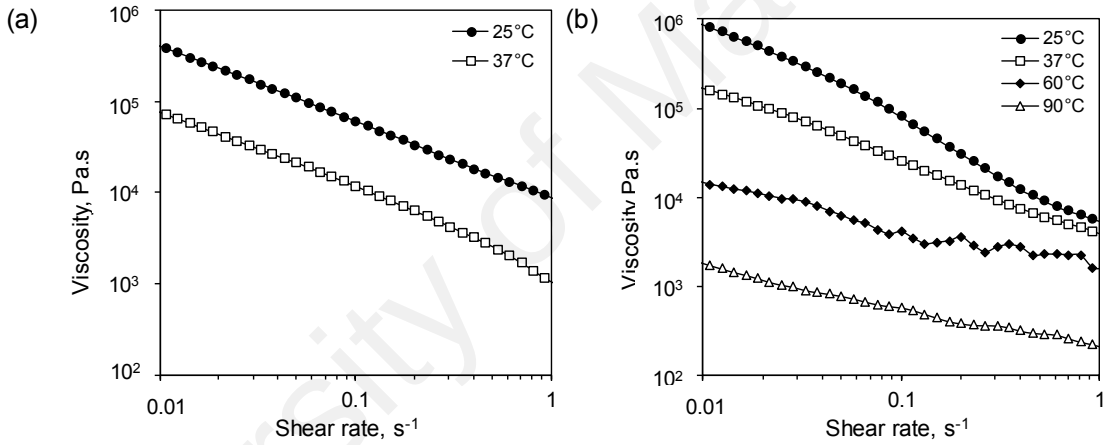

Figure 4.8 : Viscosity,η versus shear rate,$\dot{\gamma}$ for (a) H_2 phase of β-Glc-$C_{10}C_6$ and (b) L_α phase of β-Mal-$C_{10}C_6$ at selected temperatures.

Lyotropic Study

The flow behaviour of the lyotropic V_2 of β-Glc-$C_{10}C_6$ and L_α phase of β-Mal-$C_{10}C_6$ formed at the selected water concentrations are depicted in Figure 4.9 and Figure 4.10 respectively. The lyotropic liquid crystal phases also behaved as a shear thinning fluid like those of the thermotropic mesophases. With the exception of *Ia*3*d* cubic phase of 80% (w/w) at 25°C, all other lyotropic cubic and lamellar viscosities were much lower than that of the thermotropic mesophases over the whole range of shear rate.

The cubic phase is an isotropic liquid crystal phase known to be a more rigid and viscous phase than the lamellar and hexagonal phase. Understanding the rheological properties of cubic phase is also challenging since their response to stress is the result of several relaxation mechanisms. For instance, Montalvo, et al. (Montalvo et al., 1996) reported that the viscosity of cubic phase made from cationic surfactant, hexadecyltrimethylammonium bromide (CTAB) i.e. CTAB/benzyl alcohol/water system could not be measured from flow experiments, even though it showed very interesting elastic properties. Nevertheless, in this work, we were able to measure the viscosity of lyotropic cubic phase of the non-ionic Guerbet glucoside as shown in Figure 4.9. The presence of water in this system provided more liquidity to the system as the hydroxyl groups in the sugar head form hydrogen bond with water molecules.

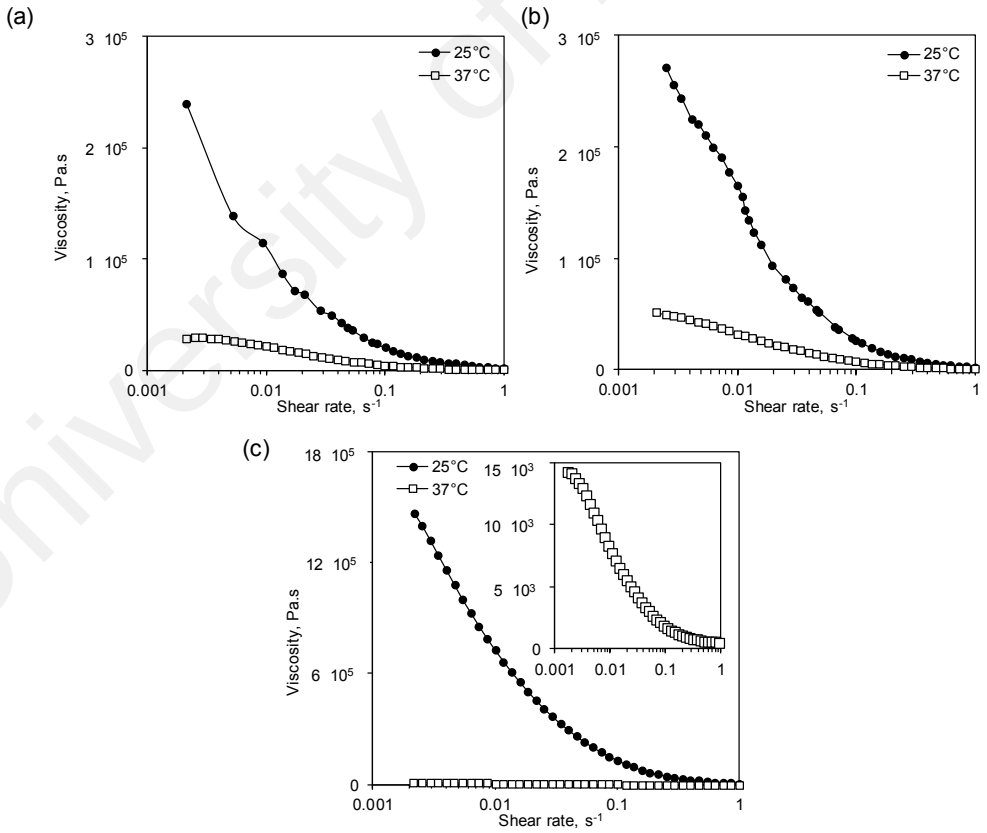

Figure 4.9 : Viscosity,η versus shear rate,$\dot{\gamma}$ for β-Glc-$C_{10}C_6$ at different water concentrations of (a) 30% (w/w), (b) 50% (w/w) and (c) 80% (w/w) and at selected temperatures. The inset shows the larger scale of shear thinning behaviour for 80% (w/w) cubic *Ia3d* phase at 37°C.

At 25°C, the coexisted *Ia*3*d* and *Pn*3*m* phase formed at lower hydration level and before excess water point i.e. 30% (w/w) has the lowest viscosity compared to the excess water condition samples i.e. the two-phase coexistence of cubic *Ia*3*d* and *Pn*3*m* phases at 50% (w/w) and cubic *Ia*3*d* phase at 80% (w/w). The effect of water concentration for other non-ionic surfactant/water systems (Soltero et al., 2007; Zhao et al., 2011) which mostly focuses on below excess water samples reported that viscosity decreased with increasing water concentration. Nonetheless, the higher viscosity values observed for the cubic phase at 50% (w/w) and 80% (w/w) had to be expected since the cubic phase started to coexist with a water phase. In this condition, large interfaces between the cubic and water phases were formed, which were responsible for the increase in viscosity (Mezzenga et al., 2005). Generally, viscosity reduced significantly once the temperature was increased to 37°C. Despite showing the highest viscosity at 25°C, the *Ia*3*d* cubic phase of 80% (w/w) had the lowest viscosity at 37°C. The result suggested that the temperature effect was more significant at a higher hydration level, hence giving more fluidity to the cubic *Ia*3*d* cubic phase of 80% (w/w) system.

It is well known that lamellar aggregates are able to slide between bilayers and into flowing condition when stress is applied (Zhao et al., 2011). The added water acts as lubricant, and thus, enhancing fluidity to the system. As a result, the viscosities of lyotropic lamellar phase of β-Mal-$C_{10}C_6$ at selected water concentrations (see Figure 4.10) were much lower than the thermotropic lamellar phase (see Figure 4.8(b)). At 25°C, the lowest viscosity value was observed for the L_α phase at 30% (w/w). The viscosity slowly increased at 50% (w/w) and the highest viscosity value was observed for L_α phase at 80% (w/w). At these excess water condition, L_α phase coexisted with the water phase and introduced more interfaces between the lamellar and water phases, resulting in an increase in the viscosity. Unlike the thermotropic lamellar phase, the lyotropic lamellar phase had minimal temperature effect on the viscosity over the whole range of shear rate.

Exceptionally, L_α phase at 80% (w/w) exhibited notable reduction in viscosity when the sample was heated at 37°C and 60°C. An anomalous viscosity was observed for this sample at 90°C which might imply that water evaporation had occurred, causing it to be less fluid and hence, increasing its viscosity.

The lyotropic L_α phase of maltoside had a lower viscosity compared to lyotropic V_2 phase of glucoside. This is reasonable because the lipid layers could move over one another easily in the lamellar phase, reducing the viscosity to a smaller value than in the the cubic phase which had less easy flow direction because the aggregates repelled one anoother in a three-dimensional network. In addition, more hydroxyl groups in the *β*-Mal-$C_{10}C_6$ could form intermolecular hydrogen bonds with water molecules, thereby increasing the fluidity of the L_α phase.

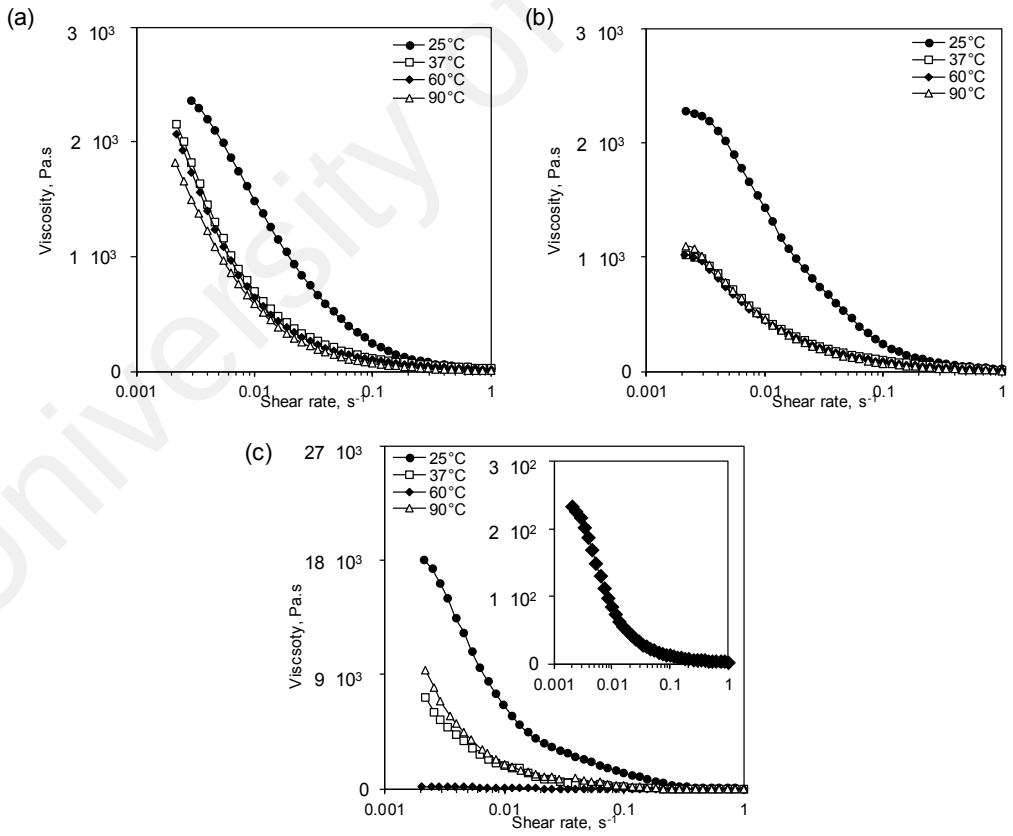

Figure 4.10 : Viscosity,η versus shear rate,$\dot{\gamma}$ for *β*-Mal-$C_{10}C_6$ at different water concentrations of (a) 30% (w/w) (b) 50% (w/w) (c) 80% (w/w) and at selected temperatures. The insets show the larger scale of shear thinning behaviour at designated temperatures.

4.4.2 Amplitude Sweep

Amplitude sweep is generally used to describe the deformation behaviour of the mesophase and determine the limit of linear viscoelastic (LVE) region. When *G' > G"*, the sample exhibit gel-like or solid structure and can be called as viscoelastic solid material. If *G" > G'*, then the sample display fluid structure and it can be called as viscoelastic fluid (Mezger, 2014).

Thermotropic Study

The LVE region for the H_2 phase of *β*-Glc-$C_{10}C_6$ is shown in Figure 4.11(a). The plot shows that the stiffness of this phase differed by a factor of 10 in the *G'* values (20000 Pa at T = 25°C and 2000 Pa at T = 37°C). This indicated that the force needed to deform the H_2 phase at lower temperature was one hundred times greater than at the higher temperature. It could also be seen that at 25°C, *G'* was greater than *G"* which meant that the phase was a viscoelastic solid which explained the significantly higher force needed to deform it. Interestingly, as the temperature increased to 37°C, *G"* was greater than *G'* which indicated that the sample was now behaving as a viscoelastic fluid. This transformation might be related to the fact that *β*-Glc-$C_{10}C_6$ had the low clearing temperature of 59°C, thus a slight increase in temperature would result in a transition to isotropic state, which made the sample flow easily.

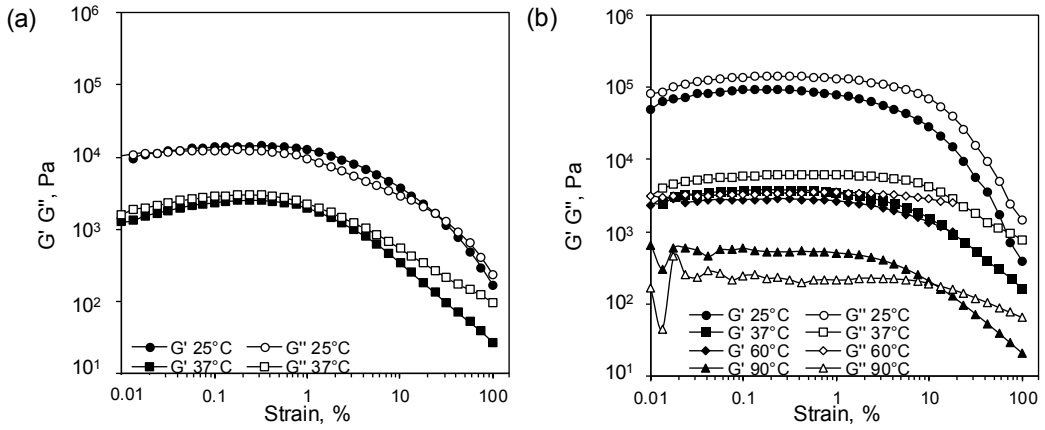

Figure 4.11 : Storage modulus, *G'* and loss modulus, *G"* versus strain for (a) H_2 phase of *β*-Glc-$C_{10}C_6$ and (b) L_α phase of *β*-Mal-$C_{10}C_6$ at selected temperatures.

With the exception of temperature at 90°C, *G"* dominated *G'* at all temperatures indicating the L_α phase of *β*-Mal-$C_{10}C_6$ displayed a fluid structure known as viscoelastic liquid (see Figure 4.11(b)). Although it appeared to be solidified at room temperature, it is a hygroscopic material due to the presence of seven hydroxyl (–OH) group within the molecule. While the viscoelastic behaviour is a function of temperature, the LVE region mostly remains invariant (see Table 4.6) at the selected temperatures. However, Niraula and coworkers had reported that the width of the LVE region is a function of the length of the hydrocarbon tail (Niraula et al., 2004).

We noted the anomalous behaviour of L_α phase at 90°C i.e. *G'* larger than *G"*. This observed result indicaed that the sample underwent some degree of damage at high temperature and loses its liquid crystalline structure. The LVE region is tabulated in Table 4.6 as the reference for the strain in frequency sweep experiment. From the data, L_α phase of *β*-Mal-$C_{10}C_6$ was suspected of damage at 90°C and was not further discussed in subsequent experiments.

Table 4.6 : The LVE region limit of H_2 phase of *β*-Glc-$C_{10}C_6$ and L_α phase of *β*-Mal-$C_{10}C_6$ at selected temperatures.

Lipid	Mesophase	Temperature (°C)	LVE limit (%)
***β*-Glc-$C_{10}C_6$**	H_2	25	0.32
		37	0.24
***β*-Mal-$C_{10}C_6$**	L_α	25	0.32
		37	0.32
		60	0.32
		90	0.76

Lyotropic Study

Figure 4.12 shows the strain test of lyotropic cubic phase of *β*-Glc-$C_{10}C_6$ at different water concentrations which revealed the dominance of a solid-like behaviour over a wide range of water concentration since *G'* was greater than *G"* value. The *G'* value increased as a function of water concentration and temperature. It is also worth mentioning that the transition from elastic to viscous behaviour was delayed as the water concentration increased. The viscous behaviour of the coexisted *Ia*3*d* cubic phase at 30% (w/w) started to dominate at strain ~1% and it gradually increased to ~10% strain at 80% (w/w). Overall, the cubic structure started to rupture at around 0.1% as characterized by the steady decrease in the *G'* value. When the strain was approximately 3%, the viscous behaviour became dominant whereby *G"* value became greater than *G'* value particularly at 37°C. Hence, a strain value of 0.01% was selected for the frequency sweep test to ensure the integrity of the sample structure. *Ia*3*d* cubic phase at 80% (w/w) (see Figure .12(c)) showed a significant increase in G" followed by decreasing at a higher strain region. This effect is termed weak strain overshoot (Hyun et al., 2011) and it is related to the deformation of the *Ia*3*d* structure that underwent stiffening which required a greater deformation to break (Mendozza et al., 2019). The *Ia*3*d* cubic phase was reported to demonstrate higher rigidity than the *Pn*3*m* symmetry because the topological characteristics of the former had a more compact space filler than the latter (Speziale et

al., 2018). The presence of a lower rigidity *Pn*3*m* cubic phase in coexisted *Ia*3*d*/*Pn*3*m* system might have rendered this effect less pronounced in 30% (w/w) and 50%(w/w) samples.

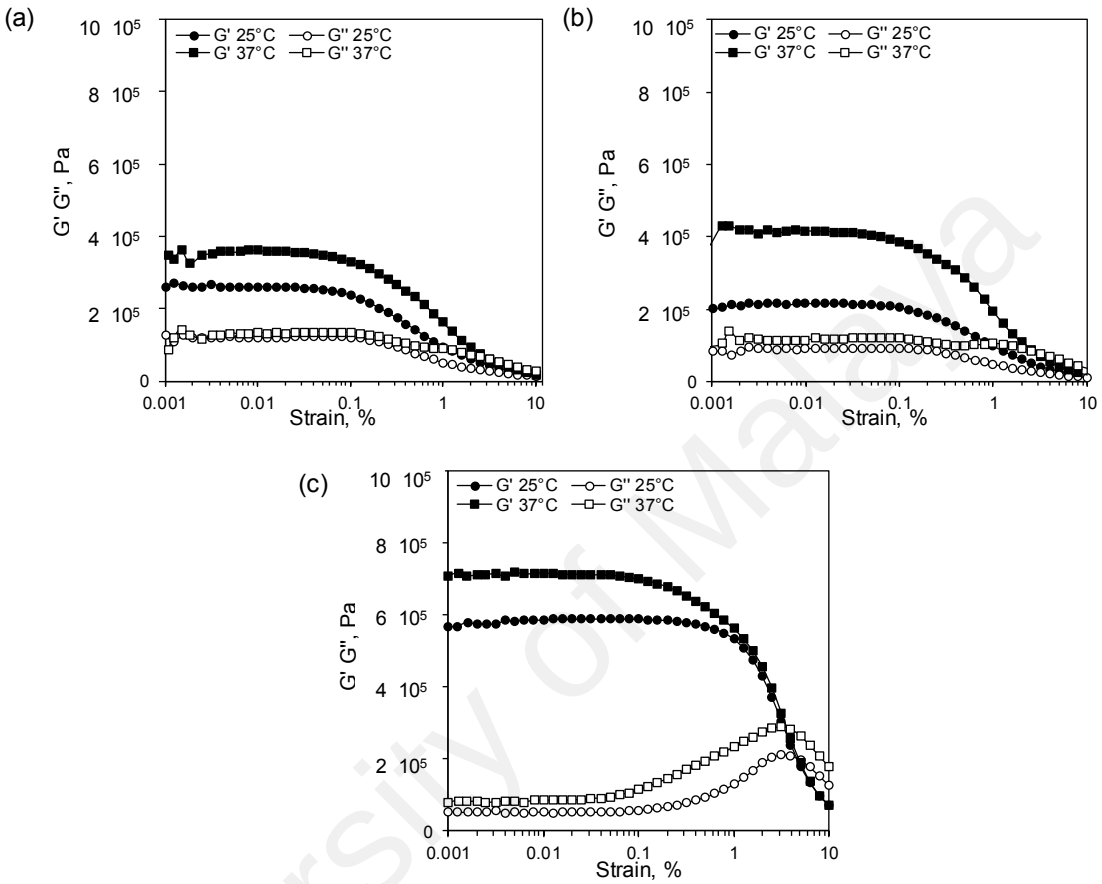

Figure 4.12 : Storage modulus, *G'* and loss modulus, *G"* versus strain for *β*-Glc-$C_{10}C_6$ at different water concentrations of (a) 30% (w/w) (b) 50% (w/w) and (c) 80% (w/w) and at selected temperatures.

The strain test for the L_α phase of *β*-Mal-$C_{10}C_6$ is shown in Figure 4.13. The result showed the dominance of *G'* over *G"* at all range tested, demonstrating the gel-like structure in this system. A similar result was reported by other researchers (Lauger et al., 1995; Montalvo et al., 1996; Németh et al., 1998). At 30% (w/w), *G'* was dominant over a wide range of strain. At middle water concentration of 50% (w/w), the storage moduli response became lower, implying less force was needed to disrupt the lamellar structure. Finally, at high water content of 80% (w/w), *G'* was steadily greater than *G"* at all

temperature tested. The measurement at 90°C has been excluded from discussion since evaporation of water was anticipated at high temperature.

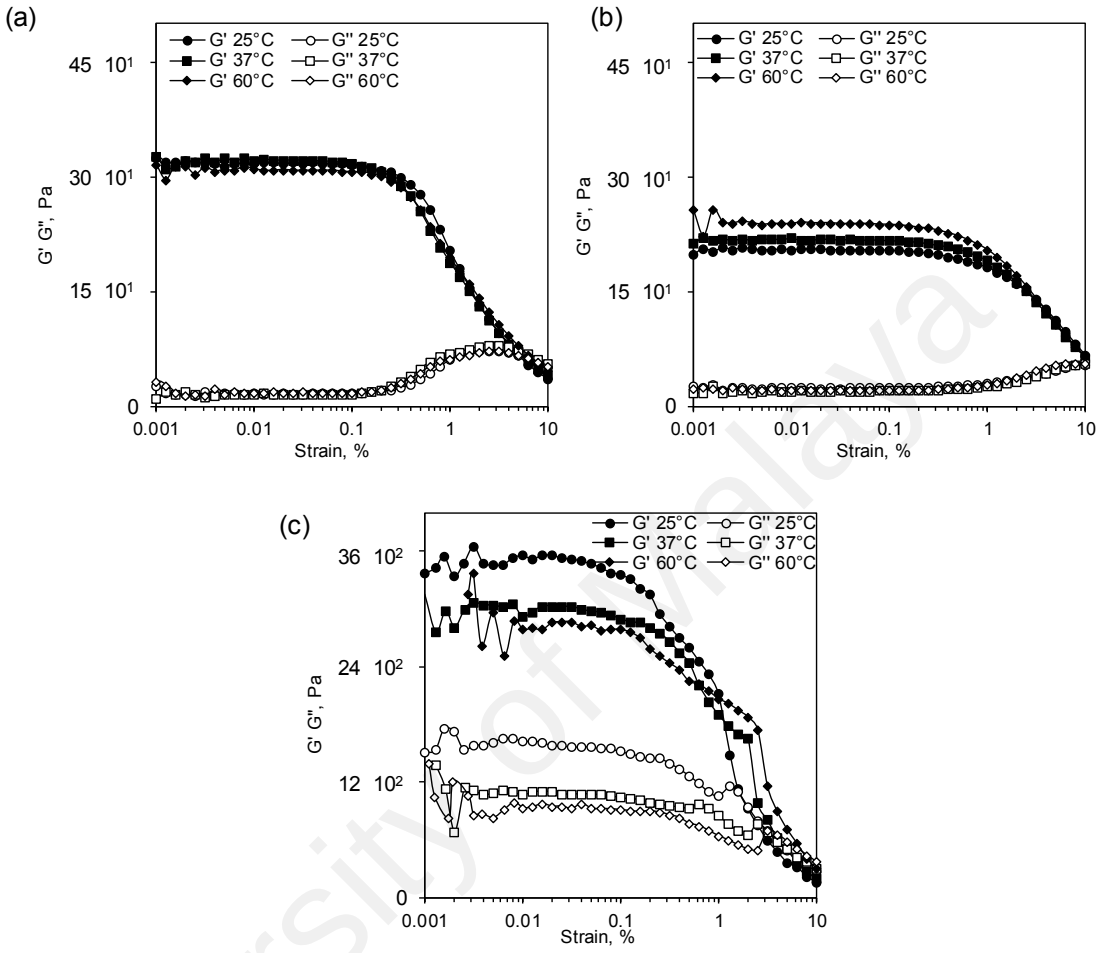

Figure 4.13 : Storage modulus, *G'* and loss modulus, *G"* versus strain for *β*-Mal-$C_{10}C_6$ at different water concentrations of (a) 30% (w/w) (b) 50% (w/w) and (c) 80% (w/w) and at selected temperatures.

4.4.3 Frequency Sweep

The general behaviour of a structured non-Newtonian fluid as a function of the shear frequency has been discussed in Figure 2.21 of Chapter 2. This figure is very useful in the interpretation of the response of all different liquid crystalline phases to frequency-dependent shear deformation in the linear viscosity regime (Mezzenga et al., 2005). By measuring the storage *G'* and loss *G"* moduli as a function of shear frequency, ω, we

would be able study the property of viscoelastic behaviour in materials (Speziale et al., 2018).

Thermotropic Study

The viscoelastic properties of the thermotropic phases for both glycolipids are shown in Figure 4.14. It is worth mentioning that the effect of pre-shear treatment is negligible in this work. Overall, *G'* and *G"* increased with the frequency, indicating that the H_2 and L_α phases followed the typical viscoelastic *G'*, *G"* response for non-Newtonian fluid at the selected temperatures. The values of *G'* and *G"* of H_2 phase exhibited different behaviours as the frequency increased (see Figure 4.14 (a)). At low frequencies, *G'* had a lower value than *G"*, and the dominant behaviour was viscoelastic fluid. As the frequency increased, both *G'* and *G"* at 25°C and 37°C increased, and eventually, at a specific point, *G'* overtook *G"*. The inverse of the frequency, ω, at which this crossover occurred is called the longest relaxation time, τ_{max}. The τ_{max} value referred to the characteristic time at which the structured fluid relaxes back to the equilibrium configuration when perturbed by shear oscillations (Mezzenga et al., 2005). The values of crossover at 25°C and 37°C for this H_2 phase of were ω = 0. 6 rad s^{-1}; τ_{max} = 1.8 s and 1.8 rad s^{-1}; τ_{max} = 0.6 s respectively. At this point, *G'* was equal to *G"* and this behaviour was consistent with transition to flow behaviour (see Figure 2.21) which indicated that the H_2 phase of *β*-Glc-$C_{10}C_6$ exhibited a viscoelastic behaviour. Further increasing the frequency, *G'* had a higher value than *G"* and at this stage, the viscoelastic solid dominated. Within the permitted strain, only the viscous regime and transition-to-flow region were present and no significant rubbery plateau condition was observed in the H_2 phase.

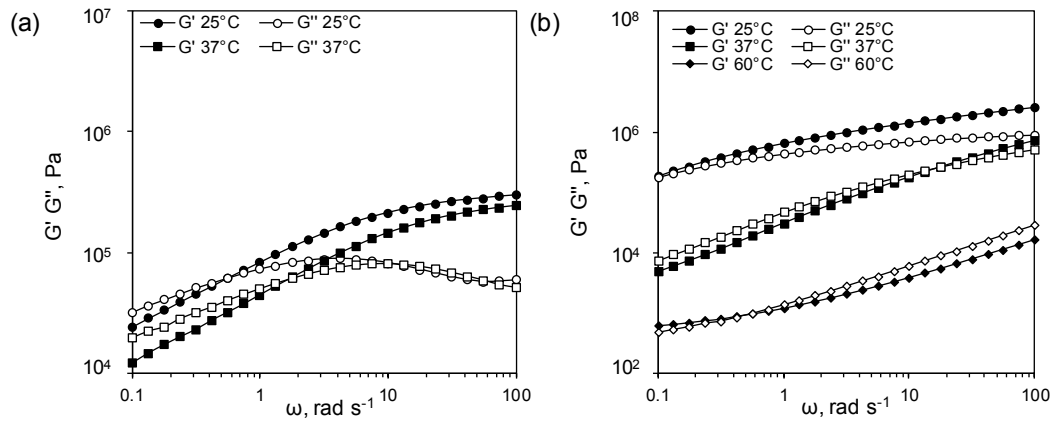

Figure 4.14 : Storage modulus, *G'* and loss modulus, *G"* versus angular frequency, ω for (a) H_2 phase of *β*-Glc-$C_{10}C_6$ and (b) L_α phase of *β*-Mal-$C_{10}C_6$ at selected temperatures. The strain for H_2 phase and L_α phase is 0.24% and 0.32% respectively.

From the graph shown in Figure 4.14(b), the *G'* and *G"* value for L_α phase of *β*-Mal-$C_{10}C_6$ consistently decreased by a magnitude of 10 as the temperature increased. At 25°C, *G'* had a higher value than *G"* over the whole angular frequency range indicating viscoelastic solid dominated. The presence of moisture in *β*-Mal-$C_{10}C_6$ at 25°C could explain the difference in viscoelastic behaviour during strain test (see Figure 4.11(b)) which could have occurred during sample loading. When the temperature increased to 37°C, *G"* was larger than *G'* at low and middle frequencies until a crossover was observed at 17.8 rad s^{-1} which corresponded to a τ_{max} value of 0.06 s. The behaviour was attributed to the transition to flow region in Figure 2.21 which implied that the L_α phase at 37°C behaves as a viscoelastic fluid capable of flowing under shear at low and middle frequencies but exhibiting an elastic behaviour at higher frequencies. At 60°C, *G'* had a higher value than *G"* at lower frequencies. *G"* increased smoothly until a crossover occurred at ω = 0.42 rad s^{-1} (τ_{max} = 2.4 s). The behaviour observed corresponded to the leathery transition (Figure 2.21) which indicated that the increase in *G"* was sharper than *G'* due to dissipation mechanism or short relaxation time responses (Mezzenga et al., 2005). Also, when comparing the stiffness between the thermotropic H_2 phase (*β*-Glc-$C_{10}C_6$) and L_α phase (*β*-Mal-$C_{10}C_6$), the former had lower stiffness than the latter. The

higher intermolecular hydrogen bond network in each maltose headgroup perhaps supported the observation.

Lyotropic Study

The frequency sweep measurements in the lyotropic cubic phase of β-Glc-$C_{10}C_6$ containing different water concentrations are presented in Figure 4.15. All water contents exhibited *G' > G"* in the whole range of frequency and temperature tested, an obserbation termed rubbery plateau. A similar trend was found in other cubic phase systems (Mendozza et al., 2019; Mezzenga et al., 2005; Speziale et al., 2018). Nevertheless, the *Ia*3*d* cubic phase of β-Glc-$C_{10}C_6$ at 80% (w/w) showed higher values of the G' than the coexisted *Ia*3*d* and *Pn*3*m* cubic phases at 30% (w/w) and 50% (w/w), which implied a higher strength and mechanical rigidity of the former over the latter (see Figure 8(d), blue markers). The relaxation time, τ_{max} of the lyotropic cubic phases of β-Glc-$C_{10}C_6$ could be ascribed as the diffusion time of the molecules of glycolipid at the water−glycolipid interface (Mezzenga et al., 2005; Speziale et al., 2018). However, these values could not be extracted in these cases due to experimental limitations. Nonetheless, these values were anticipated to be high since the transition to flow toward the viscous regime, which corresponded with the region after the crossover of the two curves when *G" < G'* happened at much lower frequencies. Currently, the explanation for relaxation time of cubic phase is still not well understood as it is thought that they experience several types of relaxation mechanisms which is still under debate (Jones & McLeish, 1995).

Similarly, Figure 4.16 shows *G'* dominating over the *G"* within the measured frequency range, indicating gel type structure in lyotropic L_α phase of β-Mal-$C_{10}C_6$. In general, the *G'* value at all water concentrations was nearly constant in the whole frequency or increased slightly at higher frequency. The frequency independent of lamellar phase has also been observed in other system. For instance, the flow study of

triethylene glycol mono *n*-decyl ether ($C_{10}C_3$) in C-orientation revealed similar time-independent behaviour (Medronho et al., 2007).

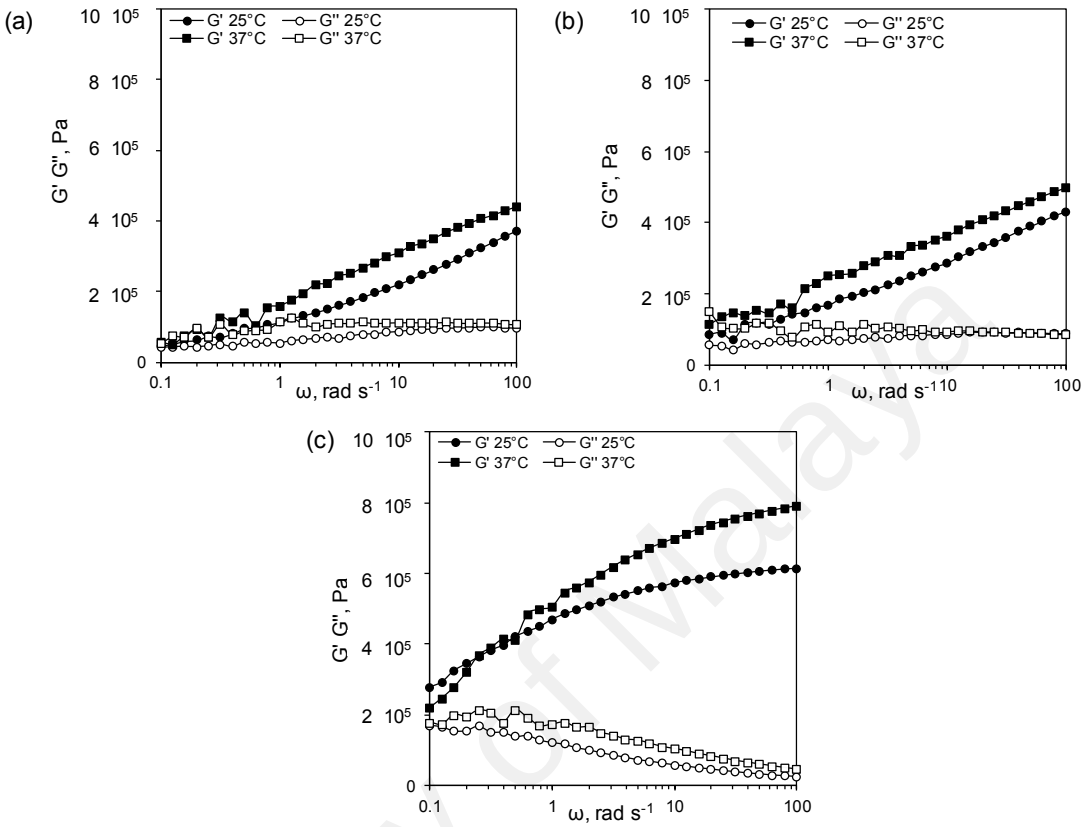

Figure 4.15 : Storage modulus, *G'* and loss modulus, *G"* versus angular frequency, ω for *β*-Glc-$C_{10}C_6$ at different water concentrations of (a) 30% (w/w), (b) 50% (w/w) and (c) 80% (w/w) and at selected temperatures.

Nevertheless, the structural strength was also influenced by water concentration. Even though the strain and time-dependent behaviour of lamellar phase showed gel-like behaviour, yet the lamellar phase itself was the most liquid-like among all lyotropic phases. This shows that the lamellar phase of *β*-Mal-$C_{10}C_6$/water had low structural strength. Moreover, the *G'* value was the highest at 80% (w/w) concentration which demonstrated the dependence of *G'* moduli on the water concentration, a common occurrence for the lamellar phase (Berni et al., 2002). From the *G'* and *G"* values, we could see that the lyotropic cubic phase (*β*-Glc-$C_{10}C_6$) was much stiffer than the lamellar phase of (*β*-Mal-$C_{10}C_6$).

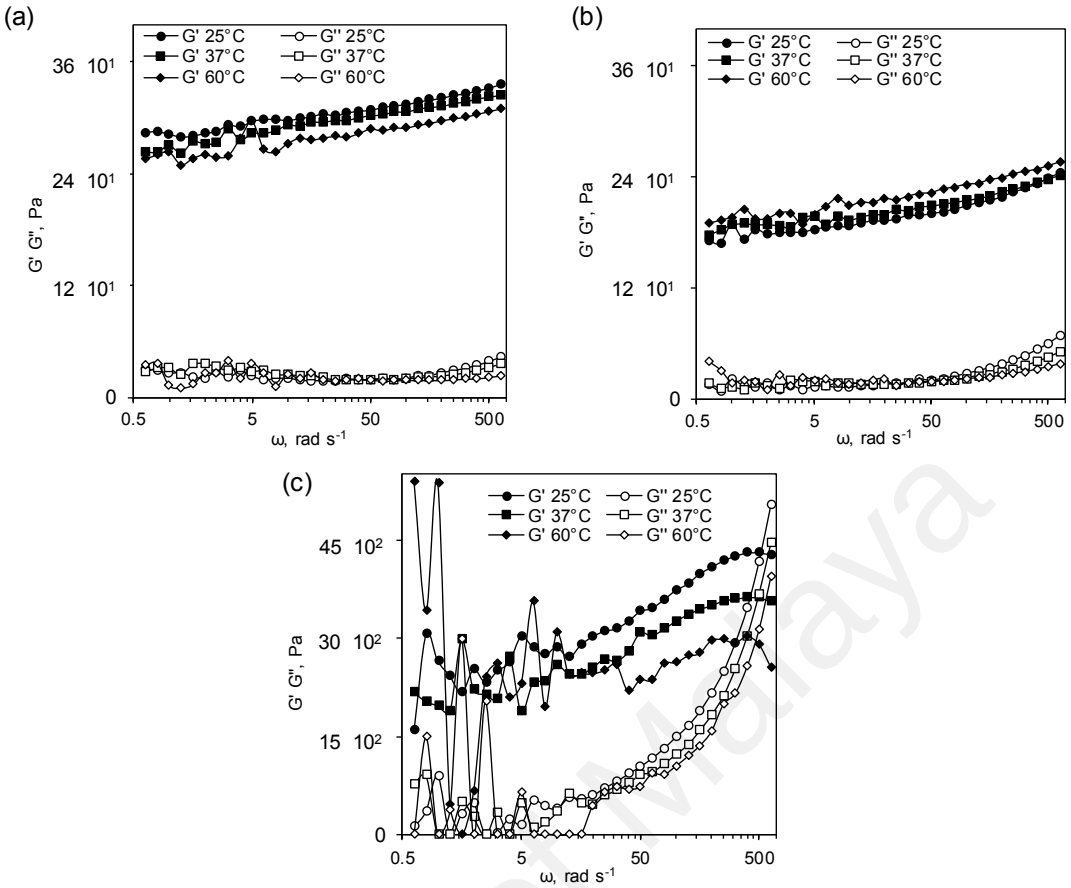

Figure 4.16 : Storage modulus, *G'* and loss modulus, *G"* versus angular frequency, ω for *β*-Mal-$C_{10}C_6$ at different water concentrations of (a) 30% (w/w), (b) 50% (w/w) and (c) 80% (w/w) and at selected temperatures.

CHAPTER 5: CONCLUSION

In this study, two Guerbet glycosides namely β-Glc-$C_{10}C_6$ and β-Mal-$C_{10}C_6$ were synthesized. The effect of different head group size on the mesophases and their rheological behaviour was investigated in the thermotropic and lyotropic condition. In anhydrous state, β-Glc-$C_{10}C_6$ having monosaccharide as the head group exhibited inverse hexagonal phase, H_2 while β-Mal-$C_{10}C_6$ having disaccharide as the head group exhibited lamellar phase, L_α. The maltoside showed higher clearing temperature, T_c than the glucoside due to the presence of extra glucose unit in the maltoside, hence, more energy was needed to break the hydrogen bonding resulting in higher T_c. In hydrated state, β-Glc-$C_{10}C_6$ formed viscous isotropic phase known as the cubic phase, V_2 while β-Mal-$C_{10}C_6$ remained as L_α phase at the selected water concentration.

Regardless of head group size, all mesophases exhibited shear thinning behaviour. However, H_2 phase of β-Glc-$C_{10}C_6$ showed lower viscosity than the L_α phase of β-Mal-$C_{10}C_6$ due to the structure difference in which seven hydroxyl groups in the latter increased the hydrogen bond network and cause more resistance for the L_α phase to flow. As expected, the lyotropic L_α phase of maltoside had lower viscosity than the lyotropic V_2 phase of glucoside. This observation was attributed by the lipid layers which could move over one another easily in the L_α phase. In addition, the formation of an intermolecular hydrogen bond between hydroxyl groups in maltoside with water molecules further increased the fluidity of this phase.

Subsequent frequency sweep which were obtained within the linear viscoelastic regime showed that the thermotropic H_2 (β-Glc-$C_{10}C_6$) L_α (β-Mal-$C_{10}C_6$) phases followed the typical viscoelastic *G'*, *G"* response for non-Newtonian fluid at the designated temperatures. In the lyotropic V_2 phase (β-Glc-$C_{10}C_6$) demonstrated that *G'* steadily increased as the frequency increase and it was expected to hit a plateau at a very high

frequency region. Meanwhile, the lyotropic L_α phase (β-Mal-$C_{10}C_6$) was frequency-independent with a lower magnitude of structural strength than the V_2 phase.

Based on the research objectives, the rheological behaviour of liquid crystalline phases of branched chain glycolipids have been successfully investigated. Each compound showed promising results for instance, both compounds displayed shear thinning behaviour which is a desirable characteristic for cosmeceutical applications however, in-depth studies on their dispersed phase i.e. droplet size is necessary to ensure system stability and product quality. Furthermore, the self-assembly exhibited by glycolipids has the potential to be utilized in drug delivery. For future work, proper investigation for the compatibility between the lipids, the desired drugs and biological system is necessary for the safety and performance efficiency.

REFERENCES

Abeygunaratne, S., Hashim, R., & Vill, V. (2006). Evidence for uncorrelated tilted layer structure and electrically polarized bilayers in amphiphilic glycolipids. *Physical Review E, 73*(1), 011916.

Ahmad, N., Ramsch, R., Esquena, J., Solans, C., Tajuddin, H. A., & Hashim, R. (2012). Physicochemical characterization of natural-like branched-chain glycosides toward formation of hexosomes and vesicles. *Langmuir, 28*(5), 2395–2403.

Ahmadi, S., Achari, V. M., Nguan, H., & Hashim, R. (2014). Atomistic simulation studies of the α/β-glucoside and galactoside in anhydrous bilayers: effect of the anomeric and epimeric configurations. *Journal of molecular modeling, 20*(3), 2165.

Araki, J., Wada, M., Kuga, S., & Okano, T. (1999). Influence of surface charge on viscosity behavior of cellulose microcrystal suspension. *Journal of Wood Science, 45*(3), 258–261.

Attard, G. S., Blackaby, W. P., & Leach, A. R. (1994). The aggregation behaviour of two structurally isomeric glycolipids. *Chemistry and Physics of Lipids, 74*(1), 83–91.

Barnes, H. A., Hutton, J. F., & Walters, K. (1989). *An introduction to rheology*. Amsterdam, Netherlands: Elsevier.

Barón, M. (2001). Definitions of basic terms relating to low-molar-mass and polymer liquid crystals (IUPAC Recommendations 2001). *Pure and Applied Chemistry, 73*(5), 845–895.

Barra, G., & Mitchell, J. R. (2013). The rheology of caramel. *Current Nutrition & Food Science, 9*(1), 15–25.

Berni, M. G., Lawrence, C. J., & Machin, D. (2002). A review of the rheology of the lamellar phase in surfactant systems. *Advances in Colloid and Interface Science, 98*(2), 217–243.

Blanchet, C. E., Hermes, C., Svergun, D. I., & Fiedler, S. (2015). A small and robust active beamstop for scattering experiments on high-brilliance undulator beamlines. *Journal of Synchroton Radiation, 22*(2), 461–464.

Boyd, B. J., Drummond, C. J., Krodkiewska, I., & Grieser, F. (2000). How chain length, headgroup polymerization, and anomeric configuration govern the thermotropic and lyotropic liquid crystalline phase behavior and the air−water interfacial adsorption of glucose-based surfactants. *Langmuir, 16*(19), 7359-7367.

Brooks, N. J., Hamid, H. A. A., Hashim, R., Heidelberg, T., Seddon, J. M., Conn, C. E., Mirzadeh Husseini, S. M., Zahid, N. I., & Hussen, R. S. D. (2011). Thermotropic and lyotropic liquid crystalline phases of Guerbet branched-chain-D-glucosides. *Liquid Crystals, 38*(11–12), 1725–1734.

Bushby, R. J., & Lozman, O. R. (2002). Discotic liquid crystals 25 years on. *Current Opinion in Colloid & Interface Science, 7*(5), 343–354.

Carlton, R. A. (2011). Polarized light microscopy, *Pharmaceutical microscopy* (pp. 7–64). New York, USA: Springer.

Chandrasekhar, S. (1992). *Liquid Crystals*. (2 ed.). Cambridge: Cambridge University Press.

Chandrasekhar, S., & Ranganath, G. (1990). Discotic liquid crystals. *Reports on Progress in Physics, 53*(1), 175–191.

Chen, Y., Ma, P., & Gui, S. (2014). Cubic and hexagonal liquid crystals as drug delivery systems. *BioMed Research International, 2014*(4), 815981–815981.

Collings, P. J., & Hird, M. (1997). *Introduction to liquid crystals: Chemistry and physics*. London, UK: CRC Press.

Costantino, V., Fattorusso, E., Mangoni, A., Di Rosa, M., & Ianaro, A. (1999). Glycolipids from sponges. VII. 1 simplexides, novel immunosuppressive glycolipids from the Caribbean sponge Plakortis simplex. *Bioorganic & Medicinal Chemistry Letters, 9*(2), 271–276.

Dembitsky, V. M. (2004). Astonishing diversity of natural surfactants: 1. Glycosides of fatty acids and alcohols. *Lipids, 39*(10), 933–953.

Demus, D., Goodby, J. W., Gray, G. W., Spiess, H. W., & Vill, V. (2011). *Handbook of liquid crystals, volume 2A: Low molecular weight liquid crystals I: Calamitic liquid crystals*. Weinheim, Federal Republic of Germany: John Wiley & Sons.

Demus, D., Goodby, J. W., Gray, G. W., Spiess, H. W., & Vill, V. (2011). *Handbook of liquid crystals, volume 2B: Low molecular weight liquid crystals II*. Weinheim, Federal Republic of Germany: John Wiley & Sons.

Dierking, I. (2003). *Textures of liquid crystals*. Weinheim, Federal Republic of Germany: John Wiley & Sons.

Dierking, I. (2014). Chiral liquid crystals: Structures, phases, effects. *Symmetry, 6*(2), 444–472.

Dimitruk, P., & Davidson, M. W. (2013). Miscroscope alignment. Retrieved on October 14th, 2018 from https://www.olympus-lifescience.com/en/microscope-resource/primer/techniques/polarized/polmicroalignment/

Ding, J., Tracey, P. J., Li, W., Peng, G., Whitten, P. G., & Wallace, G. G. (2013). Review on shear thickening fluids and applications. *Textiles and Light Industrial Science and Technology, 2*(4), 161–173.

Duer, M. J. (2008). *Solid state NMR spectroscopy: Principles and applications*. London, UK: Blackwell Science Ltd.

Elbadawi, A., Siddig, M., A. Siddig, A., Jan, L. S., & Radiman, S. (2015). Influence of nanosize silica particles on the rheological behaviour of lyotropic cubic phase of glucopone (APG) surfactant. *International Journal of Materials Science and Applications, 4*(2), 130–137.

Ermakov, S., Beletskii, A., Eismont, O., & Nikolaev, V. (2016). Brief review of liquid crystals, *Liquid crystals in biotribology: Synovial joint treatment* (pp. 37–56). Cham, Federal Republic of Germany: Springer.

Fairhurst, C. E., Fuller, S., Gray, J., Holmes, M. C., & Tiddy, G. J. (1998). Lyotropic surfactant liquid crystals, *Handbook of liquid crystal: High molecular weight liquid crystals* (pp. 341–392). Weinheim, Federal Republic of Germany: John Wiley & Sons.

Ferrer, M., Comelles, F., Plou, F. J., Cruces, M. A., Fuentes, G., Parra, J. L., & Ballesteros, A. (2002). Comparative surface activities of di- and trisaccharide fatty acid esters. *Langmuir, 18*(3), 667–673.

Friedel, G. (1922). Les états mésomorphes de la matière. *Annales de Physique, 9*(18), 273–474.

Gaisford, S., Kett, V., & Haines, P. (2016). *Principles of thermal analysis and calorimetry: 2nd edition*. Cambridge, UK: Royal Society of Chemistry.

George, J., & Sabapathi, S. (2015). Cellulose nanocrystals: Synthesis, functional properties, and applications. *Nanotechnology, Science and Applications, 8*, 45–54.

Goodby, J. W. (1998). Liquid crystals and life. *Liquid Crystals, 24*(1), 25–38.

Goodby, J. W., & Gray, G. W. (1998). Guide to the nomenclature and classification of liquid crystals, *Handbook of liquid crystal: Fundamentals* (pp. 17–23). Weinheim, Federal Republic of Germany: John Wiley & Sons.

Günther, H. (2013). *NMR spectroscopy: Basic principles, concepts and applications in chemistry*. Weinheim, Federal Republic of Germany: John Wiley & Sons.

Haines, P. J. (2012). *Thermal methods of analysis: Principles, applications and problems*. England, UK: Springer Science & Business Media.

Hakomori, S.-i. (2008). Structure and function of glycosphingolipids and sphingolipids: Recollections and future trends. *Biochimica et Biophysica Acta, 1780*, 325-346.

Hashim, R., Hashim, H. H. A., Rodzi, N. Z. M., Hussen, R. S. D., & Heidelberg, T. (2006). Branched chain glycosides: Enhanced diversity for phase behavior of easily accessible synthetic glycolipids. *Thin Solid Films, 509*(1–2), 27–35.

Hashim, R., Mirzadeh, S. M., Heidelberg, T., Minamikawa, H., Yoshiaki, T., & Sugimura, A. (2011). A reevaluation of the epimeric and anomeric relationship of glucosides and galactosides in thermotropic liquid crystal self-assemblies. *Carbohydrate Research, 346*(18), 2948–2956.

Hashim, R., Sugimura, A., Minamikawa, H., & Heidelberg, T. (2012). Nature-like synthetic alkyl branched-chain glycolipids: A review on chemical structure and self-assembly properties. *Liquid Crystals, 39*(1), 1–17.

Hashim, R., Zahid, N. I., Aripin, N. F. K., Ogawa, S., & Sugimura, A. (2018). Dry thermotropic glycolipid self-assembly: A review. *Journal of Oleo Science, 67*(6), 615–668.

Heberle, F. A., Pan, J., Standaert, R. F., Drazba, P., Kučerka, N., & Katsaras, J. (2012). Model-based approaches for the determination of lipid bilayer structure from small-angle neutron and X-ray scattering data. *European Biophysics Journal, 41*(10), 875–890.

Hemming, F. W. (1985). Chapter 4 - plycosyl phosphopolyprenols, *Glycolipids* (Vol. 10, pp. 261–305). Amsterdam, Netherlands: Elsevier Science Publishers B. V.

Hengemihle, F. H., McGinnis, G. D., Prince, S., & Templeton, C. (1984). Thermal decomposition of anomeric glycopyranosides. *Journal of Analytical and Applied Pyrolysis, 6*(3), 317–323.

Heywood, W. E., Camuzeaux, S., Doykov, I., Patel, N., Preece, R.-L., Footitt, E., Cleary, M., Clayton, P., Grunewald, S., & Abulhoul, L. (2015). Proteomic discovery and

development of a multiplexed targeted MRM-LC-MS/MS assay for urine biomarkers of extracellular matrix disruption in mucopolysaccharidoses I, II, and VI. *Analytical Chemistry, 87*(24), 12238–12244.

Hoogboom, J., Rasing, T., Rowan, A. E., & Nolte, R. J. (2006). LCD alignment layers. controlling nematic domain properties. *Journal of Materials Chemistry, 16*(14), 1305–1314.

Hruska, K. S., LaMarca, M. E., Scott, C. R., & Sidransky, E. (2008). Gaucher disease: Mutation and polymorphism spectrum in the glucocerebrosidase gene (GBA). *Human Mutation, 29*(5), 567–583.

Hyde, S. T. (2001). Identification of lyotropic liquid crystalline mesophases, *Handbook of applied surface and colloid chemistry* (Vol. 2, pp. 299–332). Florida, USA: John Wiley & Sons.

Hyun, K., Wilhelm, M., Klein, C. O., Cho, K. S., Nam, J. G., Ahn, K. H., Lee, S. J., Ewoldt, R. H., & McKinley, G. H. (2011). A review of nonlinear oscillatory shear tests: Analysis and application of large amplitude oscillatory shear (LAOS). *Progress in Polymer Science, 36*(12), 1697-1753.

Iglauer, S., Wu, Y., Shuler, P., Tang, Y., & Goddard, W. A. (2010). New surfactant classes for enhanced oil recovery and their tertiary oil recovery potential. *Journal of Petroleum Science and Engineering, 71*(1), 23–29.

Imura, T., Hikosaka, Y., Worakitkanchanakul, W., Sakai, H., Abe, M., Konishi, M., Minamikawa, H., & Kitamoto, D. (2007). Aqueous-phase behavior of natural glycolipid biosurfactant mannosylerythritol lipid A: Sponge, cubic, and lamellar phases. *Langmuir, 23*(4), 1659–1663.

Israelachvili, J. (1994). The science and applications of emulsions — An overview. *Colloids and Surfaces A: Physicochemical and Engineering Aspects, 91*, 1–8.

Jákli, A., & Saupe, A. (2006). *One-and two-dimensional fluids: Properties of smectic, lamellar and columnar liquid crystals*. London, UK: CRC Press.

Ji, Q., Kamiya, S., Jung, J.-H., & Shimizu, T. (2005). Self-assembly of glycolipids on silica nanotube templates yielding hybrid nanotubes with concentric organic and inorganic layers. *Journal of Materials Chemistry, 15*(7), 743–748.

Jones, J., & McLeish, T. (1995). Rheological response of surfactant cubic phases. *Langmuir, 11*(3), 785–792.

Jones, J., & McLeish, T. (1999). Concentration fluctuations in surfactant cubic phases: Theory, rheology, and light scattering. *Langmuir, 15*(22), 7495–7503.

Karukstis, K. K., Duim, W. C., van Hecke, G. R., & Hara, N. (2012). Biologically relevant lyotropic liquid crystalline phases in mixtures of n-octyl-*β*-D-glucoside and water. determination of the phase diagram by fluorescence spectroscopy. *The Journal of Physical Chemistry B, 116*(12), 3816–3822.

Kawamoto, H., Hosoya, T., Ueno, Y., Shoji, T., & Saka, S. (2014). Thermal stabilization and decomposition of simple glycosides in the presence of aromatic substances in closed ampoules: The role of OH···π hydrogen bonding. *Journal of Analytical and Applied Pyrolysis, 109*, 41–46.

Kazemi, M., Varshosaz, J., & Tabbakhian, M. (2018). Preparation and evaluation of lipid-based liquid crystalline formulation of fenofibrate. *Advanced Biomedical Research, 7*(1), 126–132.

Kinjo, Y., Wu, D., Kim, G., Xing, G.-W., Poles, M. A., Ho, D. D., Tsuji, M., Kawahara, K., Wong, C.-H., & Kronenberg, M. (2005). Recognition of bacterial glycosphingolipids by natural killer T cells. *Nature, 434*(7032), 520–525.

Kren, V., & Martínková, L. (2001). Glycosides in medicine:"The role of glycosidic residue in biological activity". *Current Medicinal Chemistry, 8*(11), 1303–1328.

Lafiandra, D., Masci, S., Sissons, M., Dornez, E., Delcour, J. A., Courtin, C. M., & Caboni, M. F. (2012). Chapter 6 - kernel components of technological value. In M. Sissons, J. Abecassis, B. Marchylo, & M. Carcea (Eds.), *Durum wheat* (2nd ed., pp. 85–124). Minnesota, USA: AACC International Press.

Lalitha, K., Gayathri, K., Prasad, Y., Saritha, R., Thamizhanban, A., Maheswari, C., Sridharan, V., & Nagarajan, S. (2018). Supramolecular gel formation based on glycolipids derived from renewable resources. *Gels, 4*(1), 1–12.

Langner, M., Praefcke, K., Krüerke, D., & Heppke, G. (1995). Chiral radial pentaynes exhibiting cholesteric discotic phases. *Journal of Materials Chemistry, 5*(4), 693–699.

Lauger, J., Linemann, R., & Richtering, W. (1995). Shear orientation of a lamellar lyotropic liquid crystal. *Rheologica Acta, 34*(2), 132–136.

Li, X., Cao, H., Gao, S., Pan, F., Weng, L., Song, S., & Huang, Y. (2008). Preparation of body armour material of Kevlar fabric treated with colloidal silica nanocomposite. *Plastics, Rubber and Composites, 37*(5–6), 223–226.

Liang, Q., Liu, P., Liu, C., Jian, X., Hong, D., & Li, Y. (2005). Synthesis and properties of lyotropic liquid crystalline copolyamides containing phthalazinone moiety and ether linkages. *Polymer, 46*(16), 6258–6265.

Liew, C. Y., Salim, M., Zahid, N. I., & Hashim, R. (2015). Biomass derived xylose Guerbet surfactants: Thermotropic and lyotropic properties from small-angle X-ray scattering. *RSC Advances, 5*(120), 99125–99132.

Liu, X., Gong, L., Xin, M., & Liu, J. (1999). The synthesis of sucrose ester and selection of its catalyst. *Journal of Molecular Catalysis A: Chemical, 147*(1), 37–40.

Manickam Achari, V., Nguan, H. S., Heidelberg, T., Bryce, R. A., & Hashim, R. (2012). Molecular dynamics study of anhydrous lamellar structures of synthetic glycolipids: Effects of chain branching and disaccharide headgroup. *The Journal of Physical Chemistry B, 116*(38), 11626-11634.

Mannock, D. A., & McElhaney, R. N. (2004). Thermotropic and lyotropic phase properties of glycolipid diastereomers: Role of headgroup and interfacial interactions in determining phase behaviour. *Current Opinion in Colloid & Interface Science, 8*(6), 426–447.

Matsumoto, Y., Alam, M. M., & Aramaki, K. (2009). Phase behavior, formation, and rheology of cubic and hexagonal phase based gel emulsions in water/tetraglyceryl lauryl ether/oil systems. *Colloids and Surfaces A: Physicochemical and Engineering Aspects, 341*(1–3), 27–32.

Medronho, B., Miguel, M. G., & Olsson, U. (2007). Viscoelasticity of a nonionic lamellar phase. *Langmuir, 23*(10), 5270–5274.

Meier, G., Sackmann, E., & Grabmaier, J. G. (2012). *Applications of liquid crystals*. Heidelberg, Federal Republic of Germany: Springer Science & Business Media.

Mendozza, M., Caselli, L., Montis, C., Orazzini, S., Carretti, E., Baglioni, P., & Berti, D. (2019). Inorganic nanoparticles modify the phase behavior and viscoelastic properties of non-lamellar lipid mesophases. *Journal of Colloid and Interface Science, 541*, 329-338.

Metzler, D. E. (2003). *Biochemistry: The chemical reactions of living cells*. (Vol. 1). California, USA: Elsevier.

Meyers, C. L. F., & Meyers, D. J. (2008). Thin-layer chromatography. *Current Protocols in Nucleic Acid Chemistry, 34*(1), 1–34.

Mezger, T. G. (2006). *The rheology handbook: For users of rotational and oscillatory rheometers*. Hannover, Federal Republic of Germany: Vincentz Network GmbH & Co KG.

Mezger, T. G. (2014). *Applied rheology*. Graz, Austria: Anton Paar GmbH.

Mezzenga, R., Meyer, C., Servais, C., Romoscanu, A. I., Sagalowicz, L., & Hayward, R. C. (2005). Shear rheology of lyotropic liquid crystals: A case study. *Langmuir, 21*(8), 3322–3333.

Misran, M., Azrah, A., & Aziz. (2008). Rheological properties of glycolipid based creams for pharmaceutical and cosmetic applications. *Nano Science & Nano Technology: An Indian Journal, 2*(1), 12–19.

Mnif, I., & Ghribi, D. (2016). Glycolipid biosurfactants: Main properties and potential applications in agriculture and food industry. *Journal of the Science of Food and Agriculture, 96*(13), 4310–4320.

Montalvo, G., Valiente, M., & Rodenas, E. (1996). Rheological properties of the L phase and the hexagonal, lamellar, and cubic liquid crystals of the CTAB/benzyl alcohol/water system. *Langmuir, 12*(21), 5202–5208.

Müller-Goymann, C. C. (2004). Physicochemical characterization of colloidal drug delivery systems such as reverse micelles, vesicles, liquid crystals and nanoparticles for topical administration. *European Journal of Pharmaceutics and Biopharmaceutics, 58*(2), 343–356.

Németh, Z., Halász, L., Pálinkás, J., Bóta, A., & Horányi, T. (1998). Rheological behaviour of a lamellar liquid crystalline surfactant–water system. *Colloids and Surfaces A: Physicochemical and Engineering Aspects, 145*(1), 107–119.

Nguan, H. S., Heidelberg, T., Hashim, R., & Tiddy, G. J. T. (2010). Quantitative analysis of the packing of alkyl glycosides: A comparison of linear and branched alkyl chains. *Liquid Crystals, 37*(9), 1205–1213.

Niraula, B., King, T. C., Chun, T. K., & Misran, M. (2004). Rheology properties of glucopyranoside stabilized oil–water emulsions: Effect of alkyl chain length and bulk concentration of the surfactant. *Colloids and Surfaces A: Physicochemical and Engineering Aspects, 251*(1), 117–132.

O'Lenick Jr, A. (2001). Guerbet chemistry. *Journal of Surfactants and Detergents, 4*(3), 311–315.

Ollikainen, I. (2015). *Rheological characterization of polysaccharide gels.* (Master's thesis, Lappeenranta University of Technology, Finland). Retrieved on April 25th , 2019 from http://lutpub.lut.fi/handle/10024/113955

Patrick, M., Zahid, N. I., Kriechbaum, M., & Hashim, R. (2018). Guerbet glycolipids from mannose: Liquid crystals properties. *Liquid Crystals, 45*(13–15), 1970–1986.

Pouzot, M., Mezzenga, R., Leser, M., Sagalowicz, L., Guillot, S., & Glatter, O. (2007). Structural and rheological investigation of *Fd*3*m* inverse micellar cubic phases. *Langmuir, 23*(19), 9618–9628.

Rädler, J. O., Koltover, I., Salditt, T., & Safinya, C. R. (1997). Structure of DNA-cationic liposome complexes: DNA intercalation in multilamellar membranes in distinct interhelical packing regimes. *Science, 275*(5301), 810–814.

Rodriguez-Abreu, C., Acharya, D. P., Aramaki, K., & Kunieda, H. (2005). Structure and rheology of direct and reverse liquid-crystal phases in a block copolymer/water/oil system. *Colloids and Surfaces A: Physicochemical and Engineering Aspects, 269*(1), 59–66.

Roman, M., Dong, S., Hirani, A., & Lee, Y. W. (2009). Cellulose nanocrystals for drug delivery, *Polysaccharide materials : Performance by design* (pp. 81–91). Washington DC, USA: American Chemical Society.

Saari, N. A. N., Mislan, A. A., Hashim, R., & Zahid, N. I. (2018). Self-assembly, thermotropic, and lyotropic phase behavior of Guerbet branched-chain maltosides. *Langmuir, 34*(30), 8962–8974.

Sadhale, Y., & Shah, J. C. (1999). Stabilization of insulin against agitation-induced aggregation by the GMO cubic phase gel. *International Journal of Pharmaceutics, 191*(1), 51–64.

Sadtler, V. M., Guely, M., Marchal, P., & Choplin, L. (2004). Shear-induced phase transitions in sucrose ester surfactant. *Journal of Colloid and Interface Science, 270*(2), 270–275.

Sagalowicz, L., Mezzenga, R., & Leser, M. E. (2006). Investigating reversed liquid crystalline mesophases. *Current Opinion in Colloid & Interface Science, 11*(4), 224–229.

Sakya, P., & Seddon, J. (1997). Thermotropic and lyotropic phase behaviour of monoalkyl glycosides. *Liquid Crystals, 23*(3), 409–424.

Sakya, P., Seddon, J., & Templer, R. (1994). Lyotropic phase behaviour of n-octyl-1-*O*-*β*-D-glucopyranoside and its thio derivative n-octyl-1-S-*β*-D-glucopyranoside. *Journal de Physique II, 4*(8), 1311–1331.

Santiago, M., & Strobel, S. (2013). Chapter 24 - Thin layer chromatography. In J. Lorsch (Ed.), *Methods in enzymology* (pp. 303–324). California, USA: Academic Press.

Saravacos, G. D. (1970). Effect of temperature on viscosity of fruit juices and purees. *Journal of Food Science, 35*(2), 122–125.

Schnablegger, H., & Singh, Y. (2013). *The SAXS guide - getting acquinted with the principle*. (4th ed.). Graz, Austria: Anton Paar GmbH.

Seddon, J. M., Ces, O., Templer, R. H., Mannock, D. A., & McElhaney, R. N. (2003). Structure and phase behaviour of synthetic glycolipids. *Molecular Crystals and Liquid Crystals, 402*(1), 77–84.

Seddon, J. M., Squires, A. M., Conn, C. E., Ces, O., Heron, A. J., Mulet, X., Shearman, G. C., & Templer, R. H. (2006). Pressure-jump X-ray studies of liquid crystal transitions in lipids. *Philosophical Transactions of the Royal Society A: Mathematical, Physical and Engineering Sciences, 364*(1847), 2635–2655.

Sengupta, A. (2013). Flow of nematic liquid crystals in a microfluidic environment, *Topological microfluidics* (pp. 83–135). Cham, Federal Republic of Germany: Springer.

Sengupta, A. (2013). Liquid crystal theory, *Topological microfluidics* (pp. 7–36). Cham, Federal Republic of Germany: Springer.

Shafizadeh, F. (1982). Introduction to pyrolysis of biomass. *Journal of Analytical and Applied Pyrolysis, 3*(4), 283–305.

Shah, J. C., Sadhale, Y., & Chilukuri, D. M. (2001). Cubic phase gels as drug delivery systems. *Advanced Drug Delivery Reviews, 47*(2), 229–250.

Singh, S., & Dunmur, D. A. (2002). *Liquid crystals: Fundamentals*. Farrer Road, Singapore: World Scientific.

Soltero, J. F. A., Alvarez-Ramírez, J. G., Fernández, V. V. A., Tepale, N., Bautista, F., Macías, E. R., Pérez-López, J. H., Schulz, P. C., Manero, O., Solans, C., & Puig, J. E. (2007). Phase and rheological behavior of the polymerizable surfactant CTAVB and water. *Journal of Colloid and Interface Science, 312*(1), 130–138.

Speziale, C., Ghanbari, R., & Mezzenga, R. (2018). Rheology of ultraswollen bicontinuous lipidic cubic phases. *Langmuir, 34*(17), 5052–5059.

Sułek, M. W., Ogorzałek, M., Wasilewski, T., & Klimaszewska, E. (2013). Alkyl polyglucosides as components of water based lubricants. *Journal of Surfactants and Detergents, 16*(3), 369–375.

Sun, S., Sun, S., Cao, X., & Sun, R. (2016). The role of pretreatment in improving the enzymatic hydrolysis of lignocellulosic materials. *Bioresource Technology, 199*, 49–58.

Taheri, A., & Mohammadi, M. (2015). The use of cellulose nanocrystals for potential application in topical delivery of hydroquinone. *Chemical Biology & Drug Design, 86*(1), 102–106.

Thaker, B., Kanojiya, J., & Tandel, R. (2010). Effects of different terminal substituents on the mesomorphic behavior of some azo-schiff base and azo-ester-based liquid crystals. *Molecular Crystals and Liquid Crystals, 528*(1), 120–137.

Tiddy, G. J. T. (1980). Surfactant-water liquid crystal phases. *Physics Reports, 57*(1), 1–46.

Tyler, A. I. I., Law, R. V., & Seddon, J. M. (2015). X-ray diffraction of lipid model membranes. In D. M. Owen (Ed.), *Methods in membrane lipids* (pp. 199–225). New York, USA: Springer New York.

van Boeckel, C. A. A., & van Boom, J. H. (1980). Synthesis of phosphatidyl-*α*-glucosyl-diacylglycerol containing palmitic and oleic acid esters. *Tetrahedron Letters, 21*(38), 3705–3708.

van Boeckel, C. A. A., Westerduin, P., & van Boom, J. H. (1981). Synthesis of 2,3-di-*O*-phytanyl-1-*O*-[glucosyl (galactosyl)-*β*(1→6)-mannosyl-*α*(1→2)-glucosyl-*α* (1→1)]-SN-glycerol. purple membrane glycolipids. *Tetrahedron Letters, 22*(29), 2819–2822.

van Thillo, E., Mertens, P., Boeykens, J., & Vandaele, F. (2002). Washington, DC Patent No. 6,461,802. U. S. P. a. T. Office.

Vertogen, G., & de Jeu, W. H. (2012). *Thermotropic liquid crystals, fundamentals*. Heidelberg, Federal Republic of Germany: Springer.

Vidyasagar, A., Handore, K., & Sureshan, K. M. (2011). Soft optical devices from self-healing gels formed by oil and sugar-based organogelators. *Angewandte Chemie International Edition, 50*(35), 8021–8024.

Vill, V., Böcker, T., Thiem, J., & Fischer, F. (1989). Studies on liquid-crystalline glycosides. *Liquid Crystals, 6*(3), 349–356.

Vill, V., Fischer, F., & Thiem, J. (1988). Helical twisting power of carbohydrate derivatives. *Z Naturforsch, 43a*, 1119–1126.

Vill, V., & Hashim, R. (2002). Carbohydrate liquid crystals: Structure–property relationship of thermotropic and lyotropic glycolipids. *Current Opinion in Colloid & Interface Science, 7*(5–6), 395–409.

Vill, V., von Minden, H. M., Koch, M. H. J., Seydel, U., & Brandenburg, K. (2000). Thermotropic and lyotropic properties of long chain alkyl glycopyranosides: Part I: Monosaccharide headgroups. *Chemistry and Physics of Lipids, 104*(1), 75–91.

von Minden, H. M., Milkereit, G., & Vill, V. (2002). Effects of carbohydrate headgroups on the stability of induced cubic phases in binary mixtures of glycolipids. *Chemistry and Physics of Lipids, 120*(1), 45–56.

von Rybinski, W., & Hill, K. (1998). Alkyl polyglycosides—properties and applications of a new class of surfactants. *Angewandte Chemie International Edition, 37*(10), 1328–1345.

Wade Jr, L. G. (2013). Nuclear magnetic resonance, *Organic chemistry* (pp. 563–568). Illinois, USA: Pearson Education Inc.

Wang, G., Chen, A., Mangunuru, H. P., & Yerabolu, J. R. (2017). Synthesis and characterization of amide linked triazolyl glycolipids as molecular hydrogelators and organogelators. *RSC Advances, 7*(65), 40887–40895.

Williams, H. D., Trevaskis, N. L., Charman, S. A., Shanker, R. M., Charman, W. N., Pouton, C. W., & Porter, C. J. (2013). Strategies to address low drug solubility in discovery and development. *Pharmacological Reviews, 65*(1), 315–499.

Wing, R. E., & BeMiller, J. N. (1969). Preparation of alkyl α-D-glucopyranosides. *Carbohydrate Research, 10*(3), 441–448.

Wyatt, D., & Dorschel, D. (1992). A cubic-phase delivery system composed of glyceryl monooleate and water for sustained release of water-soluble drugs. *Pharmaceutical Technology, 16*(10), 116–116.

Yamashita, J., Shiono, M., & Hato, M. (2008). New lipid family that forms inverted cubic phases in equilibrium with excess water: Molecular structure − aqueous phase structure relationship for lipids with 5, 9, 13, 17-tetramethyloctadecyl and 5, 9,

13, 17-tetramethyloctadecanoyl chains. *The Journal of Physical Chemistry B, 112*(39), 12286–12296.

Ye, E., Chee, P. L., Prasad, A., Fang, X., Owh, C., Yeo, V. J. J., & Loh, X. J. (2014). Supramolecular soft biomaterials for biomedical applications. *Materials Today, 17*(4), 194–202.

Yu, M., Jiang, Y., Shin, Y., Jiang, J., Yang, H., Zhang, H., Xue, J., Li, Q., & Yang, D.-K. (2018). Effect of biaxiality on chirality in chiral nematic liquid crystals. *Soft Matter, 14*(31), 6530–6536.

Zahid, N. I., Conn, C. E., Brooks, N. J., Ahmad, N., Seddon, J. M., & Hashim, R. (2013). Investigation of the effect of sugar stereochemistry on biologically relevant lyotropic phases from branched-chain synthetic glycolipids by small-sngle X-ray scattering. *Langmuir, 29*(51), 15794–15804.

Zhang, J., Hu, Y., & Li, Y. (2018). Supramolecular gels. In J. Zhang, Y. Hu, & Y. Li (Eds.), *Gel chemistry: Interactions, structures and properties* (pp. 9–59). Beach Road, Singapore: Springer Singapore.

Zhang, W., Yuan, C., Guo, J., Qiu, L., & Yan, F. (2014). Supramolecular ionic liquid gels for quasi-solid-state dye-sensitized solar cells. *ACS Applied Materials & Interfaces, 6*(11), 8723–8728.

Zhang, Y., Chen, L., & Wu, X. (2018). Thermotropic liquid crystalline and surface-active properties of n-alkyl α-D-mannopyranosides. *Journal of Molecular Liquids, 269*, 947–955.

Zhao, J., Wang, Z., Wei, X., Liu, F., Zhou, W., Tang, X., & Wu, T. (2011). Phase behaviour and rheological properties of the lamellar liquid crystals formed in dodecyl polyoxyethylene polyoxypropylene ether/water system. *Indian Journal of Chemistry, 50A*, 641–649.

LIST OF PUBLICATIONS AND PAPERS PRESENTED

PUBLICATION

1. **Mislan, A. A.**, Foong, J. L. N., Saharin S. M., & Zahid, N. I. (2019). Rheological behaviour of thermotropic and lyotropic liquid crystalline phases of Guerbet branched chain glycolipids. *Fluid Phase Equilibria, 50,* 112305.

2. Saari, N. A. N., **Mislan, A. A.**, Zahid, N. I. & Hashim, R. (2018). Self-assembly, thermotropic and lyotropic behaviour of synthetic branched-chain alkylmaltosides. *Langmuir*, *34*(30), 8962–8974.

PAPER PRESENTATION

Oral

Flow Behaviour of Liquid Crystalline Phases of Branched-Chain Glycolipids, 5th IET International Conference on Clean Energy and Technology & 4th International Conference on Global Sustainability & Chemical Engineering (CEAT-ICGSCE 2018), 5–6th September 2018, Kuala Lumpur, Malaysia.

Poster

Flow Behaviour of Liquid Crystalline Phases of A Branched-Chain Glycolipid, 7th Asian Conference on Colloid and Interface Science (ACCIS 2017), 8–11th August 2017, Kuala Lumpur, Malaysia.